ADAMTS13 RESISTANCE TO PROTEASE INHIBITION

UNRAVELING THE MECHANISM OF ADAMTS13 RESISTANCE TO PROTEASE INHIBITION

BY

KANWAL SINGH, BSc

A Thesis Submitted to the School of Graduate Studies in Partial Fulfilment of the

Requirements for the Degree

Doctor of Philosophy

McMaster University

McMaster University DOCTOR OF PHILOSOPHY (2022) Hamilton, Ontario (Health Sciences – Medical Sciences – Blood and Vasculature)

TITLE: Unraveling the mechanism of ADAMTS13 resistance to protease inhibition

AUTHOR: Kanwal Singh, BSc (University of Toronto)

SUPERVISOR: Colin A. Kretz, PhD

NUMBER OF PAGES: xxi, 223

LAY ABSTRACT

Hemostasis is the body's natural process to prevent bleeding and maintain blood flow. The ability of a blood protein, called VWF, to stop bleeding upon injury is regulated by the protein ADAMTS13. ADAMTS13 circulates in the blood for days, but its function cannot be stopped by inhibitors. Here, we investigate the mechanism by which ADAMTS13 is resistant to inhibition. We found that several structures of ADAMTS13, called domains and loops, protect it from inhibitors. Folding of the distal domains to the centre of ADAMTS13 partially protected ADAMTS13 from inhibitors. Further investigation revealed that two flexible loops close to the active site of ADAMTS13 were primarily responsible for protecting ADAMTS13 from inhibitors. We suggest that the flexibility of these loops guard against inhibition by folding across the active site. These results are important because advances have been made to use ADAMTS13 therapeutically in many clotting illnesses, such as strokes.

ABSTRACT

Background: ADAMTS13 is a metalloprotease that regulates the delicate balance between VWF multimeric length and its platelet capturing capacity. Unlike other ADAMTS and coagulation proteases, ADAMTS13 exhibits a prolonged half-life of several days as an active protease, suggesting that it is protected from inhibitors of metalloproteases in blood. Here, we investigate the mechanism by which ADAMTS13 is resistant to protease inhibition.

Methods: C-terminal domain truncations of ADAMTS13 (MDTCS and MD) and chimeras with ADAMTS5 (MD13/TCS5, M13/DTCS5, MD5/TCS13, and MD5(TCS-CUB13)) were generated. Metalloprotease domain segments from ADAMTS5 were swapped into MDTCS13 corresponding to the gatekeeper triad (R193, D217, and D252) (MDTCS-G), the variable loop (G236-S263) (MDTCS-V5), and the calcium-binding loop (R180-R193) (MDTCS-C5). MDTCS-GVC5 was generated to study these features simultaneously. Alpha 2-macrogloublin (A2M), tissue inhibitors of metalloproteinases (TIMPs), and small molecule inhibitor (Marimastat) were used as inhibitors, and tested using FRETS-VWF73 and Western blot.

Results: MDTCS, MD, MD13/TCS5, M13/DTCS5, MDTCS-G, MDTCS-V5, and MDTCS-C5 constructs were resistant to all inhibitors, whereas MD5/TCS13 was inhibited. The presence of the closed conformation attenuated MD5(TCS-CUB13) proteolysis by 50-fold, while displaying a slower rate of inhibition compared to MD5/TCS13. We report the kinetic parameters of the unique features of the

metalloprotease domain (the gatekeeper triad, the variable loop, and the calcium-binding loop). Moreover, simultaneously swapping these features sensitized MDTCS-GVC5 to Marimastat.

Conclusion: Our findings reveal that the closed conformation confers global latency, while the metalloprotease domain confers local latency of ADAMTS13. The local latency is maintained by the flexibility of the variable loop and the calcium-binding loop, which fold across the active site cleft to restrict inhibitor and substrate access. Extensive engagement of exosites by VWF can readily displace these loops, thereby activating ADAMTS13 from its latent form. Altogether, we present novel insight into the mechanism by which ADAMTS13 is resistant to protease inhibition.

ACKNOWLEDGEMENTS

2.7 seconds. That is the 0 – 100 km/h time of an Aprilia RSV4 Factory motorcycle. In the words of Drake, it goes from “0 to 100, real quick”. Straight roads are what most people prefer, but great drivers or riders prefer the challenge of winding roads that makes them adapt, while pushing their machines and themselves to the limit. In a way, graduate school is very similar; the experience goes by fast, teaches you to adapt with each outcome, and constantly pushes the frontier of science. As I prepare to defend my doctoral thesis, I would like to take the time to thank the individuals that contributed to this thesis and those who have supported me throughout my life.

First and foremost, I would like to thank God for all the blessings in my life, for giving me this opportunity, and for providing me with guidance and strength throughout difficult times. With the support of God and my loved ones, anything is possible.

To my supervisor, Dr. Colin Kretz, I am grateful for your guidance and having faith in my abilities to answer complex questions. Under your mentorship, I have grown as a person, as a student, and as a scientist. You taught me what it takes to be a great scientist, and how to analyze data critically to solve problems, despite numerous failures. Your guidance has helped me pursue my goals. When I joined your lab, you took time to teach me first-hand how to pipette and do tissue culture. Your willingness to teach and disseminate knowledge is admirable. Being your first student, I got to witness the growth of the lab, and I cannot wait to see the amazing discoveries that will come out of your lab. I truly appreciate everything you have done for me, and for all that I have learned from you. You will always remain a contributor behind my success and achievements.

Next I would like to express my gratitude to my committee members Dr. Jeffrey Weitz, Dr. Patricia Liaw, and Dr. Paul Kim. Your valuable expertise, insight, and feedback have helped strengthen this project. Your dedication and motivation for science and medicine is an inspiration to me. I want to further extend my gratitude to Dr. Jeffrey Weitz for his guidance during my comprehensive exam.

To my friends at TaARI, thank you for your continued support and kindness. It has been a pleasure to work, laugh, and learn from each of you. I will always cherish the times we had together. I cannot wait to see all the fantastic things each of you will achieve. To my military family, thank you for teaching me life-long skills, and the opportunity to serve my country. To Garinder and Raminder Parwaga, the gym has given me many things, but our friendship has been the best gift. To Narinder Bhatti, you are like a big brother to me, and for that I am truly so grateful. To you, and my motorcycle family, Aman Jamwal, and Varinder Sohi, blood makes you related, but the road makes you family.

No amount of thanks or words can express how grateful I am for my family. To my cousins, Manraj and Humraj Badwal, we share some of the most special times together, so thank you. To Amarjit Badwal and Sukhjinder Gill, thank you so much for everything you have done for me. You have always been there and supported me from the day I was born. God blessed me with a second set of parents. To Kulbir Kaur, thank you for loving me like a mother and supporting me like a friend. To my grandparents, Gulzar Singh, late Malkiat Kaur, Gurmanjit Tamber, and late Gurdev Singh, thank you for raising me, loving me, spoiling me, and protecting me from my parents when I got in

trouble. Thank you for your unconditional love, and for all the memories that I will forever cherish. To my brother Sanewal Singh, we have done everything together, shared countless laughs and memories, and you always had my back. We are each other's brother's keeper, from the womb to the tomb. To Rocky, you are such a blessing, you fill the house with so much joy, and you always leave paw prints on my heart. To my parents, Devinder Kaur and Lakhbir Singh, you worked long hours so we would have everything we needed, and you made sure that there were no shortcomings. You made sacrifices for our success, and provided endless support for our endeavours. You are my hero, my role model, and who I aspire to be. I am so grateful for everything you have done for me and Sanewal. Thank you from the bottom of my heart.

To the love of my life, Sahar Sohrabipour, you are my bestest friend, you are my everything. Thank you for your unconditional love and support. You are the best thing to happen to me. You taught me the importance of following your dreams, and to never stop chasing them no matter what obstacles are thrown in your way. Sahar, you are an inspiration to me and everyone around you. You will be extraordinary in everything you do. I cannot wait for a life together. I love you Sahar infinitely, and for eternity.

Lastly, I would like to thank the following funding agencies: CanVECTOR Studentship Award (2018), Ontario Graduate Scholarship (2019-2020), and the Canadian Armed Forces Learning Plan (2021) for financially supporting my graduate studies. I would like to further extend my gratitude to the University of British Columbia Centre for Blood Research for the Earl W. Davie Symposium travel award, and to the CanVECTOR research network and to McMaster University for multiple travel awards, which provided

me with the opportunity to present my research at multiple national and international conferences.

TABLE OF CONTENTS

LIST OF FIGURES

LIST OF TABLES

LIST OF ABBREVIATIONS

ADAMTS13 – A disintegrin and metalloproteinase with a thrombospondin type 1 motif, member 13
ADAMTSL – ADAMTS-like
ADP – Adensoine diphosphate
ANOVA – Analysis of variance
AT – Antithrombin
ATP – Adensoine triphosphate
ATS5 – ADAMTS5
A1- antitrypsin – Alpha 1-antitrypsin
A2M – Alpha 2-macroglobulin
BME – β-mercaptoethanol
BRG1 – Transcription activator BRG1
C1-inh – C1-inhibitor
C8 – Cysteine 8 (VWF)
Ca^{2+} - Calcium
COMP – Cartilage oligomeric matrix protein
COVID-19 – Coronavirus disease 2019
CTCK – C-terminal cysteine knot
DMEM – Dulbecco's modified eagle media 1x
DIC – Disseminated intravascular coagulation
EGR-1 – Early growth response protein 1
F – Factor
FBS – Fetal bovine serum
GP – Glycoprotein
HCII – Heparin cofactor II
Il – Interleukin
MMP – Matrix metalloproteinase
PAR – Protease-activated receptor
PF4 – Platelet factor 4
PTHrP – Parathyroid hormone-related protein
S100 – Calcium-binding protein
SDM – Site-directed mutagenesis
Sp1 – Transcription factor
TAFI – Thrombin activated fibrinolysis inhibitor
TFPI – Tissue factor pathway inhibitor
TGF-α – Transforming growth factor α
TIL – Trypsin inhibitor-like
TIMPs – Tissue inhibitors of metalloproteinases
TM – Thrombomodulin
TNF-α – Tumor necrosis factor α
tPA – Tissue-type plasminogen activator
TSP-1 – thrombospondin type-1 repeat

TTP – Thrombotic thrombocytopenia purpura
uPA – Urokinase-type plasminogen activator
VWD – von Willebrand disease
VWF – von Willebrand factor

LIST OF CONSTRUCTS

**Domains listed sequentially*

ADAMTS13 – Metalloprotease, disintegrin, TSP-1, cysteine-rich, spacer, TSP-1 2-8 repeats, and CUB1-2

MDTCS – Metalloprotease, disintegrin, TSP-1, cysteine-rich, and spacer domains; lacks closed conformation

MD – Metalloprotease and disintegrin domains

MD13/TCS5 – Chimeric protease: metalloprotease and disintegrin domains of ADAMT13; TSP-1, cysteine-rich, and spacer domains of ADAMTS5

M13/DTCS5 – Chimeric protease: metalloprotease domain of ADAMTS13; disintegrin, TSP-1, cysteine-rich, and spacer domain of ADAMTS5

MD5/TCS13 – Chimeric protease: metalloprotease and disintegrin domains of ADAMT5; TSP1, cysteine-rich, and spacer domains of ADAMTS13

MD5(TCS-CUB13) – Chimeric protease: metalloprotease and disintegrin domains of ADAMTS5; TSP-1, cysteine-rich, spacer domains, and closed conformation of ADAMTS13

MDTCS-G – R193A, D217A, and D252A: Mutation of the Gatekeeper triad in the metalloprotease domain using MDTCS

MDTCS-C5 – R180-R193 to ATS5 R367-L379: Corresponding ADAMTS5 calcium-binding loop swap and gatekeeper triad (R193) in the metalloprotease domain using MDTCS

MDTCS-V5 – G236-P244 to ATS5 D421-F429: Corresponding ADAMTS5 loop swap in the metalloprotease domain using MDTCS

MDTCS-GVC5 – R180-R193 to ATS5 R367-L379, D217A, and G236-S263 to ATS5 D422-S453: Corresponding ADAMTS5 calcium-binding loop, corresponding ADAMTS5 loop swap, and gatekeeper triad mutations in the metalloprotease domain using MDTCS

DECLARATION OF ACADEMIC ACHIEVEMENT

Kanwal Singh performed all the experiments, contributed to the conceptual design, data curation, analyzed and interpreted the results, and wrote this thesis.

Dr. Colin Kretz contributed to the supervision, conceptual design of the studies, obtained funding to support these studies, and reviewed the results and this thesis.

Chapter 1: Introduction

1.1 Hemostasis

Hemostasis is a crucial evolutionary product of a closed circulatory system, which evolved to prevent blood loss upon vascular injury (Gale, 2011; Versteeg et al., 2013). When vascular injury occurs, blood vessels constrict, a platelet plug is formed, and the coagulation system is initiated, thereby resulting in a fibrin/platelet mesh that stabilizes bleeding (Gale, 2011; Lippi et al., 2009; Springer, 2014). Conceptually, hemostasis can be separated into three processes: primary hemostasis (formation of a platelet plug), secondary hemostasis (deposition of fibrin), and fibrinolysis (degradation of the clot); however, these processes do not occur sequentially and can be activated simultaneously to varying degrees (Figure 1.1) (Gale, 2011; Stokol et al., 2013).

Hemostasis is a remarkably complex and delicate balance between bleeding and thrombotic “forces”. When there is an imbalance between these forces, individuals may be predisposed to excessive bleeding or thrombosis (Lippi et al., 2015). Hemostatic imbalance may be either acquired or inherited, and range in severity (Lippi et al., 2015). Common causes of bleeding conditions include deficiencies in coagulation factors (hemophilia) or von Willebrand factor (VWF) (Lippi et al., 2015). The incidence of bleeding conditions range from approximately 1 in 1000 (VWF-related) (Lillicrap & James, 2009) to 1 in 2,000,000 (FII deficiency) (Lippi et al., 2015). Hypercoagulability is a common cause of thrombotic conditions such as ischemic heart disease, ischemic stroke, atrial fibrillation, and venous thrombosis (Gale, 2011; Wendelboe & Raskob,

2016). The incidence of thrombotic conditions range from approximately 1 in 66 (ischemic heart disease) to 1 in 520 (venous thromboembolism) (Wendelboe & Raskob, 2016). Taken together, thrombosis accounts for approximately 1 in 4 deaths, and is considered the leading cause of mortality worldwide (Wendelboe & Raskob, 2016). Fortunately, significant advances in our understanding of these hemostatic conditions, availability of therapeutics, and increased public awareness have led to a steady decline in mortality from bleeding and thrombosis (Wendelboe & Raskob, 2016).

Hypercoagulability can also occur during infection, particularly in sepsis, whereby activation of the coagulation system can lead to disseminated intravascular coagulation (DIC) (Dempfle, 2004). DIC is the consumption of coagulation factors and platelets, due to microvascular thrombosis, and leads to bleeding (Dempfle, 2004). With respect to the current coronavirus disease 2019 (COVID-19) pandemic, patients with SARS-CoV-2 display a hypercoagulable state with elevations in d-dimer (Abou-ismail et al., 2020; Asakura & Ogawa, 2021). Appropriate interventional strategies targeting the dysregulation in coagulation in patients with SARS-CoV-2 may be of therapeutic importance (Abou-ismail et al., 2020; Asakura & Ogawa, 2021).

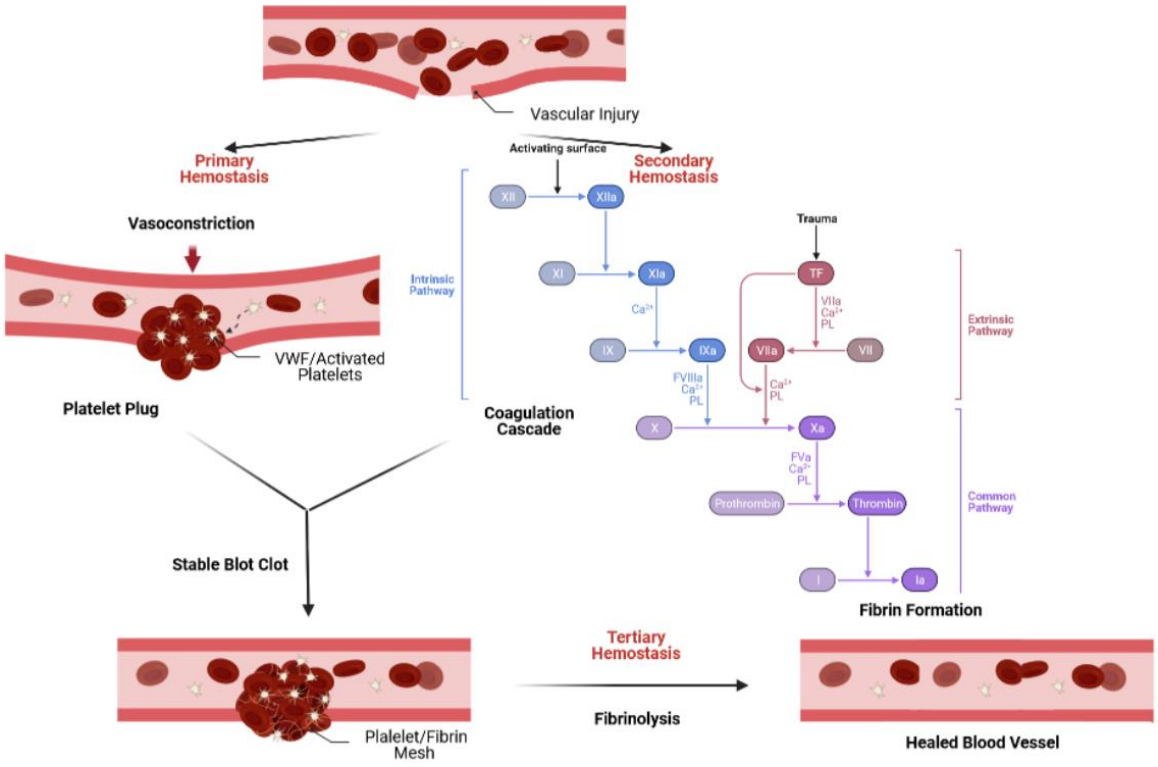
Vascular Injury
Primary Hemostasis
Activating surface
Secondary Hemostasis
Vasoconstriction
VWF/Activated Platelets
Platelet Plug
Intrinsic Pathway
XII
XIIa
XI
XIa
Ca2+
IX
IXa
FVIIIa Ca2+ PL
Coagulation Cascade
Trauma
TF
VIIa Ca2+ PL
VIIa
VII
Ca2+ PL
Extrinsic Pathway
X
Xa
FVa Ca2+ PL
Prothrombin
Thrombin
Common Pathway
I
Ia
Fibrin Formation
Stable Blot Clot
Plalelet/Fibrin Mesh
Tertiary Hemostasis
Fibrinolysis
Healed Blood Vessel

Figure 1.1. Overview of hemostasis. Hemostasis can be separated into three processes: Primary hemostasis, secondary hemostasis, and tertiary hemostasis. These processes can be activated simultaneously to varying degrees. Upon vascular injury, primary hemostasis is initiated, resulting in vasoconstriction, platelet recruitment. The subsequent adhesion, activation and aggregation of platelets, results in the formation of the platelet plug. Simultaneously, secondary hemostasis is initiated, leading to thrombin amplification and propagation that converts soluble fibrinogen into insoluble fibrin, thereby stabilizing the platelet plug. Tertiary hemostasis is the breakdown of the fibrin polymer mesh by plasmin. This process is called fibrinolysis and is an important part of wound healing, prevents clots in healthy blood vessels, and limits the size of a clot.

1.1.1 Vascular endothelium

The vascular endothelium is located at the interface between circulating blood and surrounding tissue, and consists of approximately 10^{11} cells with a combined surface area exceeding 100 m^2 (Wu & Thiagarajan, 1996). The uninjured endothelium provides a nonthrombogenic surface that does not allow platelet adherence, or activation of the coagulation system (Wu & Thiagarajan, 1996). The endothelium releases prostacyclin and nitric oxide, expresses ecto-adenosine diphosphate (ADP), thrombomodulin (TM), heparin-like molecules (heparan sulfate proteoglycan), and tissue plasminogen activator (tPA) (Wu & Thiagarajan, 1996). Prostacyclin and nitric oxide inhibit platelet activation and act as vasodilators. Ecto-adenosine diphosphatase degrades ADP and inhibits platelet aggregation. TM is a surface molecule that binds to thrombin, and facilitates activation of protein C, thereby converting thrombin to an anticoagulant enzyme. The heparin-like molecules function as a cofactor for antithrombin (AT), which serves as a potent inhibitor of coagulation. The secreted tPA activates fibrinolysis (Wu & Thiagarajan, 1996). Together, under normal conditions, the endothelium displays anticoagulant properties, which maintain blood fluidity.

1.1.2 Primary hemostasis

In contrast, injury to the endothelium results in the loss of its anticoagulant properties (Wu & Thiagarajan, 1996). Damage to the vascular endothelium causes reflex vasoconstriction, and endothelin release further constricts the damaged blood vessel (Periayah et al., 2017). This process occurs within the first 30 minutes of vascular damage, and is localized to the site of injury to restrict blood flow and prevent blood loss

(Periayah et al., 2017). The endothelium produces and secretes VWF from Weibel-Palade bodies, which functions to mediate platelet adhesion and shear-stress induced aggregation (Wu & Thiagarajan, 1996). The exposed collagen provides an anchorage site for VWF to bind and capture platelets to form the platelet plug, and releases adenosine triphosphate (ATP) and other inflammatory mediators to recruit macrophages (Periayah et al., 2017; Springer, 2014).

Following localized vasoconstriction, VWF will anchor to the exposed collagen through its A3 domain. VWF will capture platelets via interactions between its A1 domain and the glycoprotein (GP) Ibα on platelets under high shear stress exerted by flowing blood (Springer, 2014). Unfolding of VWF by shear forces exposes previously hidden platelet binding site, A1 domain, and further unfolding reveals the A2 domain for a disintegrin and metalloproteinase with a thrombospondin type 1 motif, member 13 (ADAMTS13) proteolysis (Springer, 2014). Platelet adhesion is initiated by GPIbα binding to immobilized VWF, and GPVI binding to collagen (Gale, 2011; Periayah et al., 2017). Platelets are then activated, and adhesion and aggregation is strengthened and expanded through platelet-platelet connections between GP IIb/IIIa present on platelet surfaces (Gale, 2011). Further, GP IIb/IIIa binds to multiple ligands that promote platelet-platelet aggregation such as VWF, fibrinogen, collagen, fibronectin, and vitronectin (Gale, 2011). Platelet adherence to the subendothelial collagen is strengthened through GP Ia/IIa and collagen (Gale, 2011). Platelets also release ADP and thromboxane A2 upon activation, which are important molecules for platelet aggregation (Periayah et al., 2017). Platelets contain alpha and dense granules (Blair & Flaumenhaft, 2009; Chen et

al., 2018). Activation of platelets leads to the release of VWF, platelet factor 4 (PF4), and zinc from alpha granules (Blair & Flaumenhaft, 2009; Gorodetsky et al., 1993). Whereas, dense granules release polyphosphates, ADP, ATP, and calcium (Chen et al., 2018; Prechel & Walenga, 2013). PF4 can bind and neutralize heparan sulfate on endothelial cells, thereby inhibiting AT activity, thus promoting coagulation (Prechel & Walenga, 2013). Interestingly, autoantibodies against PF4 play a pathophysiological role in heparin-induced thrombocytopenia (Prechel & Walenga, 2013).

In summary, primary hemostasis is characterized by vasoconstriction and formation of the platelet plug (Gale, 2011; Periayah et al., 2017). Vasoconstriction of the damaged blood vessel restricts blood flow, as VWF captures platelets at the site of injury, thereby resulting in the formation of a platelet plug upon platelet adhesion, activation, and aggregation (Gale, 2011; Periayah et al., 2017). This platelet plug is stabilized by the deposition of insoluble fibrin generated through the coagulation system (Gale, 2011).

1.1.3 Secondary hemostasis (coagulation system)

The coagulation system is an interaction between two independent pathways: extrinsic pathway (tissue factor pathway) and intrinsic pathway (contact pathway) that come together at the common pathway, which begins with the conversion of FX to FXa (Figure 1.2) (Harter et al., 2015; Mackman et al., 2007). The common pathway results in the conversion of prothrombin to thrombin (Harter et al., 2015; Mackman et al., 2007). The coagulation system is mediated by primarily serine proteases that are sequentially converted from zymogen to active proteases, ultimately leading to the generation of thrombin (Gale, 2011). Thrombin is the final effector protease of the coagulation system

which converts soluble fibrinogen to an insoluble fibrin network and activates platelets, thereby stabilizing the fibrin/platelet plug (Gale, 2011; Smith et al., 2016).

1.1.3.1 Extrinsic pathway (tissue factor pathway)

Upon vascular injury, the extrinsic pathway is initiated by the exposure of transmembrane receptor tissue factor (TF) expressed in the subendothelial tissue and plasma FVII/FVIIa (Mackman et al., 2007; Palta et al., 2014). TF can bind to both zymogen FVII or enzymatically active FVIIa to initiate the coagulation system (Giansily-Blaizot & Schved, 2017; Smith et al., 2016). FVII can become activated by either the TF/FVIIa complex itself, or by activated coagulation proteases, such as thrombin through feedback activation (Giansily-Blaizot & Schved, 2017). In the presence of calcium, the TF/FVIIa complex activates FX to FXa of the common pathway (Mackman et al., 2007). However, thrombin generation through this pathway is limited and can be effectively attenuated by TF pathway inhibitor (Palta et al., 2014). The TF/FVIIa complex can also activate FIX to FIXa to propagate thrombin production to ensure continuous generation of thrombin via the intrinsic pathway (Mackman et al., 2007; Palta et al., 2014; Smith et al., 2016).

1.1.3.2 Intrinsic pathway (contact pathway)

The intrinsic pathway begins by the contact activation of FXII, followed by the sequential activation of FXI and FIX (Gailani & Renné, 2007). When blood comes in contact with negatively charged molecules and surfaces such as dextran sulfate, silica, RNA, DNA, and polyphosphate, a series of contact activation reactions occur that result in the activation of FXII, prekallikrein, and FIX, and cleavage of high molecular weight

kininogen (Gailani & Renné, 2007; Grover & Mackman, 2019). Additionally, FXIIa can convert prekallikrein to α-kallikrein, which can cleave kininogen to release bradykinin, an important regulator of blood pressure and a promotor of inflammation (Gailani & Renné, 2007; Golias et al., 2007). Sequential activation of FXI by FXIIa occurs, followed by subsequent activation of FIX by FXIa (Gailani & Renné, 2007). Further, FIXa with its cofactor FVIIIa forms a tenase complex (FIXa/FVIIa), on negatively charged phospholipid surfaces and in the presence of calcium to activate FX of the common pathway (Gailani & Renné, 2007; Grover & Mackman, 2019; Palta et al., 2014). The intrinsic pathway can be activated by components of both the extrinsic and common pathways through various feedback mechanisms (Figure 1.2) (Grover & Mackman, 2019). This cross-activation plays an important role in maintaining sustained thrombin production for sufficient fibrin deposition (Grover & Mackman, 2019).

1.1.3.3 Common pathway

The common pathway is the convergence point between the extrinsic and intrinsic pathways resulting in the activation of FX (Palta et al., 2014). FX can be activated by the extrinsic complex of TF/FVIIa and calcium, and the intrinsic tenase complex of FIXa/FVIIIa on negatively charged surfaces in the presence of calcium (Gailani & Renné, 2007; Grover & Mackman, 2019; Palta et al., 2014). The resulting FXa forms a prothombinase complex with its cofactor, FVa, on a phospholipid surface in the presence of calcium that converts prothrombin into thrombin (Palta et al., 2014). Thrombin then converts circulating fibrinogen to fibrin, and activates FXIII, which covalently crosslinks the fibrin polymer network to stabilize the platelet plug (Palta et al., 2014). In addition to

converting fibrinogen to fibrin, thrombin also activates platelets via cleavage of protease-activated receptor (PAR) 1 and PAR4, and is responsible for clot propagation through positive feedback activation of the coagulation system (Gale, 2011).

1.1.4 Regulation of the coagulation system

Aside from the spatial and temporal regulation of zymogen activation steps, the coagulation system is also regulated by (a) the protein C pathway, and (b) natural protease inhibitors (Figure 1.2) (Gale, 2011; Madhusudhan et al., 2016; Palta et al., 2014). Thrombin can bind to TM on endothelial cells, and then activate protein C (Gale, 2011; Madhusudhan et al., 2016). Activated protein C with its cofactor protein S and phospholipids, proteolytically degrades and inactivates FVa and FVIIIa, thereby downregulating coagulation (Gale, 2011). Natural protease inhibitors can also downregulate the coagulation system (Madhusudhan et al., 2016; Palta et al., 2014). In particular, AT is a potent inhibitor of the intrinsic and common pathways that inhibits thrombin, FXa, FIXa, FXIa, and FXIIa (Madhusudhan et al., 2016; Palta et al., 2014). Whereas, tissue factor pathway inhibitor (TFPI) is a potent inhibitor of the extrinsic pathway that inhibits the TF/FVIIa complex (Palta et al., 2014). Other important inhibitors of coagulation include: alpha 1-antitrypsin, heparin cofactor II, C1 esterase inhibitor, and alpha 2-macroglobulin (A2M) (Palta et al., 2014). The activation of coagulation factors on surfaces of activated platelets, together with rapid inhibition of activated proteases at sites removed from on-going activation of coagulation helps restrict coagulation to the injury site. This spatial regulation of the coagulation system prevents “off-target” clot formation that may lead to organ ischemia and death (Gale, 2011). The

coagulation system is a tightly regulated system that maintains a delicate balance between procoagulant and anticoagulant forces, and any imbalance can have potentially dangerous and life-threatening consequences.

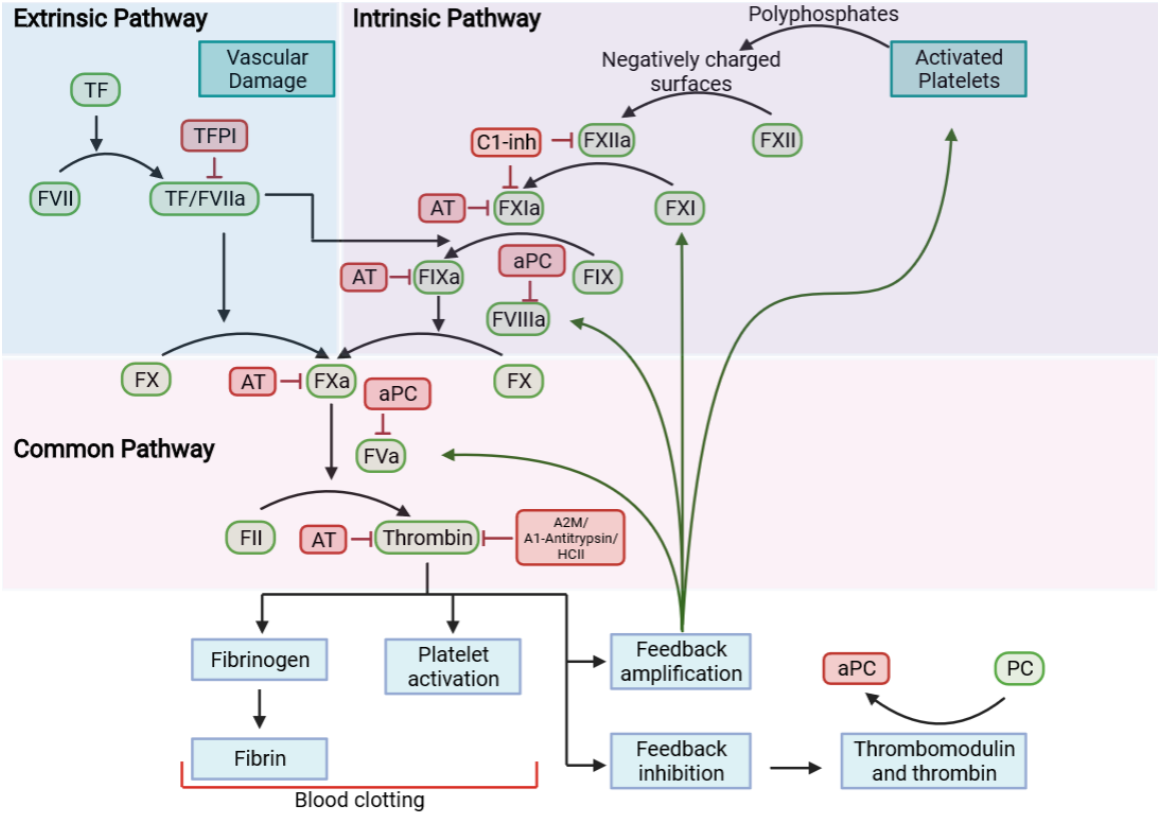
Extrinsic Pathway
Intrinsic Pathway
Common Pathway
Vascular Damage
TF
TFPI
FVII
TF/FVIIa
Polyphosphates
Negatively charged surfaces
Activated Platelets
C1-inh
FXIIa
FXII
AT
FXIa
FXI
AT
FIXa
aPC
FIX
FVIIIa
FX
AT
FXa
aPC
FX
FVa
FII
AT
Thrombin
A2M/ A1-Antitrypsin/ HCII
Fibrinogen
Platelet activation
Feedback amplification
aPC
PC
Fibrin
Feedback inhibition
Thrombomodulin and thrombin
Blood clotting

Figure 1.2. The coagulation system. Upon vascular injury, the extrinsic pathway is initiated and leads to the formation of the TF/FVIIa complex, which activates FX. The intrinsic pathway is initiated by contact activation of FXII by negatively charged surfaces such as those provided by activated platelets. The intrinsic pathway can also be initiated by the tissue factor pathway and thrombin through feedback mechanisms. The intrinsic pathway leads to the formation of the FIXa/FVIIIa tenase complex, which activates FX. The activation of FX to FXa in the common pathway converts prothrombin to thrombin. Thrombin has multiple functions: converts soluble fibrinogen to insoluble fibrin to stabilize the platelet plug, activates platelets, provides feedback amplification of the coagulation system, and provides feedback inhibition through activated protein C/TM pathway. AT inhibits thrombin, FXa, FIXa, FXIa, and FXIIa, and the inhibitory effect can be increased in the presence of heparin or heparan sulfate. Thrombin activated fibrinolysis inhibitor (TFPI) is a metalloprotease carboxypeptiase that inhibits the extrinsic pathway. Other important inhibitors of coagulation include: A2M, alpha 1-antitrypsin (A1-antitrypsin), heparin cofactor II (HCII), and C1 esterase inhibitor (C1-inh).

1.1.5 Tertiary hemostasis (fibrinolysis)

The fibrinolytic system serves to dissolve fibrin during the process of wound healing, prevent clots in healthy blood vessels, and limit the size of a clot (Gale, 2011; Palta et al., 2014). Fibrinolysis is a process that dissolves the fibrin polymer mesh into fibrin degradation products by plasmin (Palta et al., 2014). Plasmin is generated from plasminogen by tPA or urokinase plasminogen activator (uPA) (Chapin & Hajjar, 2015). Plasminogen and tPA come together on the fibrin clot surface, whereas uPA activates plasminogen in the presence of the uPA receptor (Chapin & Hajjar, 2015; Gale, 2011). Fibrinolysis or thrombosis is clinically assessed by measuring fibrin degradation products such as d-dimer, and are used in the assessment and diagnoses of pulmonary embolism, disseminated intravascular coagulation, or deep vein thrombosis (Palta et al., 2014). Inhibitors of fibrinolysis include plasmin inhibitors, plasminogen activator inhibitors, and thrombin activated fibrinolysis inhibitor (TAFI). Alpha 2-antiplasmin and A2M are potent plasmin inhibitors (Chapin & Hajjar, 2015). Plasminogen activator inhibitor 1 inhibits tPA and uPA (Chapin & Hajjar, 2015). TAFI is a metalloprotease carboxypeptidase zymogen that is activated by TM-associated thrombin (Chapin & Hajjar, 2015). Activated TAFI removes critical C-terminus positively charged lysine and arginine residues on fibrin, which in turn decreases the number of available plasminogen binding sites, thereby slowing plasmin generation (Chapin & Hajjar, 2015). The fibrinolytic system is responsible for the breakdown of fibrin during wound healing and prevents the formation of clots in healthy blood vessels (Gale, 2011; Palta et al., 2014).

Therefore, coagulation and fibrinolytic systems must be tightly regulated to maintain the delicate balance between thrombosis and hemorrhage (Palta et al., 2014).

1.2 von Willebrand factor (VWF)

VWF is a large multimeric glycoprotein that performs two hemostatic functions (De Groot et al., 2010). The primary function of VWF is to initiate platelet plug formation by capturing free flowing platelets to the site of vascular damage (Crawley et al., 2011; De Groot et al., 2010). Large VWF multimers are more effective at capturing platelets, but pose a thrombotic risk (Springer, 2014). In contrast, short VWF multimers are less effective at capturing platelets, but pose a bleeding risk (Springer, 2014). ADAMTS13 is a metalloprotease that maintains this delicate balance of VWF multimer length and the subsequent platelet capturing capacity of VWF (Sadler, 2008; Springer, 2014). The secondary function of VWF is to serve as a carrier for coagulation FVIII (De Groot et al., 2010; Shiltagh et al., 2014). Without VWF, FVIII would be prone to degradation and a short circulating half-life (De Groot et al., 2010; Shiltagh et al., 2014).

1.2.1 Synthesis and secretion of VWF

The VWF gene is located on chromosome 12 of the short arm at locus 12p13.3 (Peyvandi et al., 2011). VWF is produced in endothelial cells (plasma VWF) and megakaryocytes (platelet VWF), and is stored in Weibel-Palade bodies and α-granules, respectively (Wagner, 1990). VWF circulates in a folded globular conformation in plasma at a concentration of approximately 10 μg/mL (De Groot et al., 2010; Muia et al., 2014; Zander et al., 2015). Circulating VWF in plasma is predominantly endothelial cell–

derived, as platelets release VWF from α-granules only when activated (Ruggeri, 2003). The secretion of endothelial cell derived VWF occurs through two distinct mechanisms: basal secretion or regulated secretion (Lenting et al., 2015). In healthy individuals, basal secretion accounts for majority of circulating VWF and does not involve Weibel-Palade body exocytosis (Lenting et al., 2015). Whereas, during disease, dysregulated secretion occurs in response to endothelial cell agonists (e.g. thrombin, histamine, and cytokines) and results in the rapid release of VWF from Weibel-Palade bodies (Lenting et al., 2015; McGrath et al., 2010). Nonetheless, both endothelial cell and platelet –derived VWF play important roles in primary hemostasis (McGrath et al., 2010).

However, there are some key differences between VWF originating from endothelial cells versus megakaryocyte. Endothelial cell-VWF is constitutively secreted and undergoes proteolytic processing by ADAMTS13, whereas platelet-VWF is not constitutively secreted and does not undergo significant proteolysis, thereby lacking triplet pattern (McGrath et al., 2010; Peyvandi et al., 2011). On a multimer gel analysis, the triplet pattern is observed when VWF multimer proteolysis produces N- and C-terminal satellite bands that flank the main multimer band (James & Goodeve, 2011). Within a few hours after release from the endothelium, ultra large VWF is converted into a wide range of multimer size distributions by ADAMTS13 (X. Zhang et al., 2009). Further, endothelial cell-VWF secretion is mediated by thrombin, ADP, epinephrine, and histamine, whereas platelet-VWF secretion is mediated by thrombin, ADP, collagen, and thromboxane A2 (McGrath et al., 2010). Moreover, only endothelial cell-VWF carries FVIII (McGrath et al., 2010). Lastly, endothelial cell-VWF undergoes a set of complex

post-translational modifications including glycosylation in the rough endoplasmic reticulum and Golgi apparatus (McGrath et al., 2010; Wagner, 1990).

Interestingly, ABO blood groups account for approximately 25% variability in circulating VWF in plasma (Gill et al., 1987; McGrath et al., 2010). Type O individuals do not encode a functional AB glycosyltransferase and thus only express the H antigen. As a result, type O individuals display approximately 25% lower circulating levels of VWF, and individuals heterozygous for O display intermediate levels of VWF (McGrath et al., 2010; Swystun & Lillicrap, 2018). The lack of VWF glycosylation may result in an increased clearance of VWF in type O individuals, and to a lesser extent in those heterozygous for O (Solecka et al., 2016). Thus, this may contribute to bleeding complications for patients suffering from von Willebrand disease (VWD) and/or protection against thrombosis in the general population (Gill et al., 1987).

1.2.2 Structure of VWF

The domains of VWF are arranged in the following sequence: D1-D2-D'-D3-A1-A2-A3-D4-B1-B2-B3-C1-C2-CK (Figure 1.3) (Sadler, 1998). The multimeric chain structure of VWF is composed of numerous 270 kDa monomers, each containing binding sites for FVIII, platelets, and collagen (Matsui & Hamako, 2016). VWF consists of a signal peptide of 22 residues, a large propeptide of 741 residues, and a mature subunit of 2050 residues (Sadler, 1998). Altogether, VWF consists of 2813 residues of which 234 residues are cysteines that form paired disulfide bonds (Sadler, 1998). Cysteines are abundant in all domains except A domains, but still play a critical role in stabilizing domain structure (Crawley et al., 2011). VWF is heavily glycosylated with 10 O-linked

oligosaccharides, and 12 N-linked oligosaccharides are directly affected by an individual's blood group oligosaccharides (Sadler, 1998; Solecka et al., 2016; Wagner, 1990). In particular, four N-linked oligosaccharides at positions Asn99, Asn857, Asn2400, and Asn2790 have been identified to play an important role in synthesis and secretion of VWF (McKinnon et al., 2010).

1.2.2.1 D domains/assemblies

Each VWF monomer has multiple repeating D domains (D1, D2, D3, and D4) (Springer, 2014). Each D domain includes a cysteine-8 (C8), trypsin inhibitor-like (TIL), and E modules (Springer, 2014). The prodomain of VWF consists of the D1 and D2 domains (Springer, 2014). The D1, D2, and D'D3 domains mediate the assembly of disulfide linkage of VWF dimers in the acidic environment of the Golgi apparatus (Springer, 2014). C-terminal cysteine knot (CTCK) domain dimerizes in the endoplasmic reticulum (Springer, 2014). Multimers are formed from dimers by disulfide bonds at N-to-N and C-to-C terminal ends of each subunit (Tjernberg et al., 2004). After formation of multimers, the propeptide is cleaved off by furin; however, the propeptide remains non-covalently associated with the dimers in order to catalyze disulfide bond formation (Sadler, 1998; Tjernberg et al., 2004). The propeptide plays a critical role in the multimerization of VWF (Sadler, 1998). Premature deletion of the propeptide does not prevent transport to the Golgi apparatus, but prevents multimerization (Sadler, 1998). In terms of the D' of the D'D3 assembly, it is only composed of the TIL and E modules, and therefore, lacks the N-terminal prime D domain and C8 module (Springer, 2014). The

D'D3 domain binds FVIII, thereby playing an important role in coagulation by delivering FVIII to the site of injury (Springer, 2014).

1.2.2.2 A1 domain

With respect to structure, the A1 domain conformation is stabilized by N- and C-terminal disulfide bonds Cys1272-Cys1458 at the base of the domain, and consists of a central hydrophobic β-sheet surrounded by multiple α-helices (Figure 1.4A) (Crawley et al., 2011; Sadler, 1998). The primary function of the A1 domain of VWF is to capture platelets through GPIbα, resulting in the formation of the platelet plug (Sadler, 1998). In order to prevent spontaneous platelet binding in circulation, shear force is required to induce a conformational change that exposes the A1 domain to free flowing blood (X. Zhang et al., 2009). Mutagenesis studies identified Lys1362, Arg1392, and Arg1395 as important residues that interact with platelet GPIbα at the top of the A1 domain (Matsushita & Sadler, 1995; Sadler, 1998). Residues Glu1260-Arg1274 and Arg1450-Glu1452 at the bottom of the A1 domain comprise a regulatory region that is responsible for shielding this binding site to GPIbα until shear forces physically elongated VWF to unblock the binding site (Matsushita & Sadler, 1995). This regulatory site is of particular importance in specific gain-of-function mutations associated with VWD (Matsushita & Sadler, 1995; Sadler, 1998). In addition to platelet binding, the A1 domain can also bind heparin (Fujimura et al., 1987). Heparin can competitively inhibit platelets from binding to VWF, thereby affecting platelet plug formation during heparin administration (Fujimura et al., 1987). Although the A3 domain is the major binding site for collagen,

the A1 domain has been shown to interact with collagen IV in the basement membrane as well (Sadler, 1998), but the role of this binding in vascular biology is not well described.

1.2.2.3 A2 domain

The A2 domain of VWF harbours the Tyr1605-Met1606 cleavage site for ADAMTS13 proteolysis (Gao et al., 2006). The crystal structure of the A2 domain has identified evolutionary adaptations in the structure of VWF that regulate its platelet capturing capacity in the presence of shear forces (Q. Zhang et al., 2009). Similar to the A1 domain, the A2 domain consists of multiple α-helices and β-sheets; however, the A2 domain contains a loop instead of an α4-helix, a poorly packed central β4-sheet, *cis*-proline, and a vicinal disulfide bond (Q. Zhang et al., 2009). In contrast, the proline found at similar positions in the A1 and A3 domains is *trans* (Q. Zhang et al., 2009). The *cis*-Pro1645 is thought to play an important regulatory role in A2 domain refolding (Q. Zhang et al., 2009). The vicinal disulfide bond at Cys1669-Cys1670 is hypothesized to stabilize the A2 domain fold (Crawley et al., 2011). Since the A2 domain lacks the long range N- and C- terminal disulfide bonds, which is present in both the A1 and A3 domains, it allows the A2 domain to be completely unfolded under shear forces (Figure 1.4A and 1.4B) (Springer, 2014). Another unique feature of the A2 domain is that it contains a calcium-binding loop in the α3-β4 loop, which protects against cleavage by ADAMTS13 by promoting rapid refolding of the domain (Xu & Springer, 2012; M. Zhou et al., 2011). The Tyr1605-Met1606 cleavage site for ADAMTS13 is buried in the hydrophobic core of the β4-sheet (Q. Zhang et al., 2009). The N-linked glycan at position Asn1574 plays an important role in stabilizing the A2 domain; thus, its removal would

increase the susceptibility of the A2 domain to proteolysis due to increased unfolding (Figure 1.4B) (Crawley et al., 2011). Under shear force, the unfolding of the A2 domain begins at the C terminus and proceeds through the β4-sheet, which contains the ADAMTS13 cleavage site (Figure 1.4C) (Sing & Alexander-Katz, 2010; Springer, 2014; Q. Zhang et al., 2009). Additionally, the unfolding kinetics of the A2 domain increases exponentially with shear force (Sing & Alexander-Katz, 2010; Springer, 2014). Therefore, VWF undergoes shear force regulated cleavage by ADAMTS13 and mutations can destabilize the A2 domain in VWD (Q. Zhang et al., 2009).

1.2.2.4 A3 domain

Upon vascular injury, the A3 domain facilitates the binding of VWF to the exposed subendothelial collagen (Sadler, 1998). Shear force is necessary for platelet GPIbα binding to the A1 domain and unrevealing of the A2 domain to reveal the cleavage site for ADAMTS13 mediated proteolysis of VWF (Q. Zhang et al., 2009). The A1 domain can assist with collagen binding; however, the A1 domain plays a minor role because the removal of the A3 domain significantly impairs the ability of VWF to bind to collagen (Lankof et al., 1996). The A3 domain shares structural homology with the A1 domain, and with the A2 domain to a lesser extent (Sadler, 1998; Q. Zhang et al., 2009). The crystal structure of the A3 domain identified a central hydrophobic parallel β-sheet surrounded by seven amphipathic α-helices in an open α/β sheet or dinucleotide binding conformation (Qu & Leahy, 1995). Similar to the A1 domain, the A3 domain is connected by N- and C- terminal Cys1686-Cys1872 at the base of the domain (Figure 1.4A) (Sadler, 1998). Site-directed mutagenesis studies identified residues Asp1742,

Ser1783, and His1786 as critical residues for facilitating the binding of collagen to the A3 domain (Romijn et al., 2001, 2003). Moreover, residues Ile1738, Thr1740, Val1760, and Glu1764 play an important role in binding collagen, as mutation of these residues result in a 10-fold reduction in binding affinity (Romijn et al., 2003). The A3 domain is proposed to interact with collagen sequences containing positively charged and hydrophobic residues (Romijn et al., 2003).

1.2.2.5 CTCK domain

The CTCK domain plays an important role in the dimerization of VWF, which is required for the formation of long multimers (Y. F. Zhou & Springer, 2014). The crystal structure of the CTCK dimer identified highly elongated monomers that form antiparallel dimers consisting of two β-ribbons and four intra-chain disulfides (Cys2724 to Cys2774; Cys2739 to Cys2788; Cys2750 to Cys2754; Cys2804 to Cys2806) (Y. F. Zhou & Springer, 2014). Dimerization forms a super β-sheet and 3 inter-chain disulfide bonds between monomers (Cys2771, Cys2773, and Cys2811) (Y. F. Zhou & Springer, 2014). The CTCK domains in each monomer flank the inter-chain disulfide bonds and the backbone of hydrogen bonds in the β-sheet, creating a rigid, cross-linked structure that is highly resistant towards hydrodynamic forces, which may contribute to the efficient transmission of force between monomeric subunits in the VWF multimer (Y. F. Zhou & Springer, 2014). Interestingly, the CTCK domains of VWF share homology to neurotrophin family of growth factors and are similar to transforming growth factor-β (Sadler, 1998). In summary, the dimerization of monomers occurs tail-to-tail through disulfide bonds in the endoplasmic reticulum, then the dimers are transported to the Golgi

apparatus for head-to-head multimerization, also through disulfide bonds (Sadler, 1998). VWF also undergoes further modifications, such as removal of the prodomain and glycosylation (Sadler, 1998). The end result is a long multimeric chain of VWF monomers that can effectively capture platelets (Sadler, 1998). Mutations in the CTCK domain may manifest in VWD, as mutations may impair dimerization of monomers (Y. F. Zhou & Springer, 2014).

The C-terminal domains of VWF play an important role in binding to ADAMTS13. More specifically, D4, C1-C6, and CK domains of VWF interact with the C-terminal domains of ADAMTS13 (TSP5-8 and CUB domains) (Crawley et al., 2011). These C-terminal domains of VWF allow ADAMTS13 to bind and form a complex, and circulate in plasma (Crawley et al., 2011). The formation of this complex is a critical step in the proteolysis of VWF by ADAMTS13 in circulation (Crawley et al., 2011).

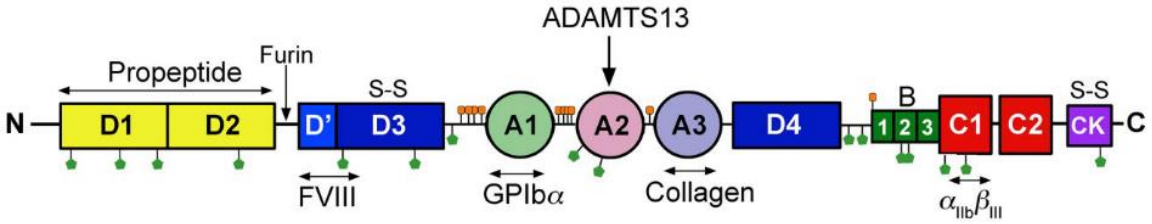

Figure 1.3. VWF domain organization. VWF is a multimeric protein composed of numerous repeating monomers. Dimerization of monomers occurs tail-to-tail at the CTCK domain through disulfide bonds in the endoplasmic reticulum. Dimers are transported to the Golgi apparatus for head-to-head multimerization through disulfide bonds at the N-terminal D assemblies. Further, modification and processing occurs, whereby VWF is N- (green lollipops) and O- (orange lollipops) glycosylated. Glycosylation is affected by ABO blood groups and plays an important role in synthesis, secretion, folding, and clearance of VWF. Another modification that occurs is the removal of the prodomain by furin. The D'D3 domains bind and transport FVIII to the site of vascular injury. The A1 domain captures platelets through GPIbα interactions, displays heparin binding, and serves as a minor binding site for collagen. The A2 domain harbours the Tyr1605-Met1606 cleavage site for proteolysis by ADAMTS13. The Tyr1605-Met1606 is buried deep within the A2 domain structure. Both A1 and A2 domains require shear force to induce a conformational change and to capture platelets (A1 domain) and reveal cleavage site for ADAMTS13 proteolysis (A2 domain). The A3 domain facilitates the binding of VWF to the exposed subendothelial collagen at the site of vascular injury. Source: Crawley et al., 2011

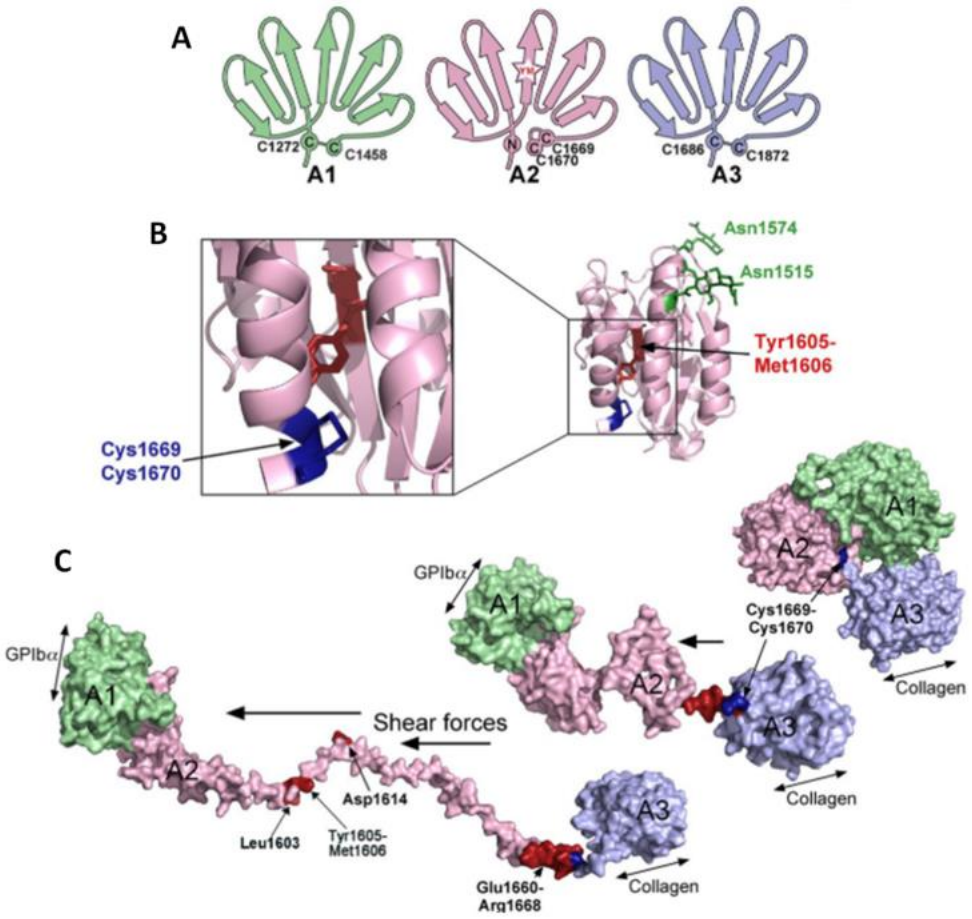
A
C1272
C1458
A1
C1669
C1670
A2
C1686
C1872
A3
B
Asn1574
Asn1515
Tyr1605-
Met1606
Cys1669
Cys1670
C
GPIbα
A1
A2
A3
Cys1669-
Cys1670
Collagen
Shear forces
Asp1614
Leu1603
Tyr1605-
Met1606
Glu1660-
Arg1668

Figure 1.4. Schematic representation of the A domains. A. The A1 and A3 domains are stabilized by N- and C-terminal disulfide bonds at the base of the domains. The A2 domain lacks the N- and C- terminal disulfide bond at the base of the domain. **B.** The A2 domain instead features a unique vicinal disulfide bond between Cys1669-Cys1670 that stabilizes the A2 fold and allows the A2 domain, thereby allowing the A2 domain to be completely elongated under shear forces for cleavage by ADAMTS13 at Tyr1605-Met1606. Residues Asn1515 and Asn1574 are N-glycosylated. Removal of N-glycan at Asn1574 increases susceptibility to proteolysis due to a conformational change that favours cleavage. **C.** Proteolysis of VWF by ADAMTS13 requires shear force that unravels the A2 domain revealing the previously hidden Tyr1605-Met1606 cleavage site. Resides Leu1603, Asp1614, and Glu1660-Arg1668 on VWF have been identified as important binding regions for ADAMTS13 exosite engagement. Source: Crawley et al., 2011

1.2.3 von Willebrand disease (VWD)

Dysfunction in VWF causes von Willebrand disease (VWD) characterized by defective platelet adhesion and aggregation (Leebeek & Eikenboom, 2016). VWD is a bleeding disorder that affects nearly 1% of the population and occurs with equal frequency among men and women (Berntorp et al., 2012; Leebeek & Eikenboom, 2016). However, symptoms of VWD are more likely to occur in women due to increased bleeding during menstrual periods, during pregnancy, and after childbirth (Kirtava et al., 2004). VWD can be subdivided into types 1, 2, and 3 (Berntorp et al., 2012; Leebeek & Eikenboom, 2016). Type 1 VWD accounts for approximately 70-80% of cases, and is characterized by a partial quantitative deficiency of VWF, caused mostly by missense mutations (Berntorp et al., 2012; Heijdra et al., 2017; Leebeek & Eikenboom, 2016).

Type 2 VWD accounts for approximately 20% of cases, and is characterized by normal to slightly reduced VWF concentration, but a reduced VWF function caused by missense mutations (Berntorp et al., 2012; Heijdra et al., 2017; Leebeek & Eikenboom, 2016). Type 2 VWD is further subdivided into types 2A, 2B, 2M, and 2N (Leebeek & Eikenboom, 2016). Type 2A is particularly pertinent to ADAMTS13. The formal definition of type 2A VWD is a loss of high molecular weight multimers (HMWM) with thrombocytopenia (Springer, 2014). There are two subtypes of type 2A VWD; Group 1 and Group 2:

Group 1 2A VWD: Lower distribution of multimers due to an impaired multimer assembly.

Group 2 2A VWD: Lower distribution of multimers because of accelerated cleavage.

Functional analysis has not yet been performed on all type 2A VWD mutations to determine their mechanism. However, mutations within the A2 domain are likely group 2, leading to destabilization of the A2 domain and accelerated degradation by ADAMTS13 at lower threshold of shear (Lynch et al., 2017). Mutations outside the A2 domain are likely group 1, due to impaired multimer assemble (Springer, 2014). Type 2B VWD can also lead to a loss of HMWM, but is caused by gain-of-function mutations in the A1 domain that enhance VWF binding to platelets and is associated with thrombocytopenia (Springer, 2014).

Type 3 VWD is the most severe and rare form of VWD accounting for less than 5% of cases (Heijdra et al., 2017). Type 3 VWF is characterized by the absence of VWF caused mostly by homozygous null mutations (Berntorp et al., 2012; Leebeek & Eikenboom, 2016). Table 1.1 provides an overview of VWD subtypes. The primary treatment for VWD is to normalize VWF and FVIII levels using desmopressin, or by Factor infusion (Leebeek & Eikenboom, 2016).

Table 1.1. Overview of VWD subtypes. Summary of each subtype of VWD including characteristics and percentage of cases that account for each subtype.

	Type 1	**Type 2**	**Type 3**
Characteristics	Quantitative	Qualitative	Quantitative
	- Reduced production/secretion - Increased clearance	- 4 Subtypes - Abnormalities in VWF	- Undetectable levels of VWF
Cases	70-80%	20%	<5%

1.3 ADAMTS protease family

The ADAMTS protease family belongs to the metzincin protease superfamily based on the conserved consensus catalytic motif containing three histidines that coordinate a zinc ion and a conserved methionine residue that provides a hydrophobic base for the zinc binding site (Gerhardt et al., 2007; Kelwick et al., 2015; Tallant et al., 2010). Moreover, the conserved methionine residue maintains the catalytic domain fold, an important determinant of substrate specificity (Gerhardt et al., 2007). The ADAMTS protease family consists of nineteen members that can be sub-grouped based on their known substrates, namely the aggrecanases or proteoglycanases (ADAMTS 1, 4, 5, 8, 9, 15, and 20), the procollagen N-propeptidases (ADAMTS 2, 3, and 14), the cartilage oligomeric matrix protein-cleaving enzymes (ADAMTS 7 and 12), the von Willebrand Factor protease (ADAMTS13), and a group of orphan enzymes with no known functions (ADAMTS 6, 10, 16, 17, 18, and 19) (Kelwick et al., 2015). Recent studies suggest that a dysfunction in members of the ADAMTS family plays a role in the pathogenesis of many diseases such as osteoarthritis (ADAMTS4 and ADAMTS5) (Tortorella et al., 2004), rheumatoid arthritis (ADAMTS7 and ADAMTS12) (Luan et al., 2008), and coronary artery disease (ADAMTS7) (Kessler et al., 2015). Table 1.2 provides an overview of the chromosomal position, major tissue expression locations, expression-inducing or repressing factors, substrates, and associated pathologies with each ADAMTS family member. The ADAMTS superfamily also consists of seven ADAMTS-like (ADAMTSL) members that participate with ADAMTS proteases in their biological processes, but are catalytically inactive and their functions are not well defined (Gao et al., 2012).

From an evolutionary perspective, the ADAMTS family can be traced back prior to the divergence of fish and mammals (Kelwick et al., 2015). For example, the sea urchin shares two genes with similarities to ADAMTS13, 16 ADAMTS genes in pufferfish, 17 genes in zebrafish, and all 19 genes in clawed frog (Kelwick et al., 2015). The diversification of the ADAMTS family during evolution likely occurred in parallel with the increased complexity of the extracellular matrix (Kelwick et al., 2015). All ADAMTS family members share a conserved domain organization: the N-terminal metalloproteinase catalytic domain responsible for proteolytic activity and the C-terminal ancillary domain(s) are responsible for facilitating substrate capture and orientation for substrate proteolysis (Figure 1.5) (Gao et al., 2012; Kelwick et al., 2015).

Although each ADAMTS protease recognizes its own specific substrate, they all employ similar cleavage mechanisms, whereby the Met-turn forms a hydrophobic pillow underneath the catalytic zinc (Gao et al., 2012; Kelwick et al., 2015). Together, the S1' specificity pocket forms a cleft into which substrates can be inserted and bind in a linear configuration (Kelwick et al., 2015). Once the substrate enters the active site cleft, a conserved glutamic acid within the zinc-binding motif is responsible for its proteolysis (Di Stasio et al., 2008; Kelwick et al., 2015). More specifically, nucleophilic attack of the catalytic solvent molecule (typically water molecule) is polarized by the glutamic acid and the zinc ion on the scissile peptide bond. (Di Stasio et al., 2008). The catalytic mechanism of MMPs consists of the Michaelis complex with the substrate comprised of the nucleophilic attack coordinated by the glutamic acid and zinc ion (Figure 1.6A) that results in the formation of a tetrahedral intermediate (Figure 1.6B), which collapses into

the final product complex (Figure 1.6C) (Tallant et al., 2010). Therefore, metalloproteases like ADAMTS13 support peptide bond hydrolysis through complex organic chemistry mechanisms. Proteases must therefore evolve complex specificity characteristics to control the timing and location of these catalytic events in order to participate in biological processes such as hemostasis.

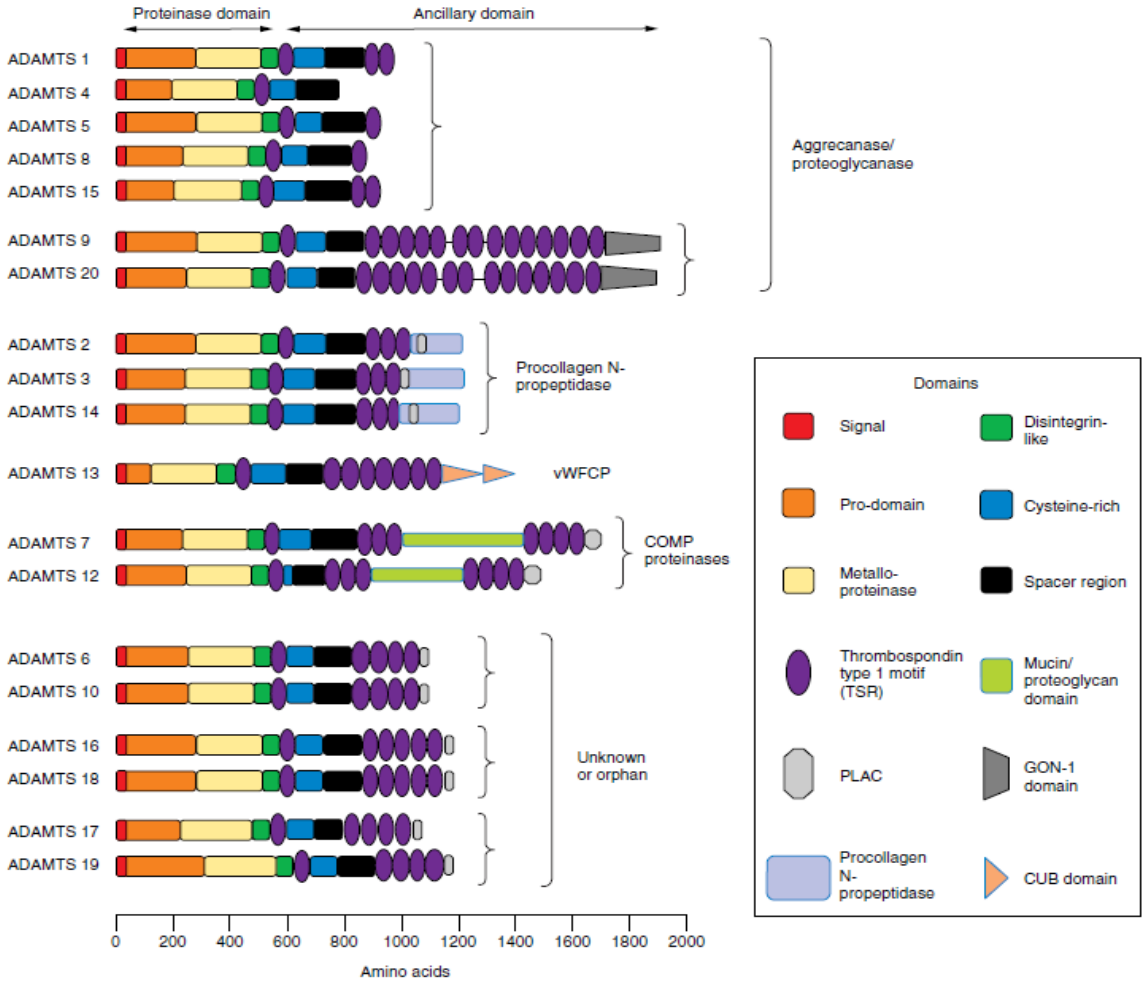

Figure 1.5. Domain organization of the ADAMTS family. All members of the ADAMTS family share the same N-terminal domain organization (MDTCS); however, they vary in their C-terminal ancillary domains. ADAMTS13 is the only member to feature CUB domains. Source: Kelwick et al., Genome Biology (2015).

Table 1.2. Characteristics of all known ADAMTS members. Overview of the chromosomal position, expression, factors inducing or repressing expression (repression shown in brackets), substrate, and pathology association of each member of the ADAMTS family. ADAMTS13 is highlighted in yellow. Adapted from: Kelwick et al., Genome Biology (2015).

Member	Chromos-omal Position	Expression	Factors inducing or (repressing) expression	Substrate(s)	Pathology association
ADAMTS1	21q21	Ovary, bronchial epithelial cells, fetal lung, placenta, fetal lung, placenta, smooth muscle, uterus, adrenal cortex, adipocyte, ciliary ganaglion, prostate, olfactory bulb, breast stromal fibroblasts, and myoepithelial cells	Progesterone, Brg1, IL-1, S100A8, S100A9, TNFα	Aggrecan, versican syndecan 4, TFPI-2, semaphoring 3C, mac02, gelatin, amphiregulin, TFG-α, heparin-binding EGF	Cancer, anti-angiogenic
ADAMTS2	5q35	Adipoctye, skeletal muscle, superior cervical ganglion, uterus, placenta, heart, liver, lung, tongue, smooth muscle, breast stromal fibroblasts	Glucocorticoids (in monocytes), IL-6	Fibrillar procollagens types I-III and V	Ehlers-Danlos syndrome type VIIc
ADAMTS3	4q21	CD105+ endothelial cells, CD34 cells, pineal gland, cartilage, bone, skeletal muscle, tendon, breast myoepithelial cells		Fibrillar procollagen tyoe II biglycan	
ADAMTS4	1q23	Ovary, spinal cord, adrenal cortex ciliary ganglion, trigeminal ganglion, brain, retina, pancreas (islets), fetal lung, breast myoepithelial cells	IL-1 + oncostatin M, TNF-α, S100A8, S100A9, leptin, IL-6 (HDAC inhibits, pentosan polysulfate)	Aggrecan, versican, reelin, biglycan, brevican, matrilin-3, A2M, COMP	Arthritis
ADAMTS5	21q21	Adipocyte, uterus, breast myoepithelial cells	IL-1, TNFα, S100A8, S100A9, leptin, IL-6	Aggrecan, versican, reelin, bigylcan, matrillin-4, brevican, A2M	Arthritis, cancer
ADAMTS6	5q12	Superior cervical ganglioin, trigeminal ganglion, appendix, heart, breast myoepithelial cells	TNFα		
ADAMTS7	5q24	Trigeminal ganglion, adrenal cortex, liver, heart, skeletal muscle, intervertebral disc, breast stromal fibroblasts	PTHrP (miR-29a/b)	COMP	Coronary artery disease (smooth muscle cell migration)
ADAMTS8	11q24	Skeletal muscle, heart, liver, superior cervical ganglion, adrenal cortex, breast stromal fibroblasts and luminal epithelial cells		Aggrecan	
ADAMTS9	3p14	Dorsal root ganglion, breast myoepithelial cells	TNFα, IL1 + oncostatin M,leptin (HDAC inhibitors)	Aggrecan, versican	Cancer
ADAMTS10	19p13	CD8+ T-cells, brain, uterus, breast stromal fibroblasts		Fibrillin-1	Weill-Marchesani syndrome
ADAMTS12	5p13	Liver, bone marrow, atrioventricular node, intervertebral		COMP	Cancer

		disc, breast stromal fibroblasts and myoepithelial cells			
ADAMTS13	9q34	Liver, CD71+ early erythroid cells, lung, thyroid, breast myoepithelial cells, platelets, cultured endothelial cells, glomerular podocytes, and astrocytes	(IL-3)	VWF	TTP
ADAMTS14	10q22	Thalamus, bone marrow, fetal thyroid, adipocyte, cerebellum, bone, skin, fibroblasts, breast myoepithelial and luminal epithelial cells		Fibrillar procollagen type I (pNα1 and pNα2 chains)	
ADAMTS15	11q24	Colon, brain, heart, uterus, muscloskeletal system, breast myoepithelial cells		Aggrecan, versican	Cancer
ADAMTS16	5p15	Follicle stimulating hormone, forskolin, transcription factors, Wilm's tumor-1, EGR-1, Sp1			Hypertension
ADAMTS17	15q26	Breast myoepithelial cells			Weill-Marchesani-like syndrome
ADAMTS18	16q23	Ciliary ganglion, heart, skin, brain, breast myoepithelial cells			
ADAMTS19	5q23	Dorsal root ganglion, breast myoepithelial cells			
ADAMTS20	2q12	Brain, appendix, heart, liver, skeletal muscle, pituitary, trigeminal ganglion, breast myoepithelial cells		Versican	

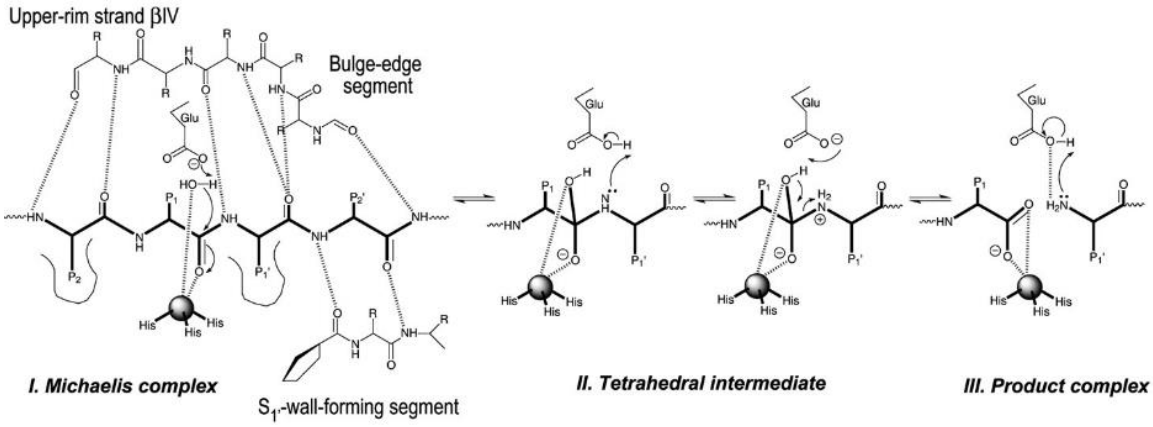

Figure 1.6. The proteolytic mechanism of Metzincin metalloproteases. A. Michaelis complex (step I) formed with the substrate, comprised of the nucleophilic attack coordinated by the glutamic acid and zinc ion. **B.** Tetrahedral intermediate (step II). **C.** Product complex (step III). Source: Tallant et al., Biochimica et Biophysica Acta (2010).

1.4 ADAMTS13 and its discovery

In 1924, Eli Moschcowitz first reported a 16 year old girl with a sudden onset of fever and hemolytic anemia, followed by death (Moschcowitz, 1925). This was the first time the disease thrombotic thrombocytopenia purpura (TTP) was described (Levy et al., 2015). For a long time, the pathophysiology of TTP remained unknown until 2001, when a genome-wide linkage analysis was performed in four TTP pedigrees, thereby localizing the responsible gene to chromosome 9q34 (Levy et al., 2001). Further investigation of this region identified mutations in a novel member of the ADAMTS family, ADAMTS13 (or formally known as the VWF-cleaving protease) (Levy et al., 2001). Today, ADAMTS13 is understood to be an important protease that maintains an appropriate size of VWF to maximize its platelet capturing capacity, and a deficiency in ADAMTS13 is responsible for TTP (Sadler, 2008). The interaction between ADAMTS13 and VWF is one small part of a larger and more complex hemostatic system that maintains the crucial balance between bleeding and thrombosis.

1.4.1 Synthesis and secretion of ADAMTS13

In situ hybridization, immunochemistry, and northern blot analysis of ADAMTS13 mRNA revealed that ADAMTS13 is predominately expressed in the liver and secreted from hepatic stellate cells (Uemura et al., 2005, 2010). More recently, ADAMTS13 has been found in platelets, cultured endothelial cells, and glomerular podocytes, but to a lesser extent (De Groot et al., 2010). ADAMTS13 has also been found in the brain, particularly astrocytes (Demircan et al., 2013; Khan et al., 2012). Here, ADAMTS13 might play an important role in protecting the brain from ischemic injury

(Demircan et al., 2013; Khan et al., 2012). Clinical studies in children suffering from advanced cirrhotic biliary atresia, whereby the bile becomes trapped and damages the liver, showed very low ADAMTS13 activity (De Groot et al., 2010; Uemura et al., 2010). In these children, ADAMTS13 activity was fully restored with a liver transplant (De Groot et al., 2010; Uemura et al., 2010). Overall, the liver is primarily responsible for producing ADAMTS13 (Uemura et al., 2010). ADAMTS13 is constitutively secreted as an active protease at a plasma concentration of approximately 1 μg/mL (Gao et al., 2006; Muia et al., 2014; Soejima et al., 2006; South et al., 2016). ADAMTS13 has a number of unique properties for a circulating protease:

1. ADAMTS13 is constitutively secreted as an active protease (Gao et al., 2006; South et al., 2016).
2. Relative to other coagulation and ADAMTS proteases, ADAMTS13 has a prolonged circulating half-life (two to four days), due in part to a lack of physiological inhibitors (Furlan et al., 1999; Scully et al., 2017).
3. The only known substrate of ADAMTS13 is VWF, and this protease displays no known off-target proteolysis (Gao et al., 2006; South et al., 2016).

These special properties separate ADAMTS13 from the other members of the ADAMTS protease family and may help explain why ADAMTS13 is resistant to natural protease inhibitors.

1.4.2 ADAMTS13 structure and function

Similar to the other members of the ADAMTS family, ADAMTS13 shares the same N-terminal MDTCS domain organization, but varies in its C-terminal domain organization (Gao et al., 2012). In particular, the N-terminus performs proteolytic activity, whereas the C-terminus variation directs substrate specificity and perhaps protease regulation (Kelwick et al., 2015; Zander et al., 2015). ADAMTS13 is a special member within the ADAMTS family, and is the only member involved in hemostasis (Kelwick et al., 2015); however, recent literature suggests that ADAMTS7 may play a role in smooth muscle migration in atherosclerosis (Kessler et al., 2015). In contrast, other ADAMTS proteases are broadly involved in matrix and cartilage homeostasis (Kelwick et al., 2015). Understanding the structure and role of each domain of ADAMTS13 is essential to understanding how ADAMTS13 is regulated, functions, and interacts with its substrate, VWF. ADAMTS13 consists of the following domains: Metalloprotease domain (M) (proteolytic site), disintegrin-like domain (D), thrombospondin type 1 (T1), cysteine-rich domain (C), spacer domain (S), seven additional thrombospondin type 1 repeats (T2-T8), and Complement components C1r/C1s, Uegf and bone morphogenic protein 1 domains (CUB1-CUB2) (Figure 1.7). Each individual domain of ADAMTS13 will be discussed in further detail below.

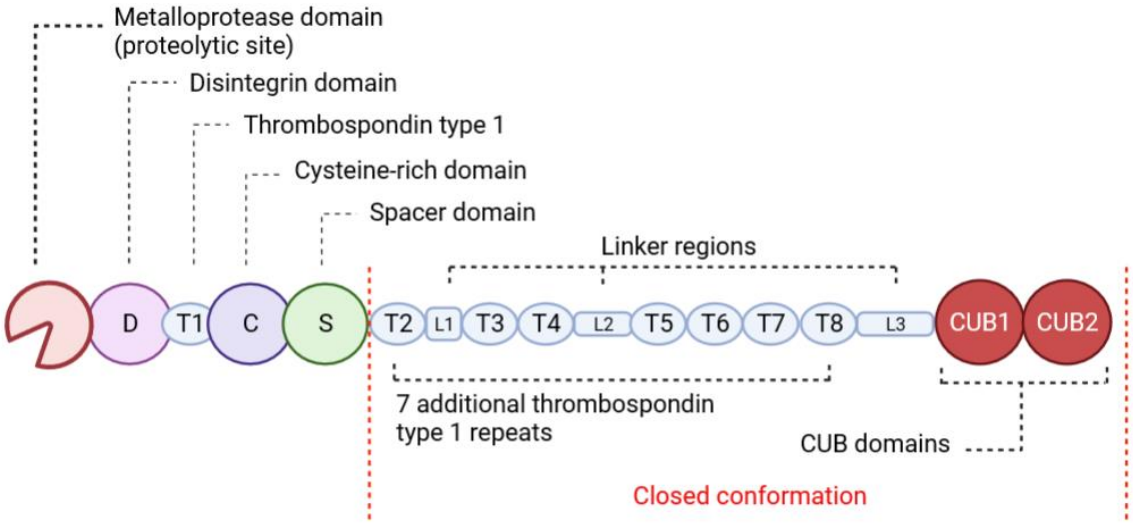

Figure 1.7 Structural organization of ADAMTS13. Metalloprotease domain (M) contains the proteolytic site, domains DTCS are important exosites for VWF binding, and T2-CUB2 comprise the closed conformation (red). CUB1-CUB2 anchor ADAMTS13 to VWF in circulation. Linker region between T2-T3, T4-T5, and T8-CUB1.

1.4.2.1 Metalloprotease domain (*M*DTCST2-T8CUB1CUB2)

ADAMTS proteases possess a propeptide preceding the metalloprotease domain (Kelwick et al., 2015; Zander et al., 2015). This propeptide functions as a molecular chaperone, and maintains latency of the newly-synthesized protease (Majerus et al., 2003; Zander et al., 2015; Zheng, 2013). The propeptide of ADAMTS13 is much smaller than in other ADAMTS proteases, and does not maintain protease latency (Majerus et al., 2003; Zheng, 2013). Mutagenesis studies that prevented the removal of the propeptide found that ADAMTS13 maintained normal VWF cleaving activity (Majerus et al., 2003). In addition, mutant forms of ADAMTS13 lacking the propeptide altogether were synthesized and secreted normally (Majerus et al., 2003). Therefore, the function of the propeptide in ADAMTS13 is currently unknown, and is likely a vestigial feature of its evolutionary history.

The metalloprotease domain contains the consensus HEXXHXBG(/N/S)BXHD catalytic motif, whereby B represents a large non-polar residue, and three histidine residues coordinate a zinc ion (Kelwick et al., 2015). Further, 14-20 residues downstream of the last histidine in the catalytic motif is a conserved methionine, defined as the "Met-turn" (Kelwick et al., 2015). This Met-turn creates a tight turn important to the structure of all metzincin metalloproteases (Kelwick et al., 2015; Zander et al., 2015). Moreover, the Met-turn provides a hydrophobic base beneath the zinc ion, which maintains the catalytic fold (Kelwick et al., 2015; Zander et al., 2015). Within the conserved zinc-binding sequence, a water molecule is polarized by Glu225 (Di Stasio et al., 2008). The resulting hydroxide molecule is hypothesized to perform a nucleophilic attack on the

backbone carbonyl group between Tyr1605-Met1606 on VWF, causing hydrolysis of the scissile bond (Di Stasio et al., 2008; Zander et al., 2015). In summary, the active site of ADAMTS13 is formed by a highly conserved 3xHis (His224, His228, and His234) zinc-binding motif, and a catalytic Glu225 (Petri et al., 2019). The S1 and S1' pockets on either side of the active site of ADAMTS13 specifically accommodate the P1 (Tyr1605) and P1' (Met1606) residues of VWF (Petri et al., 2019; South et al., 2014). In addition to the conserved catalytic site and methionine, there is also a conserved cysteine of unknown function (Zander et al., 2015). Within the metalloprotease domain, ADAMTS13 shares 29% sequence similarity with ADAMTS1 and ADAMTS5, and 33% with ADAMTS4 (Petri et al., 2019). Mutations in these regions result in reduced or no proteolytic activity (Petri et al., 2019; Zander et al., 2015).

Furthermore, ADAMTS13 contains three calcium ions important for the structural integrity. A single calcium ion is bound to the Arg180-Arg193 loop coordinated by Asp182 and Glu212, and is adjacent to the active site (Figure 1.8A). The calcium-binding loop is hypothesized to fold across the active site cleft and occlude the S1' pocket (Petri et al., 2019). Mutagenesis of the calcium-binding loop revealed significant reduction in proteolytic activity (Gardner et al., 2009). This finding suggested that the calcium-binding loop contributes to the structural integrity of the active site (Gardner et al., 2009). The remaining two calcium ions are bound in a double calcium-binding site, which stabilize another loop that connects the metalloprotease and disintegrin domains (Petri et al., 2019). Recently, it has been shown that ADAMTS13 exhibits what is defined as a "gatekeeper triad" consisting of Arg193, Asp217, and Asp252 (Figure 1.8B) (Petri et

al., 2019). The calcium-binding loop incorporates residue Arg193 (Petri et al., 2019). The ionic interaction between these three residues is suggested to block the active-site cleft and occlude the S1’ pocket, thereby maintaining a “latent” conformation (Petri et al., 2019). No other ADAMTS protease family member has been identified to have a gatekeeper triad, and the potential contribution of this feature to the regulation of ADAMTS13 is not known.

A.

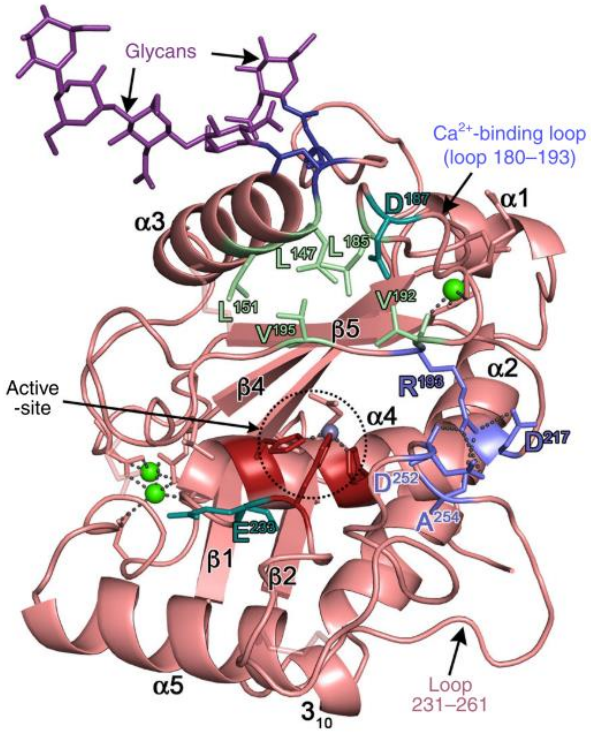
Glycans
Ca2+-binding loop
(loop 180–193)
α1
α3
D167
L147
L185
V192
L151
V195
β5
α2
R193
β4
Active
-site
α4
D217
D252
A254
E225
β1
β2
α5
Loop
231–261
310

B.

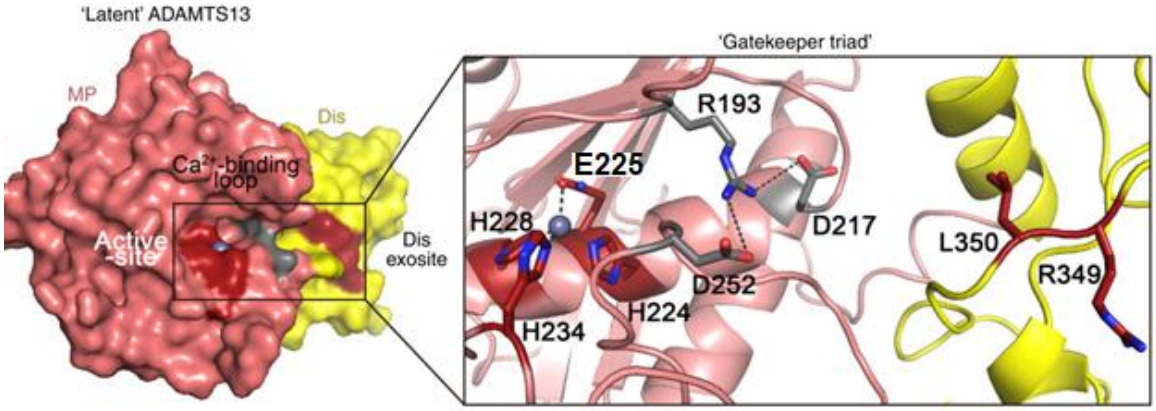
'Latent' ADAMTS13
MP
Dis
Ca2+-binding loop
Active -site
Dis exosite
'Gatekeeper triad'
R193
E225
H228
D217
D252
H224
H234
L350
R349

Figure 1.8. Metalloprotease domain calcium-binding loop and gatekeeper triad. A. The calcium-binding loop from Arg180-Arg193 is hypothesized to fold across the active site cleft and block the S1' pocket. The calcium-binding loop is coordinated by Asp182 and Glu212, and contributes to the structural integrity of the active site. Two other calcium ions are bound to a double calcium-binding site, which stabilize the loop that connects the metalloprotease and disintegrin domains (green spheres: calcium ions; grey sphere: zinc ion, purple: gatekeeper triad). **B.** Ionic interaction between Arg193 (a part of calcium-binding loop), Asp217, and Asp252 form the "gatekeeper triad". This ionic interaction is hypothesized to restrict access to the active-site cleft of ADAMTS13. This includes the S1' pocket, and the passage between the active-site and disintegrin domain (gatekeeper triad – shown in grey, active-site and disintegrin domain – shown in red). Active site composed of 3xHis (His224, His228, and His234), zinc-binding motif, and a catalytic E225 residue. Source: Petri et al., Nat Comm (2019).

1.4.2.2 Disintegrin domain (M*D*TCST2-T8CUB1CUB2)

The metalloprotease domain on its own lacks the ability to bind with specificity and cleave the Tyr1605-Met1606 cleavage site of VWF (Zander et al., 2015). The non-catalytic domains of ADAMTS13 provide the essential substrate specificity (Zander et al., 2015). The addition of the relatively short disintegrin domain (77 residues) to the metalloprotease domain restored partial substrate binding specificity and proteolytic activity (Ai et al., 2005). However, the overall proteolytic activity remained significantly reduced compared to full length ADAMTS13, suggesting that the remaining domains play an important role in substrate specificity (Ai et al., 2005). Within the disintegrin domain, Leu350 and Val352 interact in a hydrophobic manner with Ala1612 on VWF, and an ionic interaction occurs between Arg349 in the disintegrin domain and Asp1614 on VWF (Akiyama et al., 2009; Apte, 2004; De Groot et al., 2009). Mutations induced at positions Arg349, Leu350, or Val352, significantly reduce the catalytic efficiency of ADAMTS13 (De Groot et al., 2009). The crystal structure of the disintegrin domain reveals two anti-parallel β-sheets, a single N-terminal α-helix, and four disulfide bridges, which maintain the domain structure (Akiyama et al., 2009). Further, Ala276-Tyr305 loop connects the disintegrin and metalloprotease domains, which are stabilized by β-sheets and the two calcium-binding sites (Petri et al., 2019). In addition, Cys322-Cys347 is well conserved through the ADAMTS family, and may provide structural integrity of the domain (Zander et al., 2015). In summary, the disintegrin domain is a critical exosite that helps position the scissile bond for proteolysis.

1.4.2.3 TSP-1, cysteine-rich domain, spacer domain (MD*TCS*T2-T8CUB1CUB2)

The –TCS domains are essential exosites that allow for tight binding of ADAMTS13 to VWF, and are necessary for ADAMTS13 to have an effective catalytic efficiency (Zander et al., 2015). In addition, the exosite binding of –TCS domains stabilize the shear-unfolded A2 domain, preventing refolding (Feys et al., 2009). Therefore, stabilization of the shear-folded A2 domain by exosite binding, allows for sufficient time for the active site to cleave the scissile bond of VWF (Feys et al., 2009).

Proceeding the disintegrin domain is the thrombospondin type-1 repeat (T). The T domain is well conserved among the ADAMTS family (Zander et al., 2015), and consists of two β-sheets, is capped by disulfide bonds on both ends (Akiyama et al., 2009; Gao et al., 2012). Currently, no precise or unique function has been described for the T domain.

Adjacent to the T domain is the cysteine-rich domain (C). Despite sharing a low sequence similarity with the disintegrin domain (17%), the cysteine-rich domain consists of two anti-parallel β-sheets, a short α-helix, and is stabilized by six disulfide bonds similar to the disintegrin domain (Zander et al., 2015). Within the cysteine-rich domain, residues Gly471-Val474 form a hydrophobic pocket that interacts with hydrophobic VWF residues Ile1642, Trp1644, Ile1648, Leu1650, and Ile1651 (De Groot et al., 2015; Zander et al., 2015). The absence of these hydrophobic interactions have been suggested to result in a 75-to-200-fold decrease in proteolysis (De Groot et al., 2015). Therefore, these regions bind in a complementary manner that directly enhances the efficiency of proteolysis (De Groot et al., 2015).

The last domain of the –TCS region is the spacer domain (S). The spacer domain has the highest binding affinity to the unfolded A2 domain of VWF (Zander et al., 2015). Residues Leu621-Asp632 in the spacer domain form a loop that interacts with the proximal portion of the cysteine-rich domain (Akiyama et al., 2009). Both the cysteine-rich and spacer domains have been suggested to function closely and similarly to each other (Zander et al., 2015). The spacer domain is composed of 10 β-sheets that collectively form a jelly roll fold, creating a hydrophobic cluster that is surrounded by positively charged arginine residues (Akiyama et al., 2009; Zander et al., 2015).

With respect to VWF, this region of the spacer domain interacts with Asp1596-Arg1659 (Akiyama et al., 2009). Studies examining the interaction between the spacer domain and VWF have found that a removal of the spacer domain results in a 50-fold increase in K_D towards the A2 domain of VWF (VWF73), and a 20-fold decrease in overall proteolytic efficiency (k_{cat}/K_m) (Ai et al., 2005; Gao et al., 2006). Further, it has been shown that Arg660, Tyr661, and Try665 collectively are critical for VWF binding and cleavage, and are commonly found in the epitope site of ADAMTS13 antibodies (Jin et al., 2010; Pos et al., 2010).

1.4.2.4 TSP-1 repeats and CUB domains (MDTCS*T2-T8CUB1CUB2*)

In the distal regions preceding the spacer domain, more variations exist between ADAMTS proteases (Kelwick et al., 2015). ADAMTS13 is composed of seven consecutive thrombospondin type-1 repeats followed by two additional CUB domains. The number of thrombospondin type-1 repeats varies among ADAMTS proteases, and ADAMTS13 is the only member to exhibit CUB domains (Kelwick et al., 2015). The

crystal structure of the CUB domains has identified that both domains exhibit a jelly roll fold consisting of approximately 110 residues in antiparallel stranded β-sheets, characteristic of a β-sandwich structure (Kim et al., 2021). Further, the crystal structure revealed that the CUB domains of ADAMTS13 lack calcium-binding, and feature N-linked glycans (Kim et al., 2021). These unique features suggest that the function of the CUB domains in ADAMTS13 is different from other tandem CUB domains (Kim et al., 2021). The crystal structure also identified CUB P1 and P2 pockets, which are situated at the interface of CUB1 and CUB2, and between the residues that interact with the spacer domain (Kim et al., 2021).

Studies have shown that these C-terminal regions are essential for binding to globular VWF and to VWF under flowing conditions (Muia et al., 2014; South et al., 2014; Zanardelli et al., 2009). Interestingly, MDTCS truncation, which lacks thrombospondin type-1 repeats and CUB domains cleaves VWF substrates (i.e. VWF73) a with 2-fold greater efficiency than full-length ADAMTS13, with k_{cat}/K_m values of 2.0±0.60 μM x s^{-1} and 0.75±0.16 μM x $s^{-1,}$ respectively (Gao et al., 2006). However, mice lacking the CUB domains were less efficient at cleaving VWF in flow devices than ADAMTS13 derived from mice that contained the CUB domains (Banno et al., 2009). Electron microscopy images of ADAMTS13 show that N-terminal regions fold inwards, suggesting that when ADAMTS13 is not bound to VWF, the thrombospondin type-1 repeats T2-T8 fold the CUB domains toward the spacer domain (Muia et al., 2014; South et al., 2014). This conformation is termed “closed conformation”, resulting in auto-inhibition and global latency of ADAMTS13 (Figure 1.9) (Kim et al., 2021; South et al.,

2014). Linker regions exist between T2-T3, T4-T5, and T8-CUB, which provide the necessary flexibility to the TSP-1 repeats in the tail allowing ADAMTS13 to adopt the closed conformation (Figure 1.9) (Deforche et al., 2015). The closed conformation is stabilized by ionic and hydrophobic interactions between spacer and CUB domains (Figure 1.10A and Figure 1.10B) (Kim et al., 2021). The proposed interactions between spacer and CUB domains occur between the following residues:

- Ionic interactions: spacer residues Glu634 and Asp635 with CUB1 residues Lys1252 and Arg1272 (Kim et al., 2021).
- Hydrophobic interactions: spacer residues Leu591, Phe592, and Leu637 with CUB1 residues Trp1245, Leu1248, and Trp1250 (Kim et al., 2021).
- Spacer loop Arg660-Try665 forms an ionic interaction with the pocket formed by Arg1326, Arg1361, Glu1387, and Glu1389 in CUB2 (Kim et al., 2021). Spacer residue Try665 forms a cation-Pi interaction with CUB2 residue Arg1326 (Kim et al., 2021). Spacer residue Arg568 forms a salt bridge with CUB2 residue Glu1389 (Kim et al., 2021).

The closed conformation is relieved when distal C-terminal domains of ADAMTS13 interact with the distal domains of VWF (D4-CK), resulting in exposure of the spacer domain, which in turn engages the A2 domain of VWF (South et al., 2014). There are five thiol groups with thrombospondin type-1 repeats T2-T8 and a CUB-1 domain, which form disulfide interactions between ADAMTS13 and VWF, and anchors ADAMTS13 to VWF; however, this mechanism is not well understood (Zander et al.,

2015). Nevertheless, the C-terminal domains may be crucial for recognition and cleavage of VWF under arterial flow (P. Zhang et al., 2007).

Interestingly, the binding site for the CUB – spacer domain interaction has also been shown to be targeted by autoinhibitory antibodies in majority of patients (>90%) with immune TTP (Roose et al., 2018). An antibody against the spacer domain has shown to induce a conformational change in the metalloprotease domain that affects the k_{cat} of VWF cleavage, and not a K_m effect (Schelpe et al., 2020). This suggests that the closed conformation may induce some sort of long range allostery that regulates ADAMTS13 activity (Schelpe et al., 2020). In addition, the closed conformation may sterically restrict the access to the active site cleft of ADAMTS13 (Kretz et al., 2015). ADAMTS13 is the only known member of the ADAMTS family to display global latency as a result of the closed conformation (Kim et al., 2021). Therefore, the CUB-spacer domain interaction plays an important role in ADAMTS13 function and TTP pathogenesis.

In summary, the N-terminal domains of ADAMTS proteases are fairly conserved throughout the family, whereas the C-terminal domains display more variation (Kelwick et al., 2015). ADAMTS13 circulates as an active protease in a “closed conformation”, whereby the distal CUB domains interact with the proximal spacer domain (Muia et al., 2014; South et al., 2014). This “folding inwards” is described as the closed conformation and causes global latency of ADAMTS13, and is a target for autoinhibitory antibodies in patients with immune TTP (Kim et al., 2021; Roose et al., 2018). In the presence of VWF, the closed conformation is relieved, which is important under arterial conditions (Crawley et al., 2011). The metalloprotease domain contains the catalytic site, whereas

the proceeding domains are critical exosites that recognize and bind to VWF, anchoring ADAMTS13 to its substrate for proteolysis (Akiyama et al., 2009; Crawley et al., 2011; Zander et al., 2015). The metalloprotease domain features a unique "gatekeeper triad" that may resist access to the catalytic site of ADAMTS13 (Petri et al., 2019). Understanding the structure and conformation of ADAMTS13 may provide important insight into how ADAMTS13 is regulated and protected from protease inhibitors, and TTP pathogenesis.

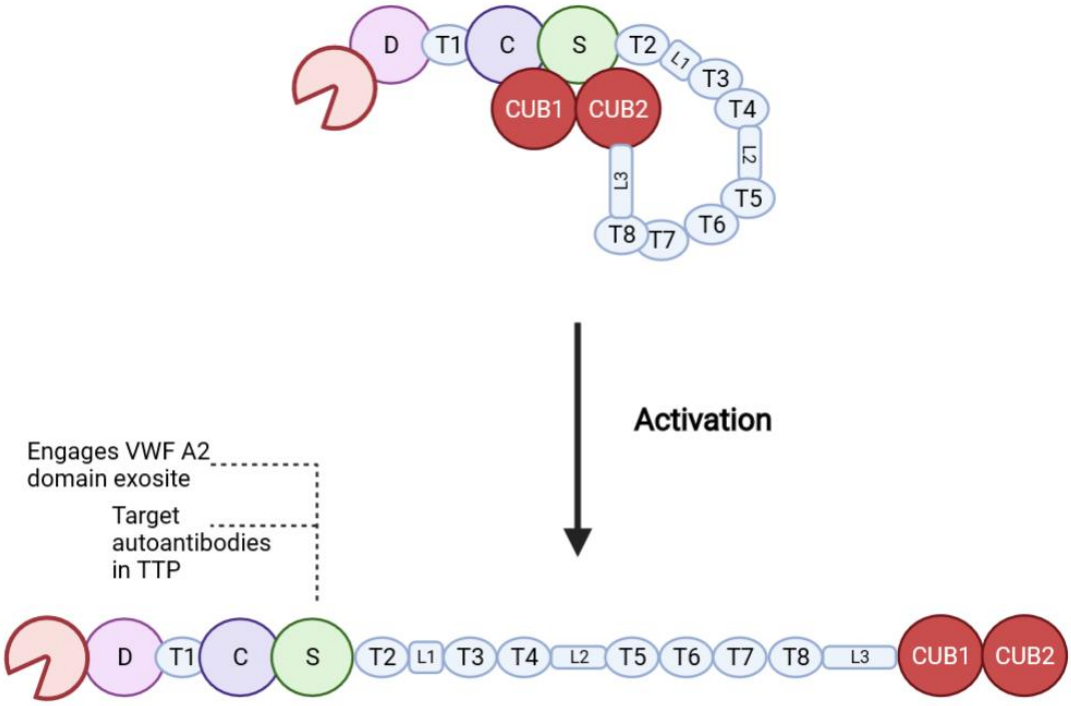

Figure 1.9. ADAMTS13 conformational activation schematic. In circulation, the CUB domains (CUB1-CUB2) bind to the spacer domain (S) resulting in auto-inhibition. Linker regions help explain the flexibility of the TSP-1 repeats (T domains). Activation occurs when distal C-terminal domains interact with the distal domains of VWF (D4-CK) resulting in the exposure of the spacer domain, which in turn engages the A2 domain of VWF. The spacer domain at sites of CUB interaction is a target for autoinhibitory antibodies in acquired TTP.

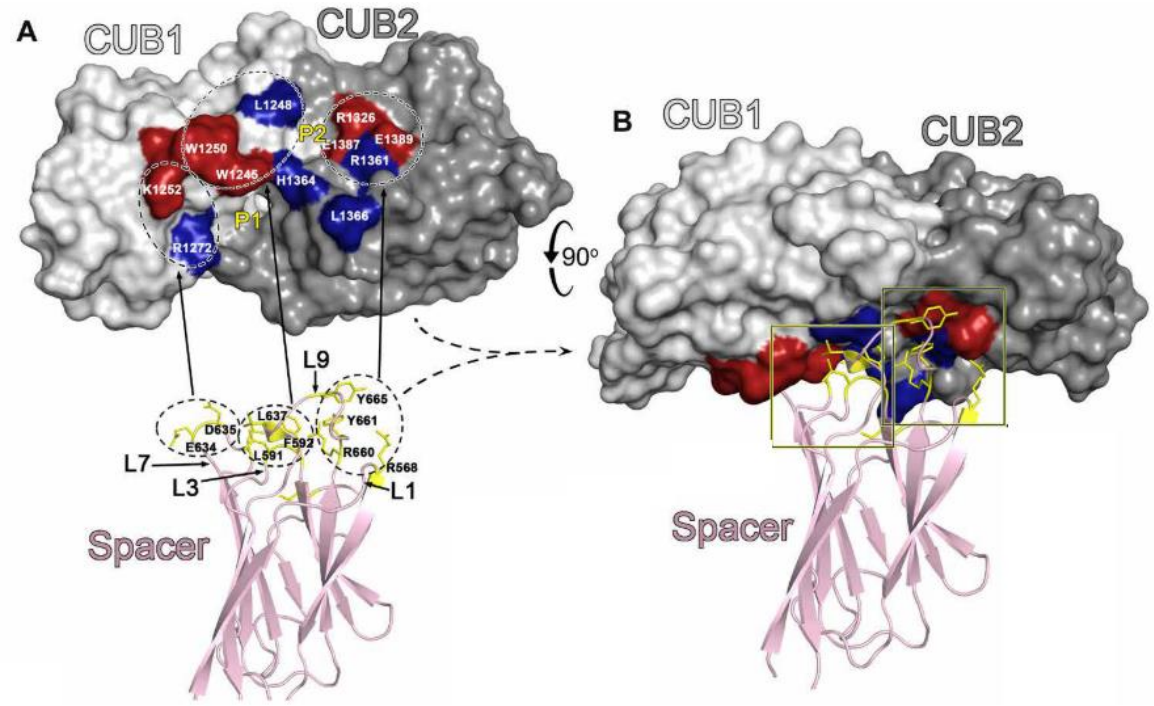
A
CUB1
CUB2
L1248
R1326
P2
E1389
W1250
E1387
R1361
W1245
H1364
K1252
P1
L1366
R1272
90°
B
CUB1
CUB2
L9
Y665
D635
L637
Y661
E634
E592
R660
L591
R568
L7
L3
L1
Spacer
Spacer

Figure 1.10. Interaction of spacer-CUB domains. A. The closed conformation of ADAMTS13 is due to ionic and hydrophobic interactions occurring between the spacer and CUB domains. Spacer residues Glu634 and Asp635 ionically interact with CUB1 residues Lys1252 and Arg1272. Hydrophobic interactions occur between spacer residues Leu591, Phe592, and Leu637 with CUB1 residues Trp1245, Leu1248, and Trp1250. The spacer loop Arg660-Try665 forms an ionic interaction with the pocket formed by Arg1326, Arg1361, Glu1387, and Glu1389 in CUB2. Moreover, spacer residue Try665 forms a cation-Pi interaction with CUB2 residue Arg1326. In addition, spacer residue Arg568 forms a salt bridge with CUB2 residue Glu1389. The P1 and P2 pockets are situated at the interface between CUB1 and CUB2. Red shows the function analysis, blue shoes the residues predicted from the refined ClusPro docking simulation. **B.** Docking model of the spacer-CUB interaction. Source: Kim et al., Science Advances (2021).

1.4.3 Global and local conformational latency

Enzymatic latency prevents proteolytic activity until conditions favour proteolysis, such as proteolytic activation (removal of prodomain), enzyme allostery, and/or activating cofactors (Kim et al., 2021). In contrast to metzincin and coagulation proteases, ADAMTS13 lacks a functional prodomain and does not require on-demand proteolytic activation, respectively (Kim et al., 2021; Majerus et al., 2003). Instead, ADAMTS13 is hypothesized to be activated allosterically by its substrate, VWF (Kim et al., 2021). Recently, the spatial and temporal regulation of ADAMTS13 has been proposed to occur by two distinct latency mechanisms: global latency and local latency (Kim et al., 2021). Global latency is conferred by the closed conformation, whereby the CUB domains interact with the spacer domain (Kim et al., 2021). The interaction between the spacer-CUB domains maintains ADAMTS13 in a compact conformation, restricts access to essential exosites, and may influence the conformation of the metalloprotease domain (Kim et al., 2021). Local latency is conferred by the metalloprotease domain, whereby the ionic interactions of the gatekeeper triad residues have been proposed to restrict access to the active site cleft (Kim et al., 2021; Petri et al., 2019). However, the exact mechanism by which the active site accessibility remains restricted is unknown. In circulation, ADAMTS13 latency may help to prevent off-target proteolysis (Kim et al., 2021). Further, activation from its latent state only occurs when ADAMTS13 interacts directly with VWF (Kim et al., 2021). The interaction between the CUB domains of ADAMTS13 and D4 domain of VWF is considered the first step in the proteolysis of VWF (Crawley et al., 2011; Kim et al., 2021). This interaction is shear-independent and

overcomes the global latency (Crawley et al., 2011; Kim et al., 2021). Next, high affinity exosite binding between the MDTCS domains of ADAMTS13 and the unravelled A2 domain of VWF occurs, thereby resulting in the final proteolysis of VWF (Crawley et al., 2011; Kim et al., 2021). This interaction is shear-dependent, and overcomes the local latency (Crawley et al., 2011; Kim et al., 2021). After cleavage of the scissile bond, the rheological shear forces have been proposed to no longer affect the cleaved A2 domain of VWF, thereby resulting in its dissociation from ADAMTS13 (Kim et al., 2021). Therefore, ADAMTS13 has been proposed to return to its globally latent and locally latent conformation (Kim et al., 2021). Consequently, the global latency and local latency regulate ADAMTS13 function in circulation.

1.4.4 ADAMTS13 docking and proteolysis of VWF

The docking of ADAMTS13 and subsequent cleavage of VWF occurs in seven distinct steps:

1. Although the proteolytic site for ADAMTS13 in the A2 domain is hidden deep within the core of VWF in circulation, a binding site for ADAMTS13 with the D4-CK region of VWF remains exposed (Figure 1.11A and 1.11B) (Crawley et al., 2011). The T5-8/CUB1CUB2 region of ADAMTS13 can reversibly bind to the D4-CK region (K_D ~80 nM) in circulation (Figure 1.11C) (Crawley et al., 2011). This binding allows ADAMTS13 and VWF complexes to form and circulate, while VWF remains in its globular form (Crawley et al., 2011).
2. Under shear forces, VWF unravels to expose the A1 domain binding site for platelet GPIbα (Crawley et al., 2011). These shear forces can overcome the

vicinal disulfide bond, unique to the A2 domain, which causes the A2 domain to unravel and elongate (Figure 1.11D) (Q. Zhang et al., 2009). Unraveling of VWF can occur upon secretion, collagen binding via A3 domain at sites of injury, or by passage through the microvasculature (Crawley et al., 2011).

3. Residues Arg660, Tyr661, and Tyr665 in the spacer domain of ADAMTS13 bind to Glu1660-Arg1668 in the unraveled A2 domain of VWF (K_D ~80 nM) (Figure 1.11E) (Crawley et al., 2011). Further binding occurs between the cysteine-rich region of ADAMTS13 and the A2 domain (Kretz et al., 2015).
4. The residue Arg349 in the disintegrin domain of ADAMTS13 binds to Asp1614 in the A2 domain (Figure 1.11F) (Crawley et al., 2011). Although this interaction has low affinity compared to the spacer-A2 domain interaction, it is a critical interaction required for proteolysis (Crawley et al., 2011).
5. The S3 subsite composed of Leu198, Leu232, and Leu274 in the metalloprotease domain bind to L1603 (P3) in the A2 domain of VWF (Figure 1.11G) (Crawley et al., 2011). Together, the engagement of these exosites position the Tyr1605 (P1)-Met1606 (P1') scissile bond over the active site of ADAMTS13 (Crawley et al., 2011).
6. The P1 and P1' residues in the A2 domain of VWF engage their respective S1 (Leu151/Val195) and S1' (Asp252-Pro256) subsite pockets in the metalloprotease domain (Figure 1.11H) (Crawley et al., 2011).
7. Proteolysis of VWF at Tyr1605-Met1606 occurs by ADAMTS13 (K_m = 0.16-1.6 μM) (Crawley et al., 2011; De Groot et al., 2009; Zanardelli et al., 2009).

VWF proteolysis by ADAMTS13 occurs at newly secreted VWF strings from endothelial cells, ultra large VWF in circulation, and at sites of vascular injury (Crawley et al., 2011). Proteolysis of VWF by ADAMTS13 is dependent on shear-induced unfolding (X. Zhang et al., 2009). The force required to unfold the domains of VWF is approximately 10 pN (Springer, 2014).

Progressive exosite engagement of ADAMTS13 by VWF is critical for proteolysis (Crawley et al., 2011). Exosite engagement positions the Tyr1605-Met1606 scissile bond over the metalloprotease domain for cleavage (Crawley et al., 2011). Moreover, exosite engagement may be necessary for access to the active site of ADAMTS13 (Kretz et al., 2015). Without exosite engagement, it is possible that the active site of ADAMTS13 remains restricted, which protects ADAMTS13 from protease inhibitors and off-target proteolysis.

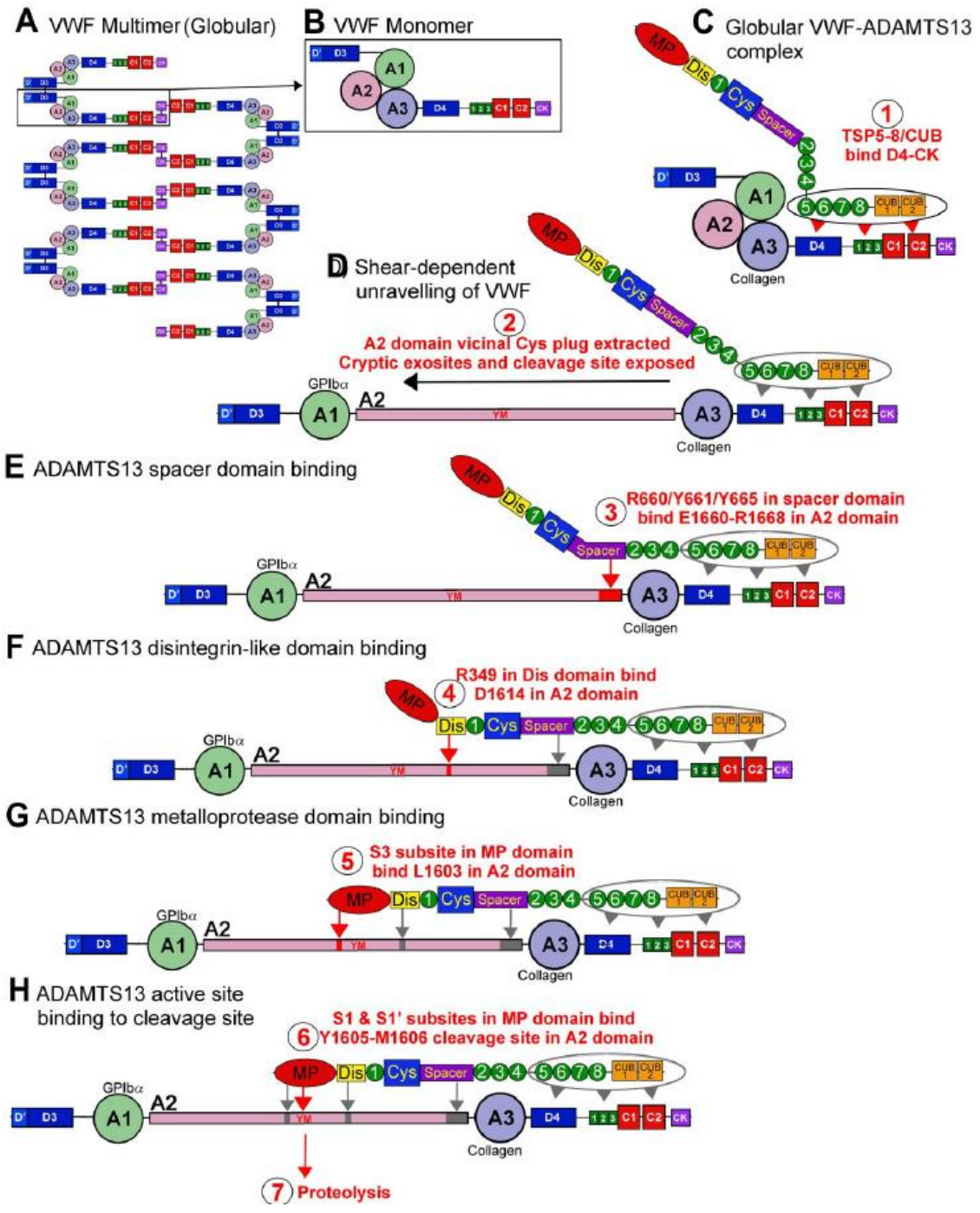
A VWF Multimer (Globular)
B VWF Monomer
C Globular VWF-ADAMTS13 complex
1 TSP5-8/CUB bind D4-CK
D Shear-dependent unravelling of VWF
2 A2 domain vicinal Cys plug extracted
Cryptic exosites and cleavage site exposed
E ADAMTS13 spacer domain binding
3 R660/Y661/Y665 in spacer domain bind E1660-R1668 in A2 domain
F ADAMTS13 disintegrin-like domain binding
4 R349 in Dis domain bind D1614 in A2 domain
G ADAMTS13 metalloprotease domain binding
5 S3 subsite in MP domain bind L1603 in A2 domain
H ADAMTS13 active site binding to cleavage site
6 S1 & S1' subsites in MP domain bind Y1605-M1606 cleavage site in A2 domain
7 Proteolysis
MP
Dis
Cys
Spacer
GPIbα
A1
A2
A3
D4
Collagen

Figure 1.11. Mechanism of VWF proteolysis by ADAMTS13. A. Head-to-head and tail-to-tail multimerization of VWF. **B.** The globular structure of a VWF monomer. **C.** ADAMTS13-VWF complex is formed and can circulate through the T5-8/CUB interaction with the D4-CK region on VWF (step 1). **D.** Shear forces unravel VWF. The A2 domain vicinal disulfide bond is relieved, allowing the A2 domain to unravel and elongate (step 2). Shear forces also expose the A1 domain binding site for platelet GPIbα. Shear forces during VWF secretion, collagen binding via A3 domain, or passage through the microvasculature can unravel VWF. **E.** ADAMTS13 spacer domain (Arg660, Tyr661, and Tyr665) binds to the A2 domain of VWF (Glu1660-Arg1668) (step 3). **F.** ADAMTS13 disintegrin domain (Arg349) binds to the A2 domain of VWF (Asp1614) (step 4). **G.** The S3 subsite pocket in the metalloprotease domain of ADAMTS13 binds to Leu1603 (P3) in A2 domain of VWF (step 5). Progressive exosite engagement of ADAMTS13 by VWF positions the Tyr1605 (P1) - Met1606 (P1') scissile bond for proteolysis. **H.** The S1 and S1' subsite pockets in the metalloprotease bind to the P1 and P1' cleavage sites in the A2 domain of VWF, respectively (step 6), thereby resulting in the proteolysis of VWF (step 7). Source: Crawley et al., Blood (2011).

1.4.5 Thrombotic thrombocytopenia purpura (TTP)

TTP is a rare microvascular thrombotic disorder with an incidence rate of 1 in 100,000 (Steinhubl et al., 1999). TTP is caused by impaired VWF cleavage by ADAMTS13, resulting in the deposition of platelet/VWF-rich thrombi in microvasculature (Sadler, 2015). Clinically, TTP is characterized by the pentad of symptoms: microangiopathic hemolytic anemia, thrombocytopenia with purpura, acute renal insufficiency, neurological abnormalities, and fever (Moake, 2002). TTP is distinguished from other microvascular thrombotic disorders by an ADAMTS13 activity of < 10% (Franchini & Mannucci, 2008). Significant reduction in ADAMTS13 activity alone may not be sufficient to cause acute episodes of TTP because patients in remission can also have ADAMTS13 activity of < 10% (Upreti et al., 2019). This has led to the "second-hit" hypothesis of TTP, which suggests that inflammatory markers and pregnancy can trigger the release of VWF from Weibel-Palade bodies (Coppo & Lämmle, 2020). Interestingly, TTP is twice as common in females than males (Terrell et al., 2010). Drastic hormonal changes and pregnancy have been found to be triggers of TTP, which may account for this sex disparity (Lattuada et al., 2003).

Deficiency in ADAMTS13 can occur by two distinct mechanisms (Cataland & Wu, 2015; Lancellotti et al., 2015). Congenital TTP is a rare autosomal recessive disease that accounts for approximately 5% of all TTP cases, and is caused by genetic mutations in ADAMTS13 either by nonsense mutations, or missense mutations that result in impaired secretion (Lancellotti et al., 2015; Romão De Souza et al., 2018). On the other hand, acquired TTP is an autoimmune response in observed commonly in patients,

whereby autoantibodies targeting ADAMTS13 inhibit its activity and/or increase its clearance from the circulation (Cataland & Wu, 2015). Although majority of patients with acquired TTP survive, relapse following remission remains an important concern (Kremer Hovinga et al., 2010). These patients require lifelong monitoring because of the episodic and cyclical nature of acquired TTP (Kremer Hovinga et al., 2010). In over 90% of patients, autoinhibitory antibodies have shown to target the spacer domain of ADAMTS13, which is crucial for both the recognition and binding of ADAMTS13 to VWF (Cataland & Wu, 2015; Roose et al., 2018; South et al., 2014) Recently, it has been observed that binding of autoinhibitory antibodies may alter the function and regulation of ADAMT13 (Roose et al., 2018; Schelpe et al., 2020). Perhaps, engagement of important exosites such as the spacer domain by inhibitors may sensitize ADAMTS13 to inhibition similar to these autoantibodies.

In terms of treatment, patients respond well to plasma exchange (Rock et al., 1991; Sadler, 2008). Plasma exchange removes auto-antibodies targeting the spacer domain of ADAMTS13, while replacing ADAMTS13 (Rock et al., 1991; Sadler, 2008). Further, patients may benefit from prophylactic immunosuppressants such as rituximab during remission, and require immediate intervention at the first sign of relapse (Cataland & Wu, 2015). To add, the use of recombinant ADAMTS13 as a potential therapeutic may be beneficial in the absence of autoinhibitory antibodies (Cataland & Wu, 2015). Recently, an anti-VWF humanized, bivalent variable-domain-only immunoglobulin fragment called caplacizumab has been developed to target the platelet-binding A1 domain of VWF and inhibit VWF/platelet interaction in patients with TTP (Scully et al.,

2019). In clinical trials caplacizumab was associated with faster normalization of platelet count and lower incidence of thrombotic events than placebo (Scully et al., 2019), Overall, understanding the regulation of ADAMTS13 may improve our understanding of TTP, and hopefully patient outcome.

1.4.6 ADAMTS13 dysfunction in sepsis

Sepsis is defined as a life-threatening organ dysfunction caused by excessive host response to infection, and is a leading cause of mortality and critical illness worldwide (Fleischmann et al., 2016; Singer et al., 2016). Activation of blood coagulation during sepsis and septic shock can lead to disseminated intravascular coagulation (DIC), which is characterized by microvascular thrombosis, consumption of clotting factors and platelets, and bleeding (Dempfle, 2004). Recent studies have suggested a reciprocal correlation between VWF and ADAMTS13 in sepsis (Kremer Hovinga et al., 2007). The extent of reduced ADAMTS13 antigen levels and activity appear strongly associated with sepsis severity and prognosis (Azfar et al., 2017; Kremer Hovinga et al., 2007). In response to inflammation, VWF is released in massive amounts from the endothelium (Ono et al., 2006). In turn, the increased levels of VWF can bind and clear limited ADAMTS13 from the circulation due to differences in their circulating half-lives (Furlan et al., 1999; Pipe et al., 2016). Cecal ligation and puncture models of sepsis in mice showed that VWF is a major determinant of decreased ADAMTS13 activity (Lerolle et al., 2009). Other suggested mechanisms that may contribute to the reduced ADAMTS13 antigen and subsequent activity in sepsis include: reduced ADAMTS13 synthesis (Uemura et al., 2010), degradation by thrombin and other proteases (Garland et al., 2017;

Levi et al., 2018), extensive neutrophil degranulation (shown to inhibit proteolytic cleavage of VWF by ADAMTS13) (Pillai et al., 2016), or impaired proteolytic activity in the presence of inflammatory mediators such as myeloperoxidase (Bernardo et al., 2019; Reiter et al., 2005). Reductions in ADAMTS13 activity may result in persistently high molecular weight VWF that may contribute to microvascular thrombosis through enhanced platelet capture (Ono et al., 2006). However, it remains unclear whether ADAMTS13 and VWF levels normalize in patients that recover from sepsis. A prolonged imbalance in ADAMTS13 and VWF may contribute to microvascular thrombosis, ischemic stroke, and organ damage in patients that survive sepsis.

1.5 Comparison of ADAMTS5 to ADAMTS13

ADAMTS5, also called aggrecanase-2, cleaves aggrecan, which is a large multi-domain proteoglycan that provides cartilage with compressibility and elasticity by regulating the movement of water molecules in the collagen network (Bondeson et al., 2008; Mosyak et al., 2008). The loss of aggrecan is a critical early step in the progression of osteoarthritis, which is a degenerative joint disorder (Bondeson et al., 2008). ADAMTS5 has been shown to contribute to structural damage of cartilage (Mosyak et al., 2008). ADAMTS5 knockout mice are protected from developing osteoarthritis; thus, inhibition of ADAMTS5 is being considered as a potential therapy for osteoarthritis (Majumdar et al., 2007).

ADAMTS5 is expressed in adipocytes, the uterus, and breast myoepithelial cells, and is secreted into the extracellular space (Bondeson et al., 2008; Kelwick et al., 2015). Structurally, ADAMTS5 and ADAMTS13 share a same N-terminal domain organization

(MDTCS); however, sequence differences within each domain give the proteases their own unique features and properties (Kelwick et al., 2015). Like ADAMTS13, ADAMTS5 consists of a catalytic metalloprotease domain, followed by a series of important exosites that provide substrate binding and specificity (Bondeson et al., 2008). Unlike ADAMTS13, ADAMTS5 has a propeptide that needs to be removed by furin for catalytic activity (Kelwick et al., 2015). The metalloprotease domain of ADAMTS5 contains the common features found in the ADAMTS family including: the active site, the catalytic zinc, calcium-binding sites, and the characteristic "met-turn" (Mosyak et al., 2008). The disintegrin domain of ADAMTS5 consists of two α-helices, two β-sheets, and several loops. The disintegrin domain has been suggested to be directly involved in aggrecan recognition (Mosyak et al., 2008). Not much is known about the –TCST2 domains of ADAMTS5; however, based on the crystal structure and our understanding of other ADAMTS proteases, it has been suggested that the remaining domains are important exosites that guide substrate specificity (Kelwick et al., 2015; Mosyak et al., 2008).

The crystal structure of the metalloprotease domain of ADAMTS5 reveals that the catalytic site is a deep, solvent-exposed cleft with access to S1' and S2' pockets, and at the center of this cleft houses the catalytic zinc (Mosyak et al., 2008). As a result, inhibitors have access to the active site of ADAMTS5, and studies exploring potential therapies for osteoarthritis have found A2M, TIMPs, and small molecule inhibitors, such as batimastat, can inhibit ADAMTS5 (Kashiwagi et al., 2001; Mosyak et al., 2008; Rasmussen & McCann, 1997; Tortorella et al., 2004). Additionally, inhibitors with small P1' moieties display the highest degree of inhibition, suggesting that smaller inhibitors

that can directly chelate zinc are more potent (Mosyak et al., 2008). In comparison, the active site of ADAMTS13 is hypothesized to be restricted by the gatekeeper triad (Petri et al., 2019), whereas the active site of ADAMTS5 remains unrestricted and exposed to substrates and inhibitors (Mosyak et al., 2008). This stark difference may explain the mechanism by which ADAMTS13 is resistant to protease inhibitors.

1.6 Protease inhibitors

Proteases are enzymes that hydrolyze peptide bonds of proteins into their individual components (Berg et al., 2002; Rudzińska et al., 2021). Proteases are classified based on their amino acid sequence in the active site or the mechanism of peptide bond cleavage (Berg et al., 2002; Rudzińska et al., 2021). Proteases can be classified into six groups: cysteine, serine (including rhomboid proteases), threonine, glutamic acid, aspartate proteases and metalloproteases (Berg et al., 2002; Rudzińska et al., 2021; Urban & Dickey, 2011). Protease inhibitors can be biological or chemical compounds that reversibly or irreversibly bind to proteases and attenuate or hinder their function (Rudzińska et al., 2021). Protease inhibitors can be classified by the type of protease they inhibit or by their mechanism of action (Rudzińska et al., 2021). Protease inhibitors have long been studied for their therapeutic potential against a wide range of diseases, viral infections, cancers, and disorders (inflammatory, respiratory, cardiovascular, and neurodegenerative) (Patick & Potts, 1998; Rudzińska et al., 2021). A2M, tissue inhibitors of metalloproteinases (TIMPs), and small molecule matrix metalloproteinase (MMP) inhibitors are three classes of inhibitors that are pertinent to ADAMTS13 because they are potent inhibitors of the metzicin protease super family.

1.6.1 Alpha 2-macroglobulin (A2M)

A2M is a pan-protease endopeptidase inhibitor capable of inhibiting many classes of proteases, including metalloproteases (Rehman et al., 2013). Interestingly, A2M inhibits proteases without covalently docking to their active site (Rehman et al., 2013). In addition to its role as a protease inhibitor, A2M also binds to cytokines and hormones to act as their carrier, and antagonizes endotoxins released from bacteria (Rehman et al., 2013). A2M is able to carry out these diverse functions because each of its four subunits consist of a bait region, an internal thioester, a receptor binding site, a transglutaminase reactive site, and a metal binding site (Rehman et al., 2013).

A2M is a tetramer of four identical 185 kDa subunits found at high plasma concentrations of approximately 2.4 mg/mL (Andersen et al., 1995; Biltoft et al., 2017; Luan et al., 2008; Rehman et al., 2013). Each subunit consists of 1451 amino acid residues, eight glycosylation sites, and eleven intra-chain disulfide bonds (Andersen et al., 1995; Rehman et al., 2013). Each homodimer is held together by a disulfide bond, which then further assembles into a tetramer through non-covalent interactions (Feldman et al., 1985; Rehman et al., 2013). Each subunit consists of a 39 amino acid cleavage region termed the “bait region”, which stretches from Pro690-Thr728 (Luan et al., 2008; Rehman et al., 2013). Proteolysis can occur anywhere along the bait region, but occurs most often within the Arg704-Val-Gly-Phe-Tyr-Glu709 interval (Rehman et al., 2013). Upon cleavage of the bait region, the internal thioester bond between Cys972 and Gln975 becomes exposed and is hydrolyzed by water (Rehman et al., 2013). Alternatively, the thioester bond can also be broken by heat and small nucleophiles (Feldman et al., 1985;

Rehman et al., 2013). Hydrolysis of the thioester bond induces conformational changes in the structure of A2M that entraps the protease, sterically blocking large substrates from reaching the protease's active site (Dangott, L. J.; Cunningham, 1982; Garcia-Ferrer et al., 2015; Rehman et al., 2013).

Although A2M is composed of four identical monomers, it only has two protease binding sites (Rehman et al., 2013). The structural model of A2M resembles a hollow cylinder composed of two identical halves (Figure 1.12A) (Feldman et al., 1985; Rehman et al., 2013). Each half is composed of two monomers with four arms, one long arm and one short arm, from each monomer (Feldman et al., 1985; Rehman et al., 2013). Upon cleavage of the bait region, the thioester located at the hinge of the long arm is exposed to solution and is hydrolysed (Feldman et al., 1985; Rehman et al., 2013). The cleaved form of A2M can be detected by SDS-PAGE at 90 kDa (Tortorella et al., 2004). Hydrolysis of the thioester causes the trap arms to swing shut, effectively trapping the protease, similar to a mouse trap analogy (Figure 1.12B) (Feldman et al., 1985; Rehman et al., 2013). Hydrolysis of the internal thioester is essential for this trapping mechanism to be successful (Feldman et al., 1985; Rehman et al., 2013). Further, it is proposed that the A2M structure becomes narrower where the two identical halves meet (Andersen et al., 1995). After cleavage of the bait region, conformational change also occurs at this site, which compacts A2M, thereby preventing the protease from escaping the "trap" (Figure 1.12C) (Andersen et al., 1995; Feldman et al., 1985). Each tetramer can inhibit two small proteases, such as trypsin (23.3 kDa) at a 2:1 protease to tetramer ratio, or one large protease, such as plasmin (83 kDa) at a 1:1 ratio (Feldman et al., 1985; Rehman et al.,

2013). Large proteases are inhibited at a 1:1 ratio because they are able to enter the second binding site through the hollow core, thus sterically blocking the site (Feldman et al., 1985). After a conformational change occurs, the receptor-binding site located on each subunit is exposed, which functions to remove the A2M-protease complex (Rehman et al., 2013). The complex is removed in circulation by receptors on hepatocytes or by fibroblast cells, monocytes/macrophages, and syncytiotrophoblasts in tissues (Rehman et al., 2013). Once the protease is successfully trapped, the A2M-protease complex is quickly removed from the body, indicated by its half-life of two-four minutes, whereas native A2M has a half-life of several hours (Rehman et al., 2013).

In terms of inhibition, A2M has been shown to inhibit many members of the ADAMTS family, including ADAMTS 1, 4, 5, 7, 10, and 12 (Kuno et al., 1999; Luan et al., 2008; Somerville et al., 2004; Tortorella et al., 2004). Therefore, the supposed resistance of ADAMTS13 to A2M poses an interesting question. A2M inhibition of ADAMTS5 is of particular interest because both ADAMTS5 and ADAMTS13 share a similar N-terminal domain organization, but lack the additional C-terminus features found in ADAMTS13.

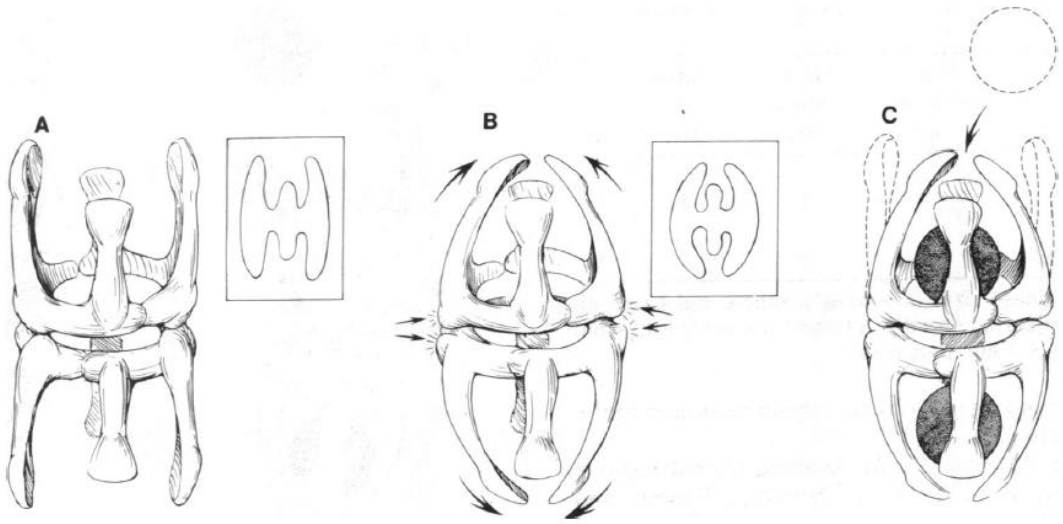

Figure 1.12. A2M schematic and mechanism of inhibition. **A.** A2M in its native state. **B.** Arrows indicate where conformational change occurs once the bait region is cleaved. **C.** Entrapment of two small proteases or one large protease (not shown). Source: Feldman et al., PNAS (1985).

1.6.2 Tissue inhibitors of metalloproteinases (TIMPs)

TIMPs are specific inhibitors of MMPs including ADAM and ADAMTS protease families (Table 1.3) (Murphy, 2011; Visse & Nagase, 2003). The TIMPs family comprises of four members: TIMP1, TIMP2, TIMP3, and TIMP4 (Visse & Nagase, 2003). In contrast to A2M, TIMPs inhibit proteases by chelating the zinc active site, thereby expelling the water molecule bound to the catalytic zinc (Visse & Nagase, 2003). Interestingly, TIMP expression patterns are not equivalent throughout the body (Murphy, 2011). They show tissue specific, constitutive, or inducible expression regulated at the transcriptional level by cytokines and growth factors (Table 1.4) (Murphy, 2011). This suggests that elevated local inhibition of metalloproteinases occurs in regions of high TIMP expression.

X-ray crystallography studies revealed that TIMPs are shaped similar to a "wedge", whereby the TIMP molecule can insert into the active site cleft of the targer protease (Gomis-Rth et al., 1997; Visse & Nagase, 2003). TIMPs are composed of an N-terminal domain of 125 amino acids and a C-terminal domain of 65 amino acids, with each domain consisting of three conserved disulfide bonds (Visse & Nagase, 2003). The conserved cysteines at position 1 and 3 in the N-terminal domain of TIMPs form disulfide bonds with the protease (Visse & Nagase, 2003). Further, Cys1 is responsible for chelating the active site of zinc with its N-terminal α-amino group and carbonyl group, resulting in the expulsion of the water molecule bound to the catalytic zinc (Visse & Nagase, 2003). Studies have shown TIMP3 to be the most potent inhibitor of the ADAMTS family including ADAMTS5; however, the mechanism(s) by which TIMP3 is

the most potent inhibitor remains unclear (Kashiwagi et al., 2001; Visse & Nagase, 2003). The inhibitory loop composed of the Cys1 in the N-terminal tail (Cys1-Thr2-Cys3-Ser4-Pro5) has been suggested to form an "inhibitory loop" with Cys68 via disulfide bond that is able to directly insert into the active site cleft to chelate the zinc, and bind to its target protease with much higher affinity (Fan & Kassiri, 2020; Kashiwagi et al., 2001). Moreover, it is possible that the structural conformation is such that TIMP3 can gain access to the active site cleft of its target protease more easily (Fan & Kassiri, 2020; Kashiwagi et al., 2001). However, the unique features of the metalloprotease domain of ADAMTS13 may protect its active site cleft from potent inhibitors like TIMPs.

Table 1.3. Inhibition of MMPs, ADAMs, and ADAMTS members by various TIMP isoforms. Source: Murphy, G., Genome Biol. (2011).

	MMPs	**ADAMs**	**ADAMTS**
TIMP1	Most	ADAM10	Unknown
TIMP2	All	ADAM12	Unknown
TIMP3	All	ADAM10, ADAM12, ADAM17, ADAM19, ADAM33	ADAMTS1, ADAMTS2, ADAMTS3, ADAMTS5, ADAMTS12
TIMP4	All	ADAM17, ADAM28	Unknown

Table 1.4. TIMP expression patterns and areas of localized concentrations. Source: Murphy, G., *Genome Biol.* (2011).

	Expression Pattern
TIMP1	Widely expressed, but localized to reproductive organs. In the central nervous system, restricted to regions associated with neuronal plasticity
TIMP2	Constitutively expressed, in most tissues, but not inducible by growth factors
TIMP3	Widely expressed, but localized to the brain, eye, and kidney
TIMP4	Is restricted to the heart, kidney, ovary, pancreas, colon, testes, brain, and adipose tissue

1.6.3 Small molecule matrix metalloprotease inhibitors

Small molecule MMP inhibitors were designed as a potential cancer therapy to mimic natural MMP inhibitor peptides; however, these inhibitors failed in clinical trials due to toxicity and adverse side effects such as musculoskeletal syndrome (Meisel & Chang, 2017). Small molecule MMP inhibitors lack specificity and were found to be potent inhibitors of the Metzincin superfamily because these inhibitors target the catalytic zinc as opposed to unique subsites within the target protease (Dorman et al., 2010). More specifically, small molecule MMP inhibitors, such as batisimat, inhibit MMPs by chelating the zinc ion through the hydroxamic group with its three side chains interfering the S1, S1' and S2' positions (Mosyak et al., 2008). Both TIMPs and small molecule MMP inhibitors target the conserved zinc ion found in the active site cleft of all MMPs (Dorman et al., 2010; Murphy, 2011).

Recently, it was demonstrated that ADAMTS13 is resistant to all four isoforms of TIMPs and small molecule MMP inhibitors, batisimat and iliomastat (Guo et al., 2016). Moreover, ADAMTS13 was found to be resistant towards all inhibitors tested (Guo et al., 2016). Specifically, TIMPs and small molecule MMP inhibitors were unable to form a tight enzyme-substrate complex with ADAMTS13, suggesting that there may be differences in the active site conformation of ADAMTS13 that protects it from inhibition (Guo et al., 2016). Perhaps inhibitors may not be able to access the active site cleft of ADAMTS13, thereby protecting ADAMTS13 from inhibition. However, the mechanism by which ADAMTS13 is resistant towards these potent protease inhibitors remains unknown.

Chapter 2: Overview of Research Project, Hypotheses, Experimental Approaches, and Objectives

2.1 Overview of research project

The goal of this project is to understand the mechanism(s) by which ADAMTS13 is resistant to protease inhibitors to better define its role in the cardiovascular system. What makes this project intriguing is that ADAMTS13 has a prolonged half-life (perhaps up to a week) in the presence of vast amounts of inhibitors, yet is actively secreted into the circulation with no off-target proteolysis. In contrast, members of the ADAMTS family and other coagulation proteases exhibit extremely shorter half-lives, are easily inhibited, are secreted in an inactive form, and display off-target proteolysis. However, the mechanism(s) by which ADAMTS13 displays these unique properties remains unknown. Further, understanding the manner by which ADAMTS13 is regulated may improve the diagnosis and treatment of acquired TTP. Moreover, this project has the potential to reveal the mechanism(s) by which other proteases in biology are resistant to inhibition, and to potentially engineer other proteases with prolonged circulating half-lives.

2.2 Hypotheses

1. The access to exosites and the active site cleft of ADAMTS13 is sterically restricted by the closed conformation.

2. The access to the active site cleft by protease inhibitors is restricted by the calcium-binding loop (R180-R193) and the variable loop (G231-S263) residing in the metalloprotease domain.
3. Progressive substrate engagement of exosites is necessary to overcome protective features of ADAMTS13 for proteolysis to occur.

2.3 Experimental approaches

1. Express and purify C-terminal domain truncations of ADAMTS13 to determine which domains of ADAMTS13 help convey resistance.
2. Clone, express, and purify chimeric proteases between ADAMTS13 and ADAMTS5 to test the role of the closed conformation and active site of ADAMTS13.
3. Develop peptides that engage the proximal exosites on ADAMTS13. These peptides are based on sequences from a previous VWF mutagenesis phage display library (Kretz et al., 2015). The purpose of these peptides is to engage important exosites of ADAMTS13, thus sensitizing ADAMTS13 to inhibition by allowing access to its active site.
4. Construct variants of MDTCS that substitute features of the metalloprotease domain with corresponding regions from ADAMTS5.

Natural and synthetic inhibitors with various mechanisms of action will be used to probe the features of ADAMTS13 that render it resistant to inhibition. Inhibition of ADAMTS13 constructs will be monitored using SDS-PAGE, Western blot, and FRETS-

VWF73 to measure activity. Specific activity of each construct will be determined using FRETS-VWF73 based on ELISA concentrations.

2.4 Specific objectives

2.4.1 Objective 1: Evaluate the role of distal domains in the resistance of ADAMTS13 to protease inhibitors.

1. Confirm ADAMTS13 resistance towards protease inhibitors.
2. Evaluate progressive domain truncations of ADAMTS13 to determine which domains help convey resistance towards protease inhibitors.

2.4.2 Objective 2: Investigate the role of the closed conformation and active site in protecting ADAMTS13 from protease inhibitors.

1. Characterize ADAMTS5 inhibition towards protease inhibitors (positive control).
2. Using chimeric constructs between ADAMTS5 and ADAMTS13, test the resistance towards protease inhibitors. Evaluate the role of the closed conformation and active site in protecting ADAMTS13 from inhibition.
3. Design peptides that engage important exosites, in an attempt to sensitize ADAMTS13 constructs to inhibition.

2.4.3 Objective 3: Identify and examine the contribution(s) of the metalloprotease domain in protecting ADAMTS13 from inhibition.

1. Evaluate the role of the gatekeeper triad (R193, D217, and D252), the calcium-binding loop (R180-R193), and the variable loop (G236-S263) in protecting

ADAMTS13 from inhibition using site-directed mutagenesis (SDM) or gene synthesis of MDTCS.

2. Attempt to sensitize MDTCS metalloprotease domain mutants to inhibition using A2M, TIMP3, and Marimastat.

Chapter 3: Material and Methods

3.1 Materials and equipment

MDTCS and MD in pcDNA 3.1-LIC were kindly provided by Dr. Tyler Beyett (University of Michigan, Ann Arbor, MI, USA). Dr. Evan Sadler kindly provided ADAMTS13, MD13TCS5, and MD5TCS13 in pcDNA 4/TO (Washington School of Medicine, St. Louis, MO, USA). MD5(TCS-CUB13) was synthesized in pUC57 and purchased from Bio Basic Canada Inc. (Markham, ON, Canada). M13/DTCS5 was synthesized in pcDNA3.1(+) and purchased from Bio Basic Canada (Markham, ON, Canada). Site-directed mutagenesis of MDTCS was synthesized and purchased from BioBasic Canada Inc. (Markham, ON, Canada). NEB 5-alpha competent E. coli were purchased from New England Biolabs (product #: C2987H; Ipswich, MA, USA). The Mini and Maxi prep DNA isolation kits were purchased from Qiagen (product #: 121123, 12162; Hilden, Germany). DNA was submitted to Mobix Laboratory at McMaster University (Hamilton, ON, Canada) for Sanger sequencing. HEK 293T cells were kindly provided by Dr. Tyler Beyett (University of Michigan, Ann Arbor, MI, USA). HEK 293T REX cells were kindly provided by Dr. Evan Sadler (Washington School of Medicine, St. Louis, MO, USA). Tissue culture cell adherent plates (10 cm^2) and flasks (T 175 cm^2) were purchased from ThermoFisher (product #: 172931, 159910; Mississauga, ON, Canada). Dulbecco's Modified Eagle Media 1x (DMEM) enriched with 4.5 g/L glucose, L-glutamine, and sodium pyruvate was purchased from Corning (product #: 10-017-CV; Manassas, VA, USA). Fetal bovine serum (FBS) was purchased from Corning (product #: 35-015-CV; Manassas, VA, USA). Penicillin-streptomycin was purchased from

ThermoFisher (product #: 15140122; Mississauga, ON). OPTI-MEM media was purchased from ThermoFisher (product #: 31985070; Mississauga, ON). Lipofectamine 3000 transfection reagent was purchased from ThermoFisher (product #: L30000001; Mississauga, ON). Transporter 5 transfection reagent was purchased from Polysciences Inc (product #: 26008-5; Warrington, PA, USA). Cloning disks used to isolate transfected colonies were purchased from Belart (product #: F37847-0001; Wayne, NJ, USA). Restriction enzymes HINDIII and NOTI were purchased from New England Biolabs (product #: R3104S, R3189S; Ipswich, MA, USA). T4 DNA Ligase was purchased from New England Biolabs (product #: M0202S; Ipswich, MA, USA). Dr. Evan Sadler kindly provided pcDNA 4/TO (Washington School of Medicine, St. Louis, MO, USA). Ampicillin was purchased from Sigma-Aldrich (product #: A9393, Oakville, ON, Canada). Zeocin and Blasticidin S HCl, Freestyle 293 expression media, and AEBSF protease inhibitor were purchased from ThermoFisher (product #: R25001, A1113902, 12338018, 78431; Mississauga, ON, Canada). Heparin sodium salt was purchased from EMD Millipore Corp. (product #: 2608411; Billerica, MA, USA). Q-Sepharose FF resin for purification was purchased from Sigma-Aldrich (product #: GE17-0510-01; Oakville, ON, Canada). HisPur Ni-NTA resin for purification of His-tag was purchased from ThermoFisher (product #: 88221; Mississauga, ON, Canada). Strep-Tactin II resin and resin specific buffers were purchased from IBA-Lifesciences (product #: 2-1201-002; Gottingen, Germany). Amylose resin high flow was purchased from New England Biolabs (product #: E8022S; Ipswich, MA, USA). Nanodrop One (ThermoFisher, Mississauga, ON, Canada) was used to measure A_{280}. Centrifugal concentrators were

purchased from EMD Millipore Corp. (product # Amicon Ultra-15; Billerica, MA, USA). PD-10 desalting columns were purchased from ThermoFisher (product #: Cytiva 17085101; Mississauga, ON, Canada). TEV protease was purchased from New England Biolabs (product #: P8112S; Ipswich, MA, USA). Highly purified A2M (bioultra, ≥98%) was purchased from Sigma-Aldrich (prodyct #: M6159; Oakville, ON, Canada). TIMP 1, 2, 3, and 4 were purchased from R&D Systems (product #: 970-TM, 971-TM, 973-TM, 974-TSF; Oakville, ON, Canada). Marimastat, ilomastat, and batimastat were purchased from Sigma-Aldrich (product #: M2699, M5939, SML0041;Oakville, ON, Canada). Pre-cast gels (Mini-PROTEAN TGX) at 4 to 20% gradient or 7.5% were purchased from Bio-Rad (product #: 4561096, 4561023; Mississauga, ON, Canada). Loading dye buffer (4x) and protein ladder (Precision Plus Protein) were purchased from Bio-Rad (product #: 1610747, 1610374; Mississauga, ON, Canada). β-meracaptoethanol (BME) was purchased from Sigma-Aldrich (M6250; Oakville, ON, Canada). SYPRO Ruby stain, Western blot apparatus, and nitrocellulose membrane were purchased from Bio-Rad (product #: 1703125, 1620112; Mississauga, ON, Canada). Protein gel analysis was conducted using Image Lab software (version 5.2.1) using the ChemiDoc MP imager System from Bio-Rad (Mississauga, ON, Canada). Metalloprotease antibody, ADAMTS5 antibody, A2M antibody were purchased from Abcam (product #: AB28274, AB41037, EPR4432; Cambridge, UK) and G1-IGD-G2 antibody was purchased from R&D Systems (product #: MAB1220; Oakville, ON, Canada). V5 antibody was purchased from Thermofisher (product #: R960-25; Mississauga, ON, Canada). Anti-rabbit, anti-goat, and anti-mouse HRP conjugated secondary antibodies were purchased from Bio-Rad (product

#: 1706515, 1721034, 1706516; Mississauga, ON, Canada). Clarity luminol and Clarity peroxide solutions were purchased from Bio-Rad (product #: 1705061; Mississauga, ON, Canada). ADAMTS13 Quantikine ELISA kit was purchased from R&D Systems (product #: DADT130; Oakville, ON, Canada). FRETS-VWF73 was purchased from AnaSpec (product #: AS-637228-05; Fremont, CA, USA). SpectraMax M3 from Molecular Devices (San Jose, CA, USA) was used to measure ELISA and FRETS-VWF73 assay. ADAMTS13, MDTCS, and ADAMTS5 were purchased from R&D Systems (product #: 6156-AD-020, 4245-AD-020, 2198-AD-020; Oakville, ON, Canada). ADAMTS5 substrate, G1-1GD-G2 (aggrecan fragment) was purchased from R&D Systems (product #: 1220-PG; Oakville, ON, Canada). Disintegrin peptides were synthesized and purchased from BioBasic Canada Inc. (Markham, ON, Canada).

3.2 Construction of stable cell lines for ADAMTS13 deletion constructs and ADAMTS13/ADAMTS5 chimeras

3.2.1 Bacterial transformation and Maxi-Prep

Stable cell lines were generated for deletion constructs: MDTCS(A75-W688) and MD(A75-L374) in pcDNA 3.1-LIC were kindly provided by Dr. Tyler Beyett. Chimeric constructs: MD13(A75-W387)TCS5(N569-T863) and MD5(M1-G568)TCS13(S388-A685) in pcDNA 4/TO were kindly provided by Dr. Evan J. Sadler. MD5(M1-G568)(TCS-CUB13(R386-T1427)) was developed in-house in pcDNA 4/TO (Section 3.3) All constructs were C-terminus 6xHis-tagged (except for MDTCS and MD which were N-terminus) for Ni-NTA purification. ADAMTS13, MD13/TCS5, MD5/TCS13, and MD5(TCS-CUB13) were also C-terminus V5-tagged for detection

(GKPIPNPLLGLDST) (Table 3.1). To increase the expression of the MD construct a large MBP solubility enhancer tag was added to the N-terminus (MKIEEGKLVIWINGDKGYNGLAEVGKKFEKDTGIKVTVEHPDKLEEKFPQVAAT GDGPDIIFWAHDRFGGYAQSGLLAEITPDKAFQDKLYPFTWDAVRYNGKLIAYPI AVEALSLIYNKDLLPNPPKTWEEIPALDKELKAKGKSALMFNLQEPYFTWPLIAA DGGYAFKYENGKYDIKDVGVDNAGAKAGLTFLVDLIKNKHMNADTDYSIAEAA FNKGETAMTINGPWAWSNIDTSKVNYGVTVLPTFKGQPSKPFVGVLSAGINAAS PNKELAKEFLENYLLTDEGLEAVNKDKPLGAVALKSYEEELAKDPRIAATMENA QKGEIMPNIPQMSAFWYAVRTAVINAASGRQTVDEALKDAQTDYDIPGTENLYF QSNA). All constructs were transformed into NEB 5-alpha Competent E. coli (New England Biolabs, Ipswich, MA; product #: C2987H) according to manufacturer's instructions and maxi-prep (Qiagen, Hilden, Germany; product #: 121123) were performed on all constructs to increase DNA template available for transfection. Small samples of all DNA templates were sent to the Mobix Laboratory at McMaster University (Hamilton, ON, Canada) for Sanger sequencing to ensure the correct sequence of each construct.

Table 3.1. Pertinent details of each ADAMTS13 deletion construct and ADAMTS13/ADAMTS5 chimera.

Construct (sequence)	Vector	Cell type	Tag	Selection
FL-ADAMTS13	pcDNA 4/TO	HEK 293T REX	His, V5	Zeo, Blast, induce with tet
MDTCS (A75-W688)	pcDNA 3.1-LIC	HEK 293T	His	Zeo
MD (A75-L374)	pcDNA 3.1-LIC	HEK 293T	His	Zeo
MD13 (A75-W387) TCS5 (N569-T863)	pcDNA 4/TO	HEK 293T	His, V5	Zeo, induce with tet, add heparin
M13 (A75-Q300) / DTCS5 (G482-C930)	pcDNA 3.1(+)	HEK 293T	Strep, V5	G418
MD5 (M1-G568) / TCS13 (S388-A685)	pcDNA 4/TO	HEK 293T	His, V5	Zeo, induce with tet
MD5 (M1-G568) / (TCS-CUB13(R386-T1427))	pcDNA 4/TO	HEK 293T	His, V5	Zeo, induce with tet

3.2.2 Lipofectamine 3000 Transfection

HEK 293T cells were cultured in DMEM (Corning, Manassas, VA, USA; product #: 10-017-CV) supplemented with 10% FBS (Corning, Manassas, VA, USA; product #: 35-015-CV) and 1% penicillin-streptomycin (ThermoFisher, Mississauga, ON, Canada; product #: 15140122), and plated on a 10 cm dish (ThermoFisher, Mississauga, ON, Canada; product #: 172931). The cells were transfected using Lipofectamine 3000 transfection reagent kit at 70% confluency (ThermoFisher, Mississauga, ON, Canada; product #: L30000001). Transfection was performed using two Eppendorf tubes consisting of the following mixture:

Tube A: 500 µL of OPTI-MEM media (ThermoFisher, Mississauga, ON, Canada; product #: 31985070) and 45 µL of Lipofectamine 3000.

Tube B: 500 µL of OPTI-MEM, 20 µg of DNA, and 40 µL of P3000 (from Lipofectamine 3000 kit.

Tubes A and B were mixed well and incubated separately for 5 minutes at room temperature. After 5 minutes, the tubes were mixed together and incubated for 20 minutes at room temperature. After 20 minutes, the complete media was aspirated off the cells and washed with 5 mL of OPTI-MEM. The OPTI-MEM was removed and the DNA/Lipofectamine reagent mixture was added to the plate. The mixture was incubated on the cells for 4 to 5 hours. The reaction was stopped with the addition of 6 mL of complete media (DMEM supplemented with 10% FBS and 1% penicillin-streptomycin).

At 90% confluency, the cells were trypsinized, and a dilution series was performed (1/10, 1/100, 1/1,000, and 1/10,000) in selection media containing DMEM

supplemented with 10% FBS, 1% penicillin-streptomycin, and 300 µg/mL Zeocin (ThermoFisher, Mississauga, ON, Canada; product #: R25001). Each diluted cell suspension was re-plated onto a 10 cm^2 dish in selection media to isolate cells with a stably integrated ADAMTS13 variant expressing plasmid. Every 2 to 3 days the selection media was changed until the cells formed individual colonies. Selection media was then removed and isolated colonies were collected using cloning disks (Belart, Wayne, NJ, USA; product #: F37847-0001) pre-soaked in 0.25% Trypsin-EDTA (1x) for 5 minutes at 37°C. Each cloning disk harbouring the colony was placed into an individual well of a 24-well plate containing the same selection media. Cells were grown to 90% confluency, then screened to identify the highest expression levels. Cells containing the ADAMTS13 truncation or ADAMTS13 active site (MD13TCS5) were screened using FRETS-VWF73 activity assay (Section 3.8.4). To screen for the highest expressing cells containing the ADAMTS5 active site (MD5TCS13 and MD5(TCS-CUB13)) media was collected and concentrated. Highest expression was determined by Western blot using anti-ADAMTS5 antibody (Abcam, Cambridge, UK; product #: AB41037) and verified by band intensity using densitometry (Section 3.8.2).

3.3 Construction of MD5(TCS-CUB13) construct

MD5(TCS-CUB13) is a chimeric protease constructed by swapping the MD domains of ADAMTS13 with ADAMTS5. This construct theoretically tests the impact of the closed conformation of ADAMTS13 on the active site of ADAMTS5. The MD5(TCS-CUB13) DNA template was synthesized and purchased from Bio Basic Canada Inc. (Markham, ON, Canada). To construct a MD5(TCS-CUB13) stable cell line,

the template was first transformed using NEB 5-alpha Competent E.coli, and was purified using a maxi-prep kit (Section 3.2.1). Both the MD5(TCS-CUB13) insert in pUC57 and expression vector pcDNA4/TO were digested with HINDIII and NOTI (New England Biolabs, Ipswich, MA, USA; product #: R3104S, R3189S), and ligated into pcDNA4/TO using T4 DNA Ligase (New England Biolabs, Ipswich, MA, USA; product #: M0202S). Individual clones were selected on a LB Agar plate containing 100 µg/mL ampicillin (Sigma-Aldrich, Oakville, ON, Canada; product #: A9393). Colonies were verified by Sanger sequencing at Mobix Laboratory. Multiple colonies were successful; one was selected at random for maxi-prep to increase DNA concentration for transfection into HEK 293T cells. MD5(TCS-CUB13) stable cell line was constructed with HEK 293T cells using the methods described in Section 3.2.2.

3.4 Protein purification protocols

3.4.1 Cell Culture

All stable cell lines, including full-length ADAMTS13 and domain truncations/chimeras were cultured in DMEM supplemented with 10% FBS and 1% pen/strep. For selection, 300 µg/mL of Zeocin was used. ADAMTS13 was expressed in HEK 293T REX cells, and were selected using 5µg/mL Blasticidin S HCl (ThermoFisher, Mississauga, ON, Canada; product #: A1113902) along with 300 µg/mL Zeocin, and expression was induced with 1 µg/mL tetracycline (Sigma-Aldrich, Oakville, ON, Canada; product #: T6670). Tetracycline was used to induce expression in all constructs in the pcDNA 4/TO vector. At 70% confluency, complete media was switched to Freestyle 293 expression media (ThermoFisher, Mississauga, ON, Canada; product #:

12338018) to increase purity by reducing the protein contain from FBS. The Freestyle media contained 20 mM AEBSF (Sigma-Aldrich, Oakville, ON, Canada; product #: 78431), which prevents protein degradation. For cell lines expressing MD13TCS5, 100 µg/mL heparin (Millipore Corp., Billerica, MA, USA; product #: 2608411) was added. Freestyle media was collected every 2 days until cell death. The collected media was centrifuged at 3000 x g, filtered (0.45 Um), and then stored at -80°C until purified.

3.4.2 Q-Sepharpose FF purification

All constructs were purified using Q-Sepharose FF (Sigma-Aldrich, Oakville, ON, Canada; product #: product #: GE17-0510-01). Bed volume was adjusted based on the amount of media being purified according to the manufacturer's protocol. Q-Sepharose FF beads were added into a standard column and primed with an acid-base wash. These beads were washed with five bed volumes of 0.1 M HCl, followed by five bed volumes of 0.1 M NaOH. The beads were washed with ten bed volumes of ddH_2O to remove any residual acid or base in the beads. The column was equilibrated with ten bed volumes of 25 mM Tris-HCl (pH 8.0). The media was diluted with two volumes of 25 mM Tris-HCl (pH 8.0), then passed over the column. The column was washed with ten bed volumes of 25 mM Tris-HCl (pH 8.0). The construct was eluted with 25 mM Tris-HCl (pH 8.0), containing 1 M NaCl in 0.5 to 1 mL fractions. A_{280nm} was measured using Nanodrop One (ThermoFisher, Mississauga, ON, Canada) to determine which fractions contained the eluted protein. These fractions were pooled for Ni-NTA purification (Section 3.4.3).

3.4.3 Ni-NTA purification

To increase purity of the construct being purified, Ni-NTA purification was performed on the elution from the Q-Sepharose purification. All constructs were fused with a polyhistidine (6xHis) tag. These constructs were purified using HisPur Ni-NTA resin (ThermoFisher, Mississauga, ON, Canada; product #: 88221). Resin bed volume was adjusted according to the manufacture's specifications. The resin was centrifuged at 500 x g to remove the storage solution. The resin was then added to a standard 30 mL column and washed with 5x resin bed volume using wash solution containing 20 mM Tris-HCl, 300 mM NaCl, 20 mM Imidazole, pH 7.4. Wash buffer concentration of Tris-HCl, NaCl and Imidazole were matched in the protein sample eluted from the Q-Sepharose column, and pH was adjusted to 7.4. This modified Q-Sepharose elution was loaded onto the Ni-NTA column. The column was then washed with ten bed volumes of wash buffer. The protein was eluted in 0.5 to 1 mL fractions using elution buffer (20 mM Tris-HCl, 300 mM NaCl, 250 mM Imidazole, pH 7.4). A_{280nm} was measured using Nanodrop One, and fractions containing protein were pooled and concentrated using a centrifugal concentrator at 15,000 x g (cut-off size of concentrator was based on the size of protein).

The concentrated samples were buffer exchanged on a PD-10 column (ThermoFisher, Mississauga, ON, Canada; product #: Cytiva 17085101) into ADAMTS13 reaction buffer (50 mM Tris-HCl, 150 mM NaCl, 10 mM $CaCl_2$, 10 µM $ZnCl_2$, 0.005% Tween 20, pH 7.4). Appropriate fractions from the PD-10 were pooled and concentrated using a centrifugal concentrator, as previously described.

To increase solubility of the MD construct, a C-terminal MBP tag was added. After Q-Sepharose and Ni-NTA purifications, the MBP tag was removed using TEV protease, according to manufacturer's instructions (New England Biolabs, Ipswich, MA, USA; product #: P8112S). The MBP tag was separated from MD using Amylose Resin High Flow (New England Biolabs, Ipswich, MA, USA; product #: E8022S). The flow through containing the MD construct was concentrated and buffer exchanged into the ADAMTS13 reaction buffer to remove the EDTA, using the PD-10 column, as previously described. Appropriate fractions containing MD were then concentrated using a centrifugal concentrator. To ensure that the construct was successfully recovered, SDS-PAGE (Section 3.8.1), Western blot (Section 3.8.2), and ELISA (Section 3.8.3) (R&D Systems, Oakville, ON, Canada) were performed. SDS-PAGE total protein staining showed purity, Western blot verified the presence of the construct, and ELISA determined the final concentration. FRETS-VWF73 activity assay (Section 3.8.4) was performed for constructs containing the ADAMTS13 metalloprotease domain.

3.5 Site-directed mutagenesis or gene synthesis of mutants targeting the metalloprotease domain in pcDNA 3.1(+)

The truncated form of ADAMTS13, MDTCS (A75-W688) was used to study the role of the gatekeeper triad (R193, D217, and D252), the calcium-binding loop (R180-R193), and the variable loop (G236-S263). Site directed mutagenesis (SDM) was utilized for constructs requiring point mutations (gatekeeper triad), and constructs with larger mutations (calcium-binding loop and variable loop 236-263) were commercially synthesized (Table 3.2). These mutations targeting the metalloprotease domain were

performed in MDTCS and inserted into pcDNA 3.1(+) vector. See Table 3.3 for complete details of each MDTCS metalloprotease mutant. Similarly, chimeric construct M13(A75-Q300)/DTCS5(G482-C930) was also commercially synthesized and inserted into pcDNA 3.1(+) (Table 3.1). These constructs were synthesized and purchased from Bio Basic Canada Inc. (Markham, ON, Canada). In addition, the full-length ADAMTS13 and MDTCS construct was redesigned in pcDNA 3.1(+) to increase yield and purity, and eliminate the requirement for tetracycline to induce expression (Table 3.3). Additional C-terminal V5-tag (GKPIPNPLLGLDST) was added for detection by ELISA and Western blot, and an N-terminal Strep-tag II (WSHPQFEK) was also added for purification purposes. The Strep-tag II/Strep Tactin system provides significantly improved specificity, resulting in increased yield and purity in a single purification step. Maxi-prep was performed to increase DNA yield, as previously described in Section 3.2. These constructs were expressed in HEK 293T mammalian cells using Transporter 5 transfection reagent (Polysciences, Warrington, PA, USA; product #: 26008-5) according to the manufacturer's protocol (Section 3.5.1).

Table 3.2. SDM or gene synthesis of mutants targeting the metalloprotease domain using MDTCS in pcDNA 3.1 (+).

MDTCS pcDNA 3.1 (+)		
Construct	**Residue(s)**	**Target**
	R193A	Gatekeeper triad
	R193A and D217A	Gatekeeper triad
MDTCS-G	R193A, D217A, and D252A	Gatekeeper triad (Triple Mutant)
	D217A	Gatekeeper triad
	D217A and D252A	Gatekeeper triad
	D252A	Gatekeeper triad
	Del L175-R193	Gatekeeper triad and calcium-binding loop
MDTCS-V5	G236-P244 to ATS5 D421-F429	ADAMTS5 loop swap
MDTCS-C5	R180-R193 to ATS5 R367-L379	ADAMTS5 calcium-binding loop and gatekeeper triad (R193)
MDTCS-GVC5	R180-R193 to ATS5 R367-L379, D217A, and G236-S263 to ATS5 D422-S453	ADAMTS5 calcium-binding loop, gatekeeper, and ADAMTS5 loop swap

Table 3.3. Pertinent details of each MDTCS metalloprotease mutant.

Construct (sequence)	Abbreviation	Vector	Cell type	Tag	Selection
FL-ADAMTS13	WT-ADAMTS	pcDNA 3.1(+)	HEK 293T	Strep, V5	G418
MDTCS (A75-W688)	WT-MDTCS	pcDNA 3.1(+)	HEK 293T	Strep, V5	G418
MDTCS (R193A, D217A, and D252A)	MDTCS-G	pcDNA 3.1(+)	HEK 293T	Strep, V5	G418
MDTCS (G236-P244 to ATS5 D421-F429)	MDTCS-V5	pcDNA 3.1(+)	HEK 293T	Strep, V5	G418
MDTCS (R180-R193 to ATS5 R367-L379)	MDTCS-C5	pcDNA 3.1(+)	HEK 293T	Strep, V5	G418
MDTCS (R180-R193 to ATS5 R367-L379, D217A, and G236-S263 to ATS5 D422-S453)	MDTCS-GVC5	pcDNA 3.1(+)	HEK 293T	Strep, V5	G418

3.5.1 Transient transfection using Transporter 5 reagent

Transient transfection of MDTCS, M13/DTCS5, and mutants targeting the metalloprotease domain in MDTCS were performed using the Transporter 5 reagent. DNA (2.5 to 4 µg/10cm^2) was diluted in OPTI-MEM at 1/20th (12.5 mL) of the total cell culture volume (250 mL). Similarly, Transporter 5 reagent (4x amount of DNA used) was diluted in OPTI-MEM at 1/20th (12.5 mL) of total cell culture volume. Transporter 5 reagent/OPTI-MEM mixture was added in a dropwise manner to the DNA/OPTI-MEM mixture, and incubated for 20 minutes. After 20 minutes, the DNA/Transporter 5 complex (25 mL) was added to the remaining OPTI-MEM to be used (500 mL). For transfection, T175 flasks (5 flasks) of HEK 293T cells were plated. At 70% confluency, old media was discarded, and the cells were washed twice with sterile PBS. OPTI-MEM containing the DNA/Transporter 5 complex (50 mL) was added to each T175 flask and incubated at 37°C for 48 hours. See Section 3.6 for isolating and purifying target constructs. Alternatively, OPTI-MEM media containing the constructs were filtered and concentrated using an appropriate cut-off concentrator, and buffer exchanged. The final concentration was determined using ELISA (Section 3.8.3).

3.6 Strep-Tactin resin purification

Strep-Tactin II resin (IBA-Lifesciences, Gottingen, Germany; product #: 2-1201-002) was used to increase purity and yield of select constructs synthesized in pcDNA 3.1(+). The bed volume of Strep-Tactin resin was adjusted according to approximate yield (binding capacity up to 9 mg/mL). Strep-Tactin resin was added to a column and washed with five column volumes of wash buffer (100 mM Tris-HCl and 150 mM NaCl, pH 8.0)

via gravity flow. Conditioned media was adjusted to match Tris-HCl and NaCl concentrations and adjusted to pH 8.0. Once the conditioned media containing the target protein passed through the resin, the resin was washed five times with one column volume. The construct was eluted six times with 0.5 column volumes of elution buffer (100 mM Tris-HCl, 150 mM NaCl, and 2.5 mM desthiobiotin, pH 8.0). The target construct was eluted in the 2^{nd} to 5^{th} fraction. The desthiobiotin was removed by dialysis.

3.7 A2M buffer exchange

Human A2M was purchased from Sigma-Aldrich (Mississauga, ON, Canada; product #: M6159) in lyophilized form, and was reconstituted in 200 µL of ADAMTS13 reaction buffer. The A2M (M6159) from Sigma-Aldrich is a highly purified form of A2M that contains minimal pre-cleaved A2M than the standard prep. However, A2M was lyophilized with glycine as a stabilizer, which may interfere with the FRETS-VWF73 activity assay. To remove the glycine, a buffer exchange into the ADAMTS13 reaction buffer (50 mM Tris-HCl, 150 mM NaCl, 10 mM $CaCl_2$, 10 µM $ZnCl_2$, 0.005% Tween 20, pH 7.4) was performed using a PD-10 column (ThermoFisher, Mississauga, ON, Canada; product #: Cytiva 17085101).

3.8 Quantifying construct purification and inhibition: SYPRO, Western blot, ELISA, FRETS-VWF73, and aggrecan assay

3.8.1 SYPRO total protein stain

Total protein staining was used to visualize the purity of protein purification, to visualize the presence of the cleaved form of A2M at 90 kDa upon cleavage by a

protease, and to measure aggrecan proteolysis of protease constructs containing the ADAMTS5 metalloprotease domain. Samples were reduced using β-mercaptoethanol. These samples were further denatured by boiling for two minutes in 4x sample buffer (Bio-Rad, Mississauga, ON, Canada; product #: 1610747). Upon denaturing, protein purification samples were loaded onto a 4 to 20% polyacrylamide gradient Mini-PROTEAN TGX pre-cast gel (Bio-Rad, Mississauga, ON, Canada; product #: 4561096). A 7.5% polyacrylamide Mini-PROTEAN TGX pre-cast gel (Bio-Rad, Mississauga, ON, Canada; product #: 4561023) was used to visualize the 90 kDa cleaved form of A2M. Electrophoresis was performed at 80 V for the first 15 minutes, then at 180 V until the leading dye-front approached the end of the gel.

To stain the polyacrylamide gel with SYPRO Ruby staining (Bio-Rad, Mississauga, ON, Canada; product #: 1703125), the gel was placed into a fixative solution containing 7% acetic acid and 50% methanol in Milli-Q H_2O, then placed onto a shaker for 30 minutes. This step was repeated two times. Next, the gel was rinsed with Milli-Q H_2O and submerged in SYPRO Ruby. The gel was then covered with aluminum foil and placed on a shaker overnight at room temperature. The SYPRO Ruby was removed, and a destain solution containing 7% acetic acid and 10% methanol in Milli-Q H_2O was added. The gel was placed on the shaker for 30 minutes. This step was repeated once more. Finally, the gel was then washed with Milli-Q H_2O and imaged using Image Lab software (version 5.2.1) on the ChemiDoc MP Imager System (Bio-Rad, Mississauga, ON, Canada).

3.8.2 Western blot

Western blot was used to verify the presence of ADAMTS13 constructs, MDTCS metalloprotease domain mutants, cleaved form of A2M, and cleaved form of aggrecan. Once gel electrophoresis was completed, the 7.5% polyacrylamide gel was transferred onto a nitrocellulose membrane (Bio-Rad, Mississauga, ON, Canada; product #: 1620112) in transfer buffer consisting of 25 mM Tris-base, 190 mM glycine, and 10% methanol overnight at 30 V or 1.5 hour at 75 V. Upon completion of the transfer, the membrane was placed into a blocking solution consisting of 5% non-fat dry milk and TBS with 0.05% Tween 20 for 2 hours.

For ADAMTS13, MDTCS, MD, and MDTCS metalloprotease domain mutants, 1/1500 rabbit polyclonal primary antibody for M domain of ADAMTS13 (Abcam, Cambridge, UK; product #: AB28274) was added to new blocking solution. MD5/TCS13 and MD13/TCS5 chimeras were constructed with a V5 tag, therefore 1/1500 V5 tag polyclonal antibody (ThermoFisher, Mississauga, ON, Canada; product #: R960-25) was used. The primary antibody was incubated for 2 hours. The membrane was then washed with TBS with 0.05% Tween 20 solution, three times for 5 minutes. An anti-rabbit HRP conjugated secondary antibody (Bio-Rad, Mississauga, ON, Canada; product #: 1706515) (1/5000) was added to a new blocking solution for 1 hour. The membrane was then washed six times, with TBS with 0.05% Tween 20. A 250 µL mixture consisting of 50% Clarity luminol and 50% Clarity peroxide solution (Bio-Rad, Mississauga, ON, Canada product #: 1705061) was applied and incubated for 5 minutes, prior to imaging with the

Image Lab software (version 5.2.1) on the ChemiDoc MP Imager System (Bio-Rad, Mississauga, ON, Canada).

The bait region of A2M was detected using the same protocol described above, but with its appropriate primary and secondary antibody. Anti-A2M (Abcam, Cambridge, UK; product #: EPR4432) at 1/1500 was used as the primary antibody. Goat anti-Human HRP (Bio-Rad, Mississauga, ON, Canada; product #: 1706516) (1/5000) was used as the secondary antibody.

3.8.3 ADAMTS13 ELISA

Upon purification, ADAMTS13 ELISA was performed on each construct to determine an accurate concentration. The Human ADAMTS13 Quantikine ELISA Kit (R&D Systems, Oakville, ON, Canada; product #: DADT130) was efficiently able to detect truncated, chimeric, and SMD forms of ADAMTS13 or MDTCS. The minimal detection limit of this ELISA is 0.104 ng/ml. The plasma was diluted to 100-fold, as suggested by the manufacture's protocol. Using the pre-coated plate provided in the kit, 100 µL of supplied assay diluent RD1-89 was added into each well. Next, 50 µL of standard, control, and sample(s) were added to appropriate wells. The plate was covered with adhesive strip and incubated for 2 hours on a microplate shaker. Each well was aspirated and washed with the provided wash buffer (3x). Next, 200 µL of human ADAMTS13 conjugate was added to each well, the plate was sealed with a new adhesive strip, and incubated for 2 hours on a microplate shaker. The plate was then washed with wash buffer (3x) and 200 µL of TMB (substrate solution) was added to each well, covered from light, and incubated for 30 minutes. After 30 minutes, 50 µL of stop

solution H_2SO_4 (provided with the kit) was added to each well. Optical density of each well was determined using the SpectraMax M3 (Molecular Devices, San Jose, CA, USA) set to 450 nm.

3.8.4 FRETS-VWF73 assay

FRETS-VWF73 is a fluorescence-quenching substrate for ADAMTS13 used to measure its proteolytic activity (Kokame et al., 2005). The substrate was purchased from AnaSpec (Fremont, CA, USA; product #: AS-637228-05) at 0.1 mg in lyophilized form. DMSO (35 µL) and Milli-Q H_2O (105 µL) was added to achieve a stock concentration of 100 µM. To quantify residual protease activity, 10 µL of sample was added per well of a 96-well plate along with 90 µL FRETS-VWF73 at a final concentration of 1 µM in FRETS-VWF73 buffer (5 mM Bis-tris, 25 mM $CaCl_2$, and 0.005 % Tween 20, pH 6.0 – pre-incubated at 37 °C) for a total reaction volume of 100 µL per well. The residual activity was measured with SpectraMax M3 (Molecular Devices, San Jose, CA, USA) fluorescence mode at λ_{ex} = 340 nm and λ_{em} = 450 nm at 37 °C. Fluorescence was measured every 30 seconds for 6 hours, and the reaction rate was determined by linear regression of the initial slope using SoftMax Pro (version 5.4). This protocol was repeated with the MDTCS metalloprotease domain mutants.

3.9 Inhibition studies

3.9.1 ADAMTS13, MDTCS, MD, MD13/TCS5. M13/DTCS5, and MDTCS inhibition experiments to characterize metalloprotease domain mutants

FRETS-VWF73 activity assays were used to measure the residual activities of ADAMTS13, MDTCS, MD, MD13/TCS5, M13/DTCS5, and MDTCS metalloprotease domain mutants, following incubation with various inhibitors (Section 3.8.4). ADAMTS13, MDTCS, and MDTCS metalloprotease domain mutants (20 nM) were incubated with A2M, TIMP3, and Marimastat (250 nM) for 6 hours at 37 °C in a 22 µL reaction volume containing ADAMTS13 reaction buffer in a 96-well plate. After the 6 hour incubation with inhibitors, 10 µL of sample was added per well along with 90 µL FRETS-VWF73 at a final concentration of 1 µM (FRETS-VWF73 buffer) for a total reaction volume of 100 µL per well to quantify residual protease activity. Due to the poor activities of MD, MD13/TCS5, and M13/DTCS5 towards FRETS-VWF73, the concentrations of these variants was increased to 1 µM to meet the detection threshold. The inhibitor concentrations were increased to 2.5 µM to maintain an excess inhibitor to protease concentration. Western blot analysis was also performed to examine the capacity of the MDTCS variants to cleave the A2M bait region. In these experiments, 50 nM A2M was incubated with 250 nM MDTCS variants in a 22 µL reaction volume containing ADAMTS13 reaction buffer for 6 hours at 37 °C. Western blot was performed (Section 3.8.2) to detect the A2M cleavage product at 80 kDa. All experiments were performed at least three times.

3.9.2 ADAMTS5, MD5/TCS13, and MD5(TCS-CUB13) inhibitory experiments

The proteolytic activity of constructs containing the ADAMTS5 metalloprotease domain was determined by monitoring the cleavage of recombinant human aggrecan (R&D systems, Oakville, ON, Canada; product #: 1220-PG) by SDS-PAGE. Using the ADAMTS13 reaction buffer, inhibitors (A2M, TIMP3, Marimastat at 250 nM) were incubated with ADAMTS5 or MD5/TCS13 (20 nM) for 2 hours, followed by the addition of aggrecan (100 nM) for 1 hour. The cleaved form of aggrecan was assessed by Western blot with an anti-G1-1GD-G2 antibody (R&D Systems, Oakville, ON, Canada; product #: MAB1220) (Section 3.8.2), and expressed as the percent of aggrecan cleaved in the presence of a protease. The incubation time of the inhibitor was determined based on previous literature suggesting that two hours is a sufficient amount of time to allow for the inhibition of ADAMTS5 (Tortorella et al., 2004).

A reaction time-course was performed to quantify the capacity of MD5(TCS-CUB13) to cleave aggrecan compared to MDTCS13. Thus, 100 nM MD5(TCS-CUB13) or 25 nM MD5(TCS13) was incubated with 100 nM aggrecan in ADAMTS13 reaction buffer at 37 °C. At various time-points, aliquots were removed into stop buffer containing 50 mM EDTA before analyzing the reaction time-course by Western blot (Section 3.8.2). Proteolytic activity was expressed as the percent of aggrecan cleaved based on the presence of the cleaved form of aggrecan at 65 kDa. For inhibition studies, 100 nM MD5(TCS-CUB13) was incubated with A2M, TIMP3, or Marimastat (250 nM), followed by an 18-hour incubation of the MD5(TCS-CUB13)/inhibitor complex (based on the time-course from above) with 100 nM aggrecan. The capacity of MD5(TCS-CUB13) and

MD5(TCS13) to cleave the A2M bait region was also examined by Western blot, as described (Section 3.8.2). All experiments were performed at least three times.

Aggrecan cleavage by MD5/TCS13 and MD5(TCS-CUB13) was modeled using a non-linear regression equation:

$$Y = V_{max}*X\text{^}h/(EC50\text{^}h+X\text{^}h)$$

Where X is time (hours), Y: percentage of aggrecan cleaved, EC50: time (hours) that gives 50% aggrecan cleavage, h: hillslope factor (no unit).

3.10 Disintegrin domain engagement study

Based on the mutagenesis phage display library data on VWF73 (Kretz et al., 2015), three peptides were designed to engage the disintegrin domain. The following peptides were synthesized and purchased from Bio Basic Canada Inc (Markham, ON, Canada):

D-peptide:	SDEIKRLPGDIQ
T-VWF	TGNPASDEIKRLPGDIQ
K-VWF	KGNPASDEIKRLPGDIQ

Titration of these peptides was performed with MDTCS (20 nM) and MD (1 µM) to calculate IC50 for each VWF peptide using FRETS-VWF73 (Section 3.8.4). The peptide-MDTCS or MD interaction was modelled by a non-linear regression equation:

$$Y = (Top-Bottom)/(1+10\text{^}(X-LogIC50)) + Bottom$$

Where X: logmolar concentration (mM), Y: proteolytic activity (RFU x s^{-1} x nM^{-1}), Top and Bottom: plateaus in units of Y axis, and logIC50: peptide concentration at 50% activity. MDTCS (20 nM) and MD (1 µM) was incubated with D-peptide, T-VWF, or K-

VWF for 1 hour based on the IC50 from the non-linear regression equation, followed by 6-hour incubation with A2M, TIMP3, or Marimastat (250 nM). Activity was measured using FRETS-VWF73. Western blot was performed to assess cleavage of the bait region of A2M in the presence of VWF peptides for both MDTCS and MD (Section 3.8.2).

3.11 Kinetic analysis of MDTCS metalloprotease domain mutants

Michaelis-Menten kinetic analysis was performed for FL-ADAMTS13, WT-MDTCS, MDTCS-G, MDTCS-C5, MDTCS-V5, MDTCS-GVC5 using the FRETS-VWF73 assay (0, 0.5, 1, 2.5, and 5 µM) (Section 3.8.4). Similarly, Michaelis-Menten kinetic analysis was performed for each variant in the presence of 250 nM Marimastat using FRETS-VWF73 assay (0, 0.5, 1, 2.5, and 5 µM) (Section 3.8.4). Kinetic parameters of each variant were determined at the concentration of 20 nM. Initial rates of FRETS-VWF73 cleavage were plotted as a function of substrate concentration (µM), and fit by nonlinear regression to the Michaelis-Menten equation:

$$Y = V_{max}(X)/(K_m+X)$$

Where X is substrate concentration (µM), Y is enzyme velocity (RFU), V_{max} is the maximum rate of FRETS-VWF73 cleavage (RFU/sec) and K_m is the Michaelis-Menten constant (substrate concentration at half V_{max}; µM). k_{cat} was determined by dividing V_{max} by protease concentration. Protease performance was calculated by determining the catalytic constant (k_{cat}/K_m).

3.12 Marimastat potency experiments between ADAMTS5 and MDTCS-GVC5

The potency of Marimastat to inhibit MDTCS-GVC5 was compared against ADAMTS5. ADAMTS5-aggrecan time-course study was performed to determine the

time required for 20 nM ADAMTS5 to completely cleave 100 nM aggrecan. ADAMTS5 was incubated with aggrecan at 0, 5, 10, 15, 30, 60, and 120 minutes. The cleavage of intact aggrecan at 120 kDa was quantified by Western blot and compared to no ADAMTS5 control. Cleavage of aggrecan by ADAMTS5 was modelled using the non-linear regression equation:

$$Y = V_{max}*X\text{^}h/(EC50\text{^}h+X\text{^}h)$$

Where X: time (minutes), Y: aggrecan cleaved (%), EC50: time that gives 50% aggrecan cleavage, and h: hillslope factor (no unit).

Marimastat at concentrations of 0 nM, 0.250 nM, 2.5 nM, 25 nM, and 250 nM with 20 nM ADAMTS5 and 100 nM aggrecan was incubated based on the time required for complete cleavage of aggrecan (from above). The cleavage of intact aggrecan was quantified from the Western blot and the residual activity was expressed as a percentage. Using the same experimental design, we tested 20 nM MDTCS-GVC5 with Marimastat concentrations (0 nM, 0.250 nM, 2.5 nM, 25 nM, and 250 nM), and evaluated proteolysis using FRETS-VWF73 (1 µM) (Section 3.8.4). Both reactions were modelled by using the non-linear regression equation:

$$Y = 100/(1+X/IC50)$$

Where X: Marimastat concentration (nM), Y: residual activity (%), normalized response, and IC50: concentration of Marimastat required for 50% inhibition.

3.13 ADAMTS sequence alignment

Sequence alignment study was conducted for ADAMTS 1, 4, 5, 7, 12, and 13 using PRALINE multiple sequence alignment server (Centre for Integrative

Bioinformatics VU, http://www.ibi.vu.nl/programs/pralinewww/) and Clustal Omega multiple sequence alignment server (European Bioinformatics Institute, http://www.ebi.ac.uk/Tools/msa/clustalo/). The protein sequences used for the alignment study were retrieved from the National Center for Biotechnology Information protein database (NCBI, https://www.ncbi.nlm.nih.gov/protein/).

3.14 PYMOL visualization software

The molecular visualizations of the structures of MDTCS and ADAMTS5 bound to Marimastat were constructed with PyMOL 2.5 by Schrodinger (https://pymol.org/2/). The PDB file was retrieved from the PDB Protein Databank (https://www.rcsb.org/structure/6QIG and https://www.rcsb.org/structure/3HY7). The PDB ID: 6QIG corresponds to the crystal structure of 3H9 Fab-MDTCS (Petri et al., 2019), and the PDB ID: 3HY7 corresponds to the crystal structure of ADAMTS5 bound to Marimastat (Tortorella et al., 2009). Notably, ADAMTS5 has not been crystalized without the presence of inhibitors. The presence of inhibitors has shown to be necessary to crystalize ADAMTS5 by significantly increasing the protein unfolding temperature (approximately 27 °C), thereby increasing the stability of ADAMTS5 (Shieh et al., 2008; Tortorella et al., 2009).

3.15 AlphaFold protein structure computation

AlphaFold DB developed by DeepMind and EMBL-EBI provided a computational prediction of the structure of ADAMTS13 (Jumper et al., 2021; Varadi et al., 2022). AlphaFold is a recently developed artificial intelligence system that predicts a protein's 3D structure based on its amino acid sequence with high degree of accuracy.

The human ADAMTS13 computational structure was retrieved from https://alphafold.ebi.ac.uk/entry/Q76LX8 (PDB ID: AF-Q76LX8-F1-model_v2).

3.16 Statistical analysis

GraphPad Prism software (La Jolla, CA, USA) was used to perform statistical analyses. Values were expressed as mean ± standard deviation and p-values <0.05 were considered significant. A one-way analysis of variance (ANOVA) was performed to determine significant differences between groups followed by Tukey's multiple comparisons test. Pearson's correlation coefficient was used to calculate correlations.

Chapter 4: Results – Evaluate the Role of Distal Domains in the Resistance of ADAMTS13 to Protease Inhibitors

4.1 ADAMTS13 deletion constructs

Full-length ADAMTS13, and deletion constructs MDTCS and MD were stably integrated into mammalian 293T cells, expressed, and purified by Q-Sepharose FF and Ni-NTA. SYPRO Ruby staining was used to assess the purity of each construct, and Western blot was used to verify the presence of each construct. Full-length ADAMTS13 was detected at 180 kDa (Figure 4.1A), MDTCS was detected at 80 kDa (Figure 4.1B), and MD with its MBP tag attached was detected at 80 kDa (Figure 4.1C). Upon removal of the MBP tag by TEV protease, MD was detected at 35 kDa (Figure 4.1C). Impurities were detected on the total protein stain. However, all constructs were detected at the correct molecular weight by Western blot, and protein concentrations were quantified by ELISA. The functional activity of each ADAMTS13 construct was evaluated using FRETS-VWF73 and compared to values of commercial ADAMTS13 and MDTCS (R&D Systems) and/or with previous literature that utilized the same ADAMTS13 truncation constructs (Table 4.1) (Gao et al., 2006). Since our constructs were proteolytically active and performed similar to commercial and reported values in literature, these impurities did not affect the overall interpretation of studying the inhibition of these constructs.

A. ADAMTS13

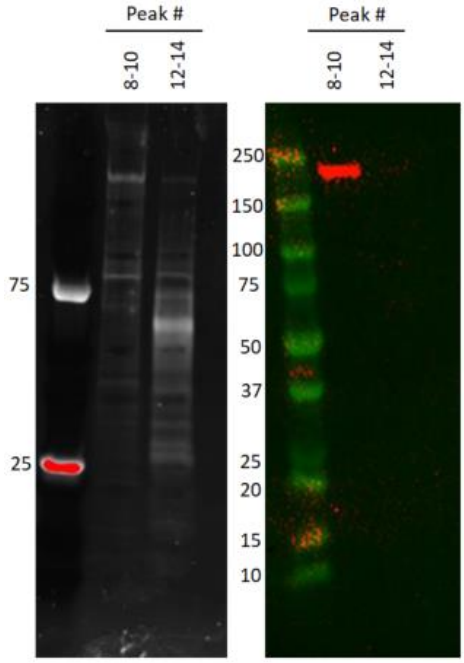

B. MDTCS

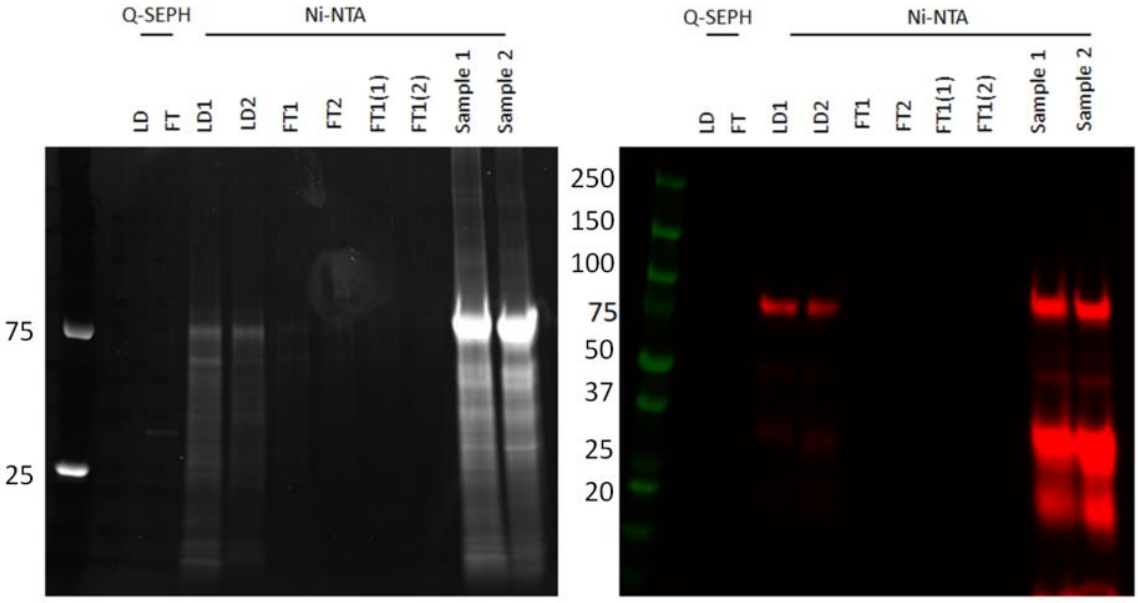

C. MD-MBP and MD

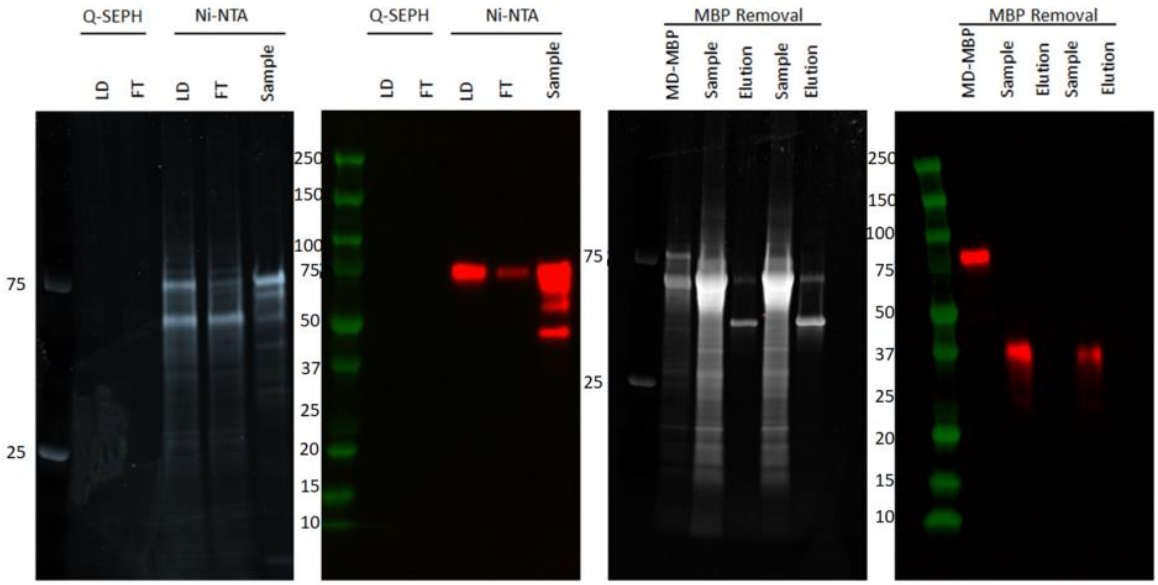

Figure 4.1. Purification of ADAMTS13 deletion constructs. A. Full-length ADAMTS13 was purified using high-performance liquid chromatography. Full-length ADAMTS13 was observed at its expected molecular weight of 180 kDa. **B.** MDTCS was observed at its expected molecular weight of 80 kDa **C.** MD with its MBP tag was observed at its expected molecular weight of 80 kDa. Upon removal of the MBP tag, MD was observed at its expected molecular weight of 35 kDa. MDTCS and MD were purified using Q-Sepherose FF, followed by Ni-NTA. All gels were performed using a 4 to 20% polyacrylamide gel under reducing conditions. Samples were diluted 1/100. SYPRO Ruby staining is shown in grey and Western blot is shown in red.

Table 4.1. Specific proteolytic activity of ADAMTS13, MDTCS, and MD determined by FRETS-VWF73. Concentrations: ADAMTS13 – 20 nM; MDTCS – 20 nM; MD – 1 µM; FRETS-VWF73 – 1 µM. Statistical analysis compared to ADAMTS13; ns $p > 0.05$, * $p \leq 0.05$, ** $p \leq 0.01$, *** $p \leq 0.001$, **** $p \leq 0.0001$.

	Proteolytic Activity (RFU x s^{-1} x nM)	**Fold change**
WT-ADAMTS13	51.52±3.98	
WT-MDTCS	92.73±4.82****	1.80 (↑)
MD	2.83±0.33****	32.77 (↓)

4.2 Confirming the resistance of ADAMTS13 towards protease inhibitors

ADAMTS13 resistance to natural and synthetic inhibitors of metalloproteases was first examined. Full-length ADAMTS13 displayed a proteolytic activity of 51.52±3.98 RFU x s^{-1} x nM^{-1}, which did not differ following a 6 hour incubation with approximately 10-fold molar excess A2M, TIMP-1, -2, -3, -4, or Marimastat (Figure 4.2A). Western blot analysis confirmed that after 6 hour incubation, ADAMTS13 did not cleave the bait region of A2M, whereas ADAMTS5 did cleave the bait region, as indicated by the presence of an 80 kDa band (Figure 4.2B). These data demonstrate that ADAMTS13 is resistant to known natural and synthetic protease inhibitors of metalloproteases.

A. Inhibitor effect on proteolysis of FRETS-VWF73 **B. A2M Western blot**

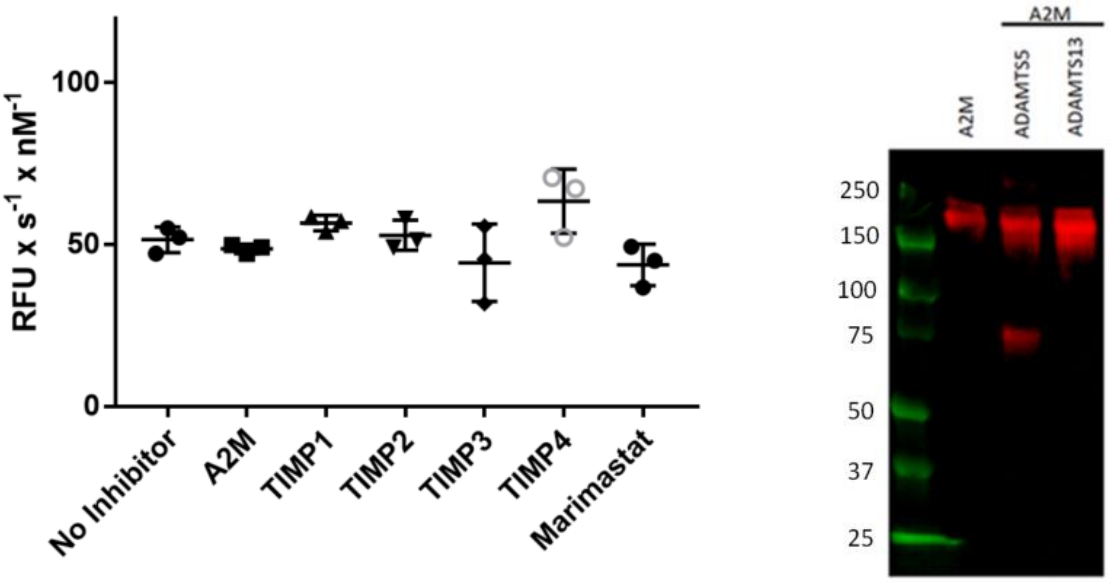

Figure 4.2. Confirming the resistance of ADAMTS13 towards protease inhibitors. A. Full-length ADAMTS13 (20 nM) was incubated with A2M, TIMP1, TIMP2, TIMP3, TIMP4, and Marimastat (250 nM) for 6 hours, and the proteolytic activity was measured using 1 μM FRETS-VWF73. ADAMTS13 displayed resistance towards all inhibitors. Proteolytic activity measured in RFU x s^{-1} x nM^{-1}. N=3. **B.** Western blot was used to identify the cleaved form of A2M at 80 kDa. ADAMTS5 was used as a positive control. Full-length ADAMTS13 was not able to cleave A2M. ADAMTS5 (250 nM), full-length ADAMTS13 (250 nM) and A2M (50 nM). N=3.

4.3 Characterizing MDTCS in the presence of inhibitors

The deletion construct MDTCS lacks the seven additional TSP-1 and two CUB domains that maintain ADAMTS13 in a closed conformation and responsible for global latency in circulation. We tested whether removing the closed conformation sensitizes MDTCS after 6 hour inhibition. MDTCS displayed a proteolytic activity of 92.73±4.82 RFU x s^{-1} x nM^{-1}, which did not differ in the presence of 10-fold molar excess A2M, TIMP-1, -2, -3, -4, or Marimastat (Figure 4.3A). As expected, the proteolytic activity of MDTCS towards FRETS-VWF73 was 2-fold greater than full-length ADAMTS13 due to the absence of the auto-inhibitory effect of the closed conformation. Resistance towards A2M was confirmed using Western blot by identifying the presence of cleaved A2M at 80 kDa after 6 hour incubation (Figure 4.3B). MDTCS did not cleave A2M, consistent with lack of inhibition observed in the FRETS-VWF73 activity assay. Therefore, MDTCS is resistant to inhibitors of metalloproteases, similar to full length ADAMTS13.

A. Inhibitor effect on proteolysis of FRETS-VWF73 **B. A2M Western blot**

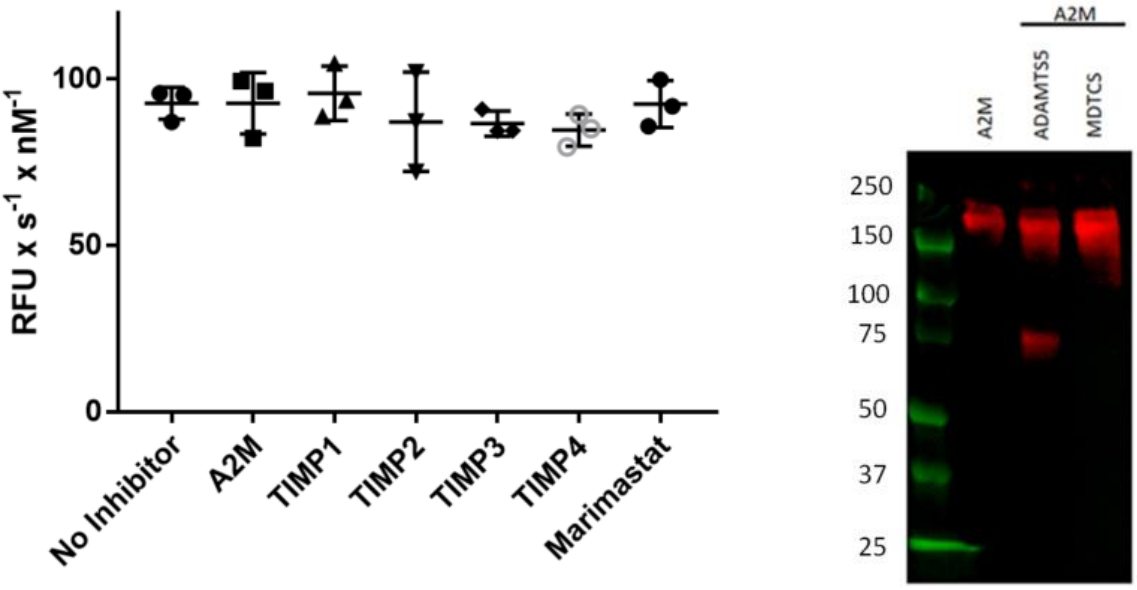

Figure 4.3. Characterizing the resistance of MDTCS towards protease inhibitors. A. MDTCS (20 nM) was incubated with A2M, TIMP1, TIMP2, TIMP3, TIMP4, and Marimastat at concentration of 250 nM for 6 hours, and the proteolytic activity was measured using 1 μM FRETS-VWF73. MDTCS displayed resistance towards all inhibitors. Proteolytic activity measured in RFU x s^{-1} x nM^{-1}. N=3. **B.** Western blot was used to identify the cleaved form of A2M at 80 kDa after 6 hour incubation. ADAMTS5 was used as a positive control. MDTCS was not able to cleave A2M. ADAMTS5 (250 nM), MDTCS (250 nM) and A2M (50 nM). N=3.

4.4 Characterizing MD in the presence of inhibitors

The MD deletion construct lacks the important exosites –TCS in addition to the closed conformation. The proteolytic activity of this construct is substantially lower than MDTCS and full length ADAMTS13. Therefore, the concentration of MD was increased to 1 μM to meet the detection threshold, and the concentration of inhibitors was increased to maintain a higher molar ratio of inhibitor to protease. MD displayed a proteolytic activity of 2.83±0.33 RFU x s^{-1} x nM^{-1}, which did not differ in the presence of molar excess A2M, TIMP-1, -2, -3, -4, or Marimastat after 6 hour incubation (Figure 4.4A). Western blot of MD did not show the cleaved form of A2M after 6 hour incubation, consistent with its resistance to inhibition observed in the FRETS-VWF73 assay. These data demonstrate that MD is resistant to known inhibitors of proteases similar to full length ADAMTS13 and truncated MDTCS.

A. Inhibitor effect on proteolysis of FRETS-VWF73 **B. A2M Western blot**

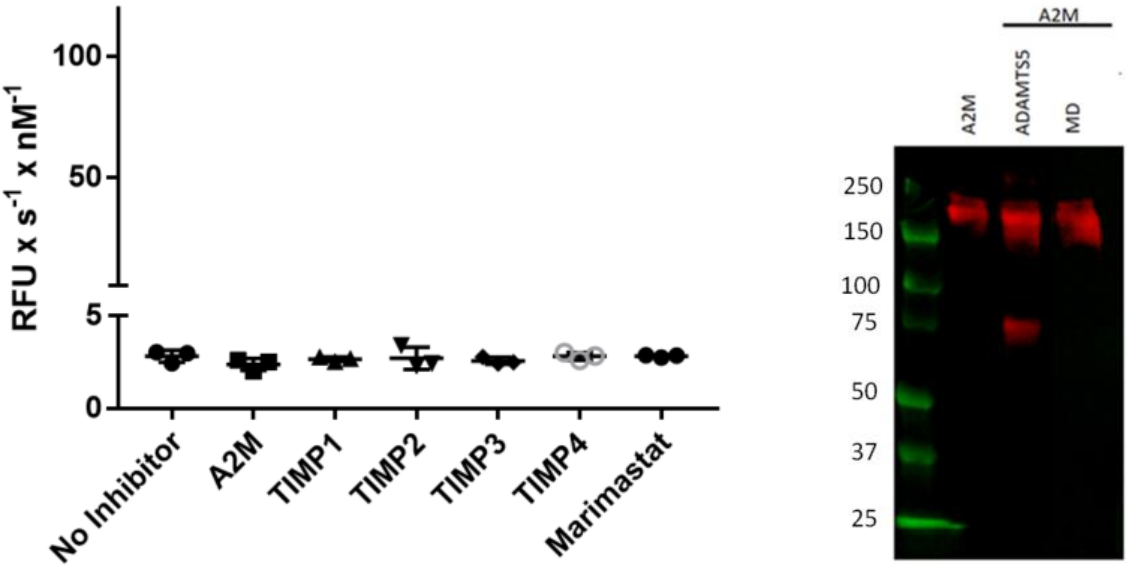

Figure 4.4. Characterizing the resistance of MD towards protease inhibitors. A. MD (1 μM) was incubated for 6 hours with A2M, TIMP1, TIMP2, TIMP3, TIMP4, and Marimastat (2.5 μM), and the proteolytic activity was measured using 1 μM FRETS-VWF73 assay. MD displayed resistance towards all inhibitors. Proteolytic activity measured in RFU x s^{-1} x nM^{-1}. N=3. **B.** Western blot was used to identify the cleaved form of A2M at 80 kDa after 6 hour incubation. MD was not able to cleave A2M. ADAMTS5 (250 nM), MD (250 nM) and A2M (50 nM). N=3.

Chapter 5: Results – Investigate the Role of the Closed Conformation and Active Site in Protecting ADAMTS13 from Protease Inhibitors

5.1 ADAMTS13/ADAMTS5 chimeric constructs

Data from the truncation studies suggest that the resistance of ADAMTS13 to inhibition can be explained by features in the metalloprotease and disintegrin domains. These data do not exclude the possibility that the closed conformation of ADAMTS13 contributes additional protection against inhibition. Based on our findings, the next step was to investigate the role of the closed conformation and the active site region of ADAMTS13 by constructing chimeric proteases with an ADAMTS protease that is known to be inhibited. Therefore, we selected ADAMTS5 because numerous studies have demonstrated that ADAMTS5 can be inhibited by multiple classes of inhibitors, including A2M (Tortorella et al., 2004), TIMP3 (Fan & Kassiri, 2020; Kashiwagi et al., 2001; Murphy, 2011), and small molecule MMP inhibitors (Meisel & Chang, 2017; Rasmussen & McCann, 1997; Tortorella et al., 2009). The goal of these chimeric constructs was to define the structural features of ADAMTS13 that render it resistant to inhibition. In addition to these chimeras, we designed peptides that engaged the disintegrin domain in an attempt to sensitize ADAMTS13 to inhibition.

Chimeric constructs MD13/TCS5, MD5/TCS13, and MD5(TCS-CUB13) were stably integrated into mammalian 293T cells, expressed, and purified by Q-Sepharose FF and NI-NTA chromatography. Chimeric construct M13/DTCS5 was transiently transfected into HEK 293T cells using Transport 5 reagent in OPTI-MEM. M13/DTCS5 was not isolated from the OPTI-MEM. After 72 hours, the OPTI-MEM was collected,

concentrated, and buffer exchanged into the ADAMTS13 reaction buffer. Total protein staining (SYPRO Ruby) was used to assess the purity of each construct. Impurities were detected on the total protein stain. All constructs were detected by Western blot V5 antibody at their correct molecular weight: MD13/TCS5 at 80 kDa (Figure 5.1A), MD5/TCS13 at 80 kDa (Figure 5.1B), MD5(TCS-CUB13) at 180 kDa (Figure 5.1C), and M13/DTCS5 at 80 kDa (Figure 5.1D). Concentrations were determined by an ELISA, which was capable of detecting both our truncated and chimeric constructs. Functional activity was pertinent to our studies; and therefore, proteolytic activity of chimeras with the active site from ADAMTS13 was verified using a FRETS-VWF73 assay (Table 5.1). These values were found to be consistent with values observed in previous literature for similar chimeric constructs (Gao et al., 2006). Chimeras with the active site from ADAMTS5 were determined proteolytically active by assessing for the cleaved form of aggrecan by Western blot (Figure 5.1E). For the purpose of studying inhibition, functional activity was more pertinent to our study, rather than the purity of our constructs/chimeras. Therefore, these impurities did not affect the overall interpretation of our results.

A. MD13/TCS5

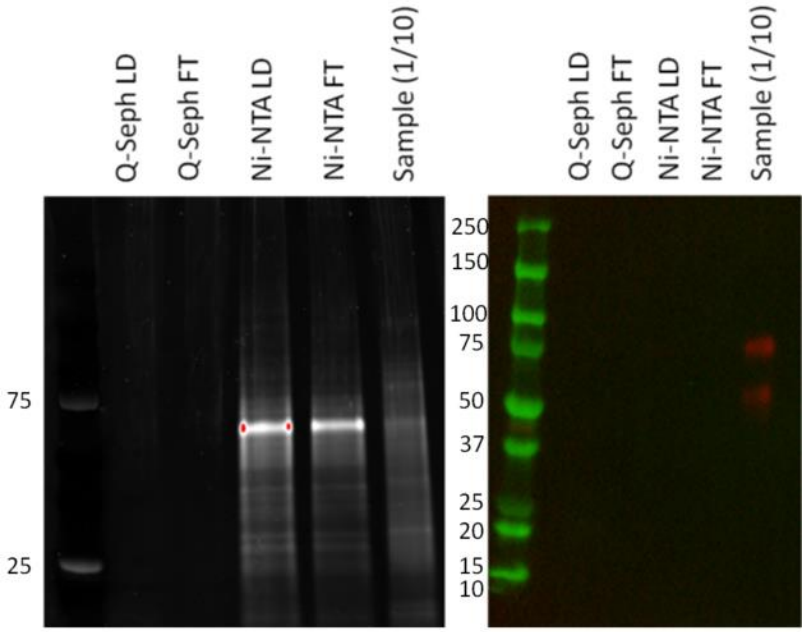

B. MD5/TCS13

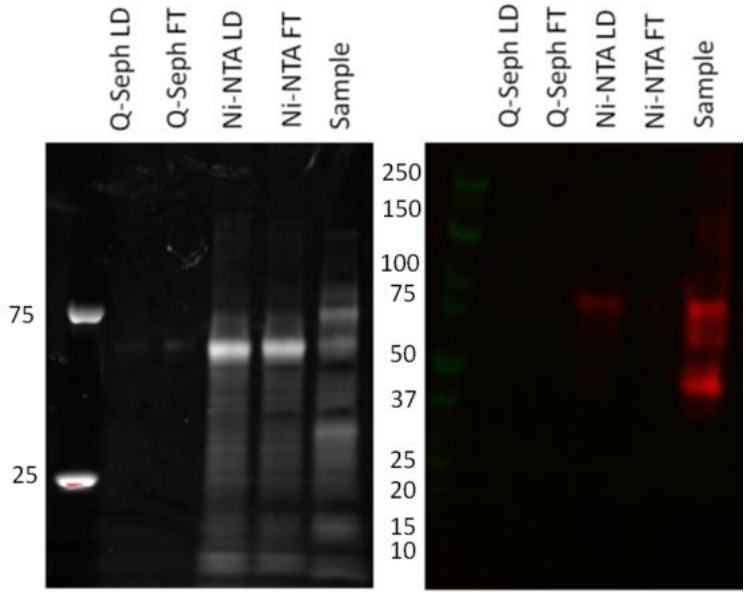

C. MD5(TCS-CUB13) **D. M13/DTCS5**

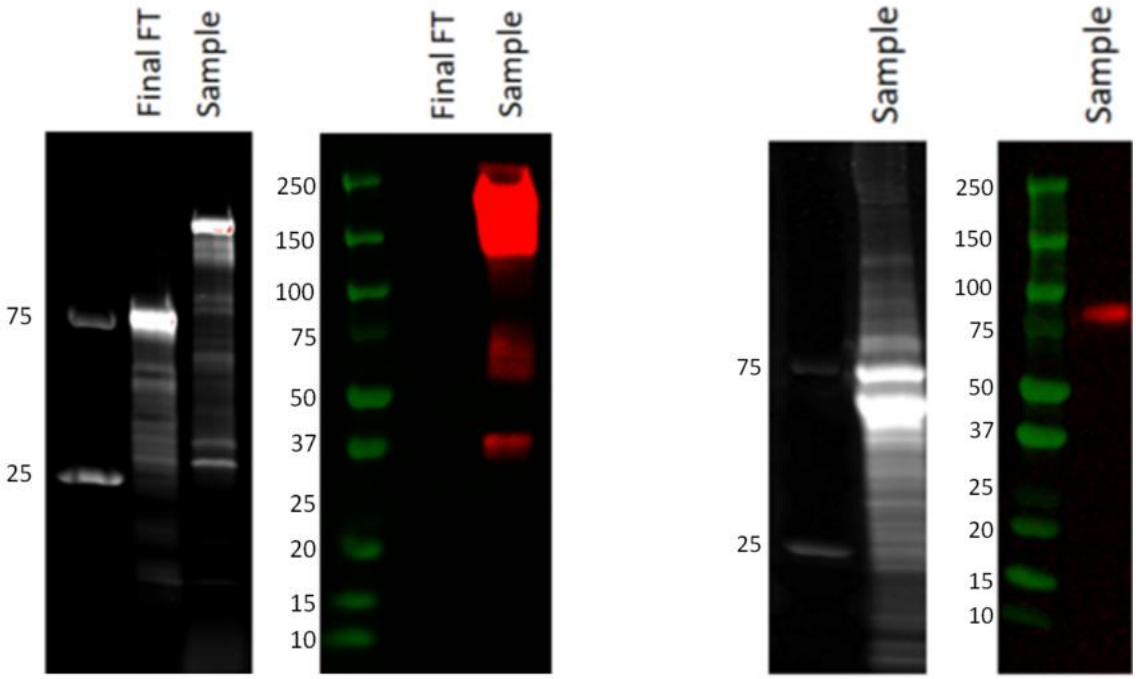

E. Confirming proteolytic activity of ADAMTS5, MD5/TCS13, and MD5(TCS-CUB13) by Western blot assessment of aggrecan

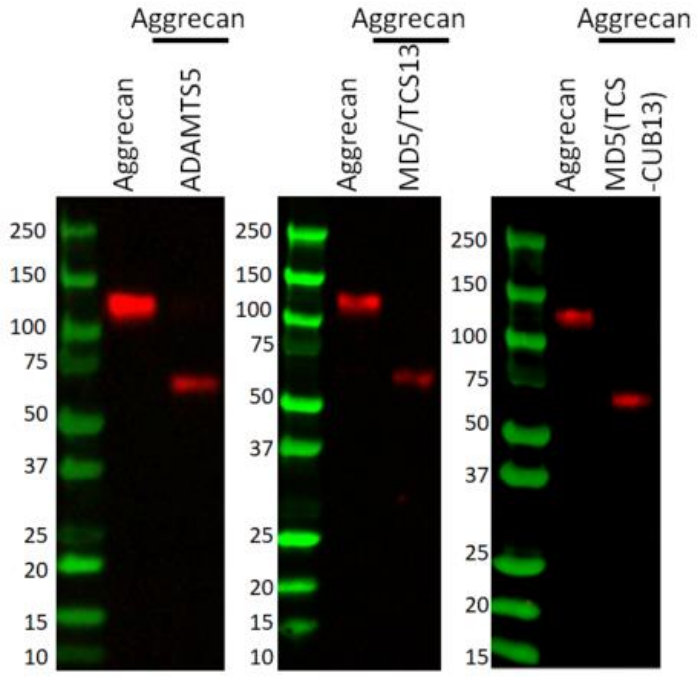

Figure 5.1. Purification of chimeric constructs. A. MD13/TCS5 was detected at 80 kDa on SYPRO and Western blot. **B.** MD5/TCS13 was detected at 80 kDa on SYPRO and Western blot. **C.** MD5(TCS-CUB13) was detected at 180 kDa on SYPRO and Western blot. **D.** M13/DTCS5 was detected at 80 kDA on SYPRO and Western blot. MD13/TCS5, MD5/TCS13, and MD5(TCS-CUB13) were purified using Q-Sepherose FF, followed by Ni-NTA. M13/DTCS5 concentrated, but not purified from OPTI-MEM. All gels were performed using a 4 to 20% polyacrylamide gel under reducing conditions. SYPRO Ruby staining is shown in grey and Western blot for V5 antibody is shown in red. E. Anti-aggrecan Western blot verifying ADAMTS5, MD5/TCS13, and MD5(TCS-CUB13) were proteolytically active by assessing the cleaved form of aggrecan at 65 kDa after 1 hour incubation. Concentrations: ADAMTS5 – 20 nM; MD5/TCS13 – 20 nM; MD5(TCS-CUB13) – 100 nM; aggrecan – 100 nM.

Table 5.1. Specific proteolytic activity of WT-MDTCS, MD13/TCS5, and M13/DTCS5 determined by FRETS-VWF73. Concentrations: WT-MDTCS – 20 nM; MD13/TCS5 – 1 µM; M13/DTCS5 – 1 µM; FRETS-VWF73 – 1 µM. Statistical analysis compared to WT-MDTCS; ns $p > 0.05$, * $p \leq 0.05$, ** $p \leq 0.01$, *** $p \leq 0.001$, **** $p \leq 0.0001$.

	Proteolytic Activity (RFU x s^{-1} x nM)	**Fold change**
WT-MDTCS	92.73±4.82	
MD13/TCS5	1.77±0.19****	52.39 (↓)
M13/DTCS5	0.03±0.02****	3091 (↓)

5.2 Characterizing ADAMTS5 inhibition towards protease inhibitors

Validating the inhibition of ADAMTS5 to protease inhibitors was an important step to ensure that ADAMTS5 can serve as a positive control for this project, and to confirm consistency with previous literature (Fan & Kassiri, 2020; Kashiwagi et al., 2001; Meisel & Chang, 2017; Rasmussen & McCann, 1997; Tortorella et al., 2004, 2009). The activity of ADAMTS5 was monitored by its ability to cleave its substrate, aggrecan (G1-IGD-G2). Western blotting was used to detect the cleaved form of aggrecan at 65 kDa (Figure 5.2A), and quantify percent cleavage (Figure 5.2B). After 1 hour, 57.17±16.91% of the aggrecan was cleaved by ADAMTS5 in the absence of inhibitors. Aggrecan cleavage was significantly reduced following a 2 hour incubation with 10-fold molar excess of A2M (10.47±3.00%, $p \leq 0.0001$), TIMP3 (4.10±2.48%, $p \leq 0.0001$), or Marimastat (0.93±1.04%; $p \leq 0.0001$). TIMP1, TIMP2, and TIMP4 did not significantly reduce the ability of ADAMTS5 to cleave aggrecan ($p > 0.05$). Therefore, future experiments focussed on exploring the capacity of A2M, TIMP3, and Marimastat to inhibit ADAMTS13 and ADAMTS5 chimeric constructs.

A. Aggrecan cleavage **B. Quantification of Western blot**

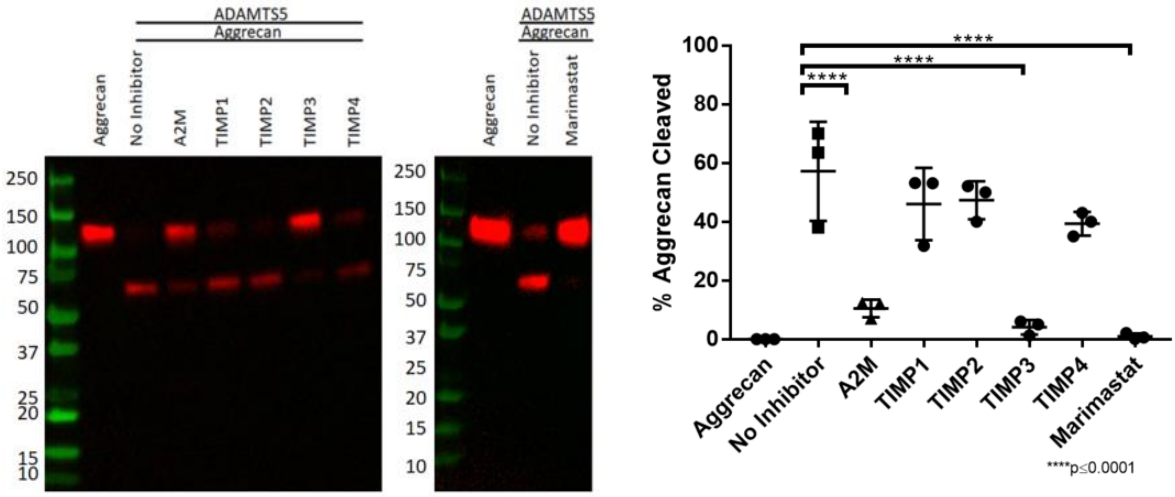

Figure 5.2. Characterizing and confirming the inhibition of ADAMTS5 towards protease inhibitors. A. Western blot assessing for cleaved aggrecan at 65 kDa (intact aggrecan: 120 kDa). ADAMTS5 (20 nM) incubated with or without inhibitors (250 nM) for 2 hours, followed by a 1 hour incubation with aggrecan (G1-IGD-G2, 100 nM). N=3. **B.** Western blot quantification expressed as percent aggrecan cleaved using anti-aggrecan antibody. A2M, TIMP3, and Marimastat were potent inhibitors of ADAMTS5. N=3, ****$p \leq 0.0001$.

5.3 Characterizing ADAMTS5/ADAMTS13 chimeric constructs towards protease inhibition

5.3.1 MD13/TCS5 chimeric construct

MD13/TCS5 consists of the MD domains from ADAMTS13 fused to the –TCS domains from ADAMTS5. Similar to the ADAMTS13 deletion construct MD, the proteolytic activity of MD13/TCS5 was also below the detection threshold of the FRETS-VWF73 assay. Therefore, concentration of MD13/TCS5 was increased to match the detection threshold, and the inhibitor concentrations were adjusted accordingly to maintain molar excess of inhibitor. MD13/TCS5 cleaved FRETS-VWF73 at a proteolytic rate of 1.77±0.19 RFU x s^{-1} x nM^{-1} (Figure 5.3A), similar to truncation construct MD. The proteolytic activity of MD13/TCS5 was not reduced following a 6-hour incubation with A2M, TIMP3, or Marimastat indicating its resistance (Figure 5.3A). MD13/TCS5 resistance to A2M was also confirmed by the absence of the 80 kDa cleavage product on a Western blot (Figure 5.3B). These observations are comparable to the MD13 deletion construct and suggest that the metalloprotease and disintegrin domains of ADAMTS13 contribute to its resistance to protease inhibitors.

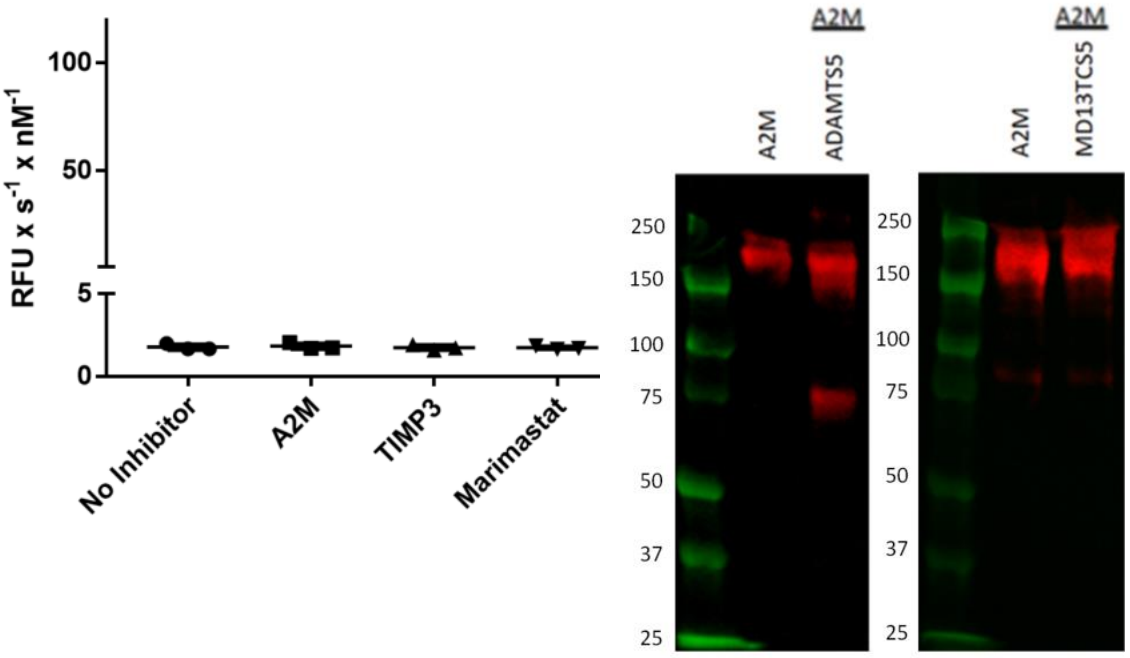

Figure 5.3. Investigating the resistance of MD13/TCS5 towards protease inhibitors. **A.** MD13/TCS5 (1 μM) was incubated with A2M, TIMP3, and Marimastat (2.5 μM) for 6 hours. Proteolytic activity was measured using a FRETS-VWF73 assay. RFU x s^{-1} x nM^{-1}. N=3. **B.** Western blot was used to assess the cleaved form of A2M (50 nM) at 80 kDa using anti-A2M antibody in the presence of MD13/TCS5 (250 nM). ADAMTS5 (250 nM) was used as a positive control. MD13/TCS5 was unable to cleave A2M. N=3. MD13/TCS5 was resistant towards A2M, TIMP3, and Marimastat.

5.3.2 M13/DTCS5 chimeric construct

The chimera M13/DTCS5 was next constructed to evaluate the contribution of the disintergrin and metalloprotease domains to ADAMTS13 resistance to inhibition. M13/DTCS5 contains the metalloprotease domain of ADAMTS13 and the DTCS exosite domains from ADAMTS5. Similar to the deletion construct MD and MD13/TCS5, M13/DTCS5 concentrations were increased to meet the detection threshold of FRETS-VWF73, and inhibitor concentrations were adjusted to maintain molar ratios comparable to previous experiments. M13/DTCS5 displayed a specific activity of 0.03±0.02 RFU x s^{-1} x nM^{-1}, approximately 100-fold lower than MD, 3000-fold lower than MDTCS, and 1700-fold lower than ADAMTS13 (Figure 5.4A and Table 5.1). These data are consistent with previous published data demonstrating the role of the disintegrin, cysteine, and spacer domains are important exosites for ADAMTS13 proteolysis of VWF and VWF73 (Gao et al., 2006; Muia et al., 2014; Petri et al., 2019). In the presence of inhibitors, after a 6-hour incubation the proteolytic activity of M13/DTCS5 was not reduced with molar excess A2M, TIMP3, or Marimastat (Figure 5.4A). Resistance to A2M inhibition was confirmed by using Western blot and confirming the absence of the A2M cleavage product at 80 kDa, as expected (Figure 5.4B). These findings suggest that the metalloprotease domain of ADAMTS13 contributes to the resistance of ADAMTS13 to protease inhibitors.

A. Inhibitor effect on proteolysis **B. A2M Western blot**

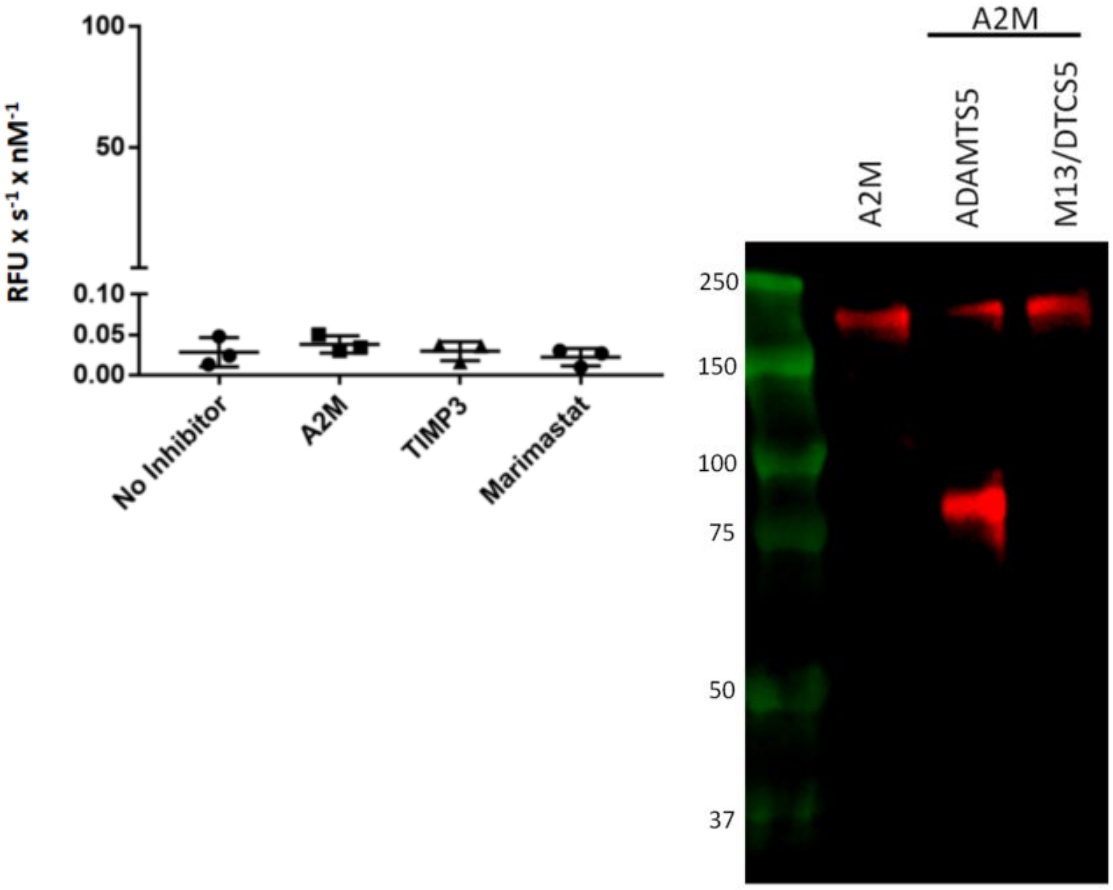

Figure 5.4. Investigating the resistance of M13/DTCS5 towards protease inhibitors. **A.** M13/DTCS5 (1 µM) was incubated with A2M, TIMP3, and Marimastat (2.5 µM) for 6 hours. Proteolytic activity was measured using a FRETS-VWF73 assay. RFU x s^{-1} x nM^{-1}. N=3. **B.** Western blot was used to assess the cleaved form of A2M (50 nM) at 80 kDa using anti-A2M antibody in the presence of M13/DTCS5 (250 nM). ADAMTS5 (250 nM) was used as a positive control. N=3.

5.3.3 MD5/TCS13 chimeric construct

The previous experiments have revealed that the metalloprotease domain of ADAMTS13 contains features that protect it from natural and synthetic protease inhibitors. However, these data do not exclude the possibility that the exosites and distal domains confer additional protections on ADAMTS13. The MD5/TCS13 chimera is the reciprocal to MD13/TCS5 chimeric construct, and consists of the active site region of ADAMTS5, and the –TCS exosite domains of ADAMTS13. The activity of MD5/TCS13 was evaluated by monitoring the cleavage of aggrecan (G1-IGD-G2) at 65 kDa by Western blot and expressed as a percentage of cleaved aggrecan. After a 1 hour incubation, MD5/TCS13 cleaved 79±2% of aggrecan (Figure 5.5A and B). To test MD5/TCS13 resistance towards protease inhibitors, MD5/TCS13 was incubated for 2 hours with the inhibitors 10-fold molar excess A2M, TIMP3, and Marimastat at followed by a 1 hour incubation with aggrecan (G1-IGD-G2). In the presence of these inhibitors no significant cleavage product of aggrecan was detected at 65 kDa ($p \leq 0.0001$) (Figure 5.5A and B). Therefore, this data suggests that the –TCS exosite domains of ADAMTS13 do not contribute to its resistance to natural and synthetic protease inhibitors.

A. Quantification of aggrecan cleavage w/ inhibitors **B. Aggrecan Western blot**

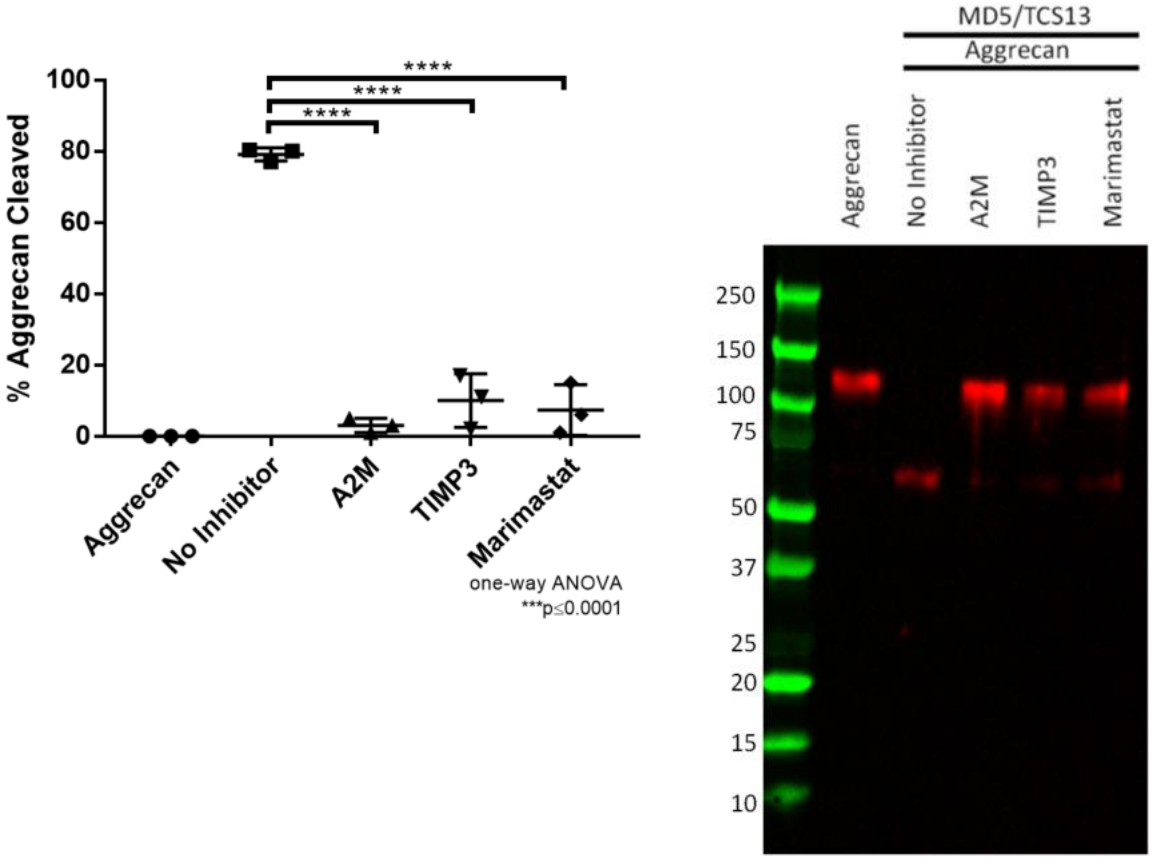

Figure 5.5. Investigating the resistance of MD5/TCS13 towards protease inhibitors. **A.** MD5/TCS13 (20 nM) was incubated for 2 hours with and without protease inhibitors (250 nM), followed by a 1 hour incubation with aggrecan (G1-IGD-G2) (100 nM). N=3; ****p≤0.0001. **B.** Western blot assessing for cleaved aggrecan at 65 kDa (intact aggrecan: 120 kDa) using anti-aggrecan antibody. Western blot quantification was expressed as percent aggrecan cleaved. N=3.

5.3.4 MD5(TCS-CUB13) chimeric construct

The previous data using MD5/TCS13 demonstrated that the –TCS exosite domains do not contribute to the resistance of ADAMTS13 to protease inhibitors. Next, the MD5(TCS-CUB13) chimera was constructed to test whether the closed conformation contributes to resistance. This construct extended MD5/TCS13 to include the 7 additional TSP-1 and tandem CUB domains that were important for maintaining ADAMTS13 in a closed conformation, and tested whether this conformation affected the capacity of the metalloprotease domain to cleave substrates or bind to inhibitors.

The time to 50% aggrecan cleavage (EC50) of MD5/TCS13 was determined to be 40±2 minutes, whereas the EC50 of 4-fold excess MD5(TCS-CUB13) was determined at 522±36 minutes (Figure 5.6A). Therefore, these data indicated that the closed conformation imposes an approximately 50-fold protection against MD5(TCS-CUB13) aggrecanase activity. Next, we compared the susceptibility of MD5(TCS-CUB13) to inhibition by A2M, TIMP3, or Marimastat. Thus, MD5(TCS-CUB13) or MD5/TCS13 was incubated with inhibitor for 2 hours, followed by incubation with aggrecan for 18 hours because our data from Figure 5.6A showed that MD5(TCS-CUB13) completely cleaves aggrecan by 18 hours. Western blot analysis demonstrates that MD5(TCS-CUB13) was unable to cleave aggrecan in the presence of protease inhibitors; therefore, the closed conformation was unable to completely protect MD5(TCS-CUB13) from inhibition (Figure 5.6B). An A2M time-course study was conducted to test whether the closed conformation affected the rate of inhibition. Western blot analysis of A2M showed that the cleaved form of A2M was initially detected after 1 hour in the presence of

MD5/TCS13; however, the cleaved form of A2M was detected after 2 hours in the presence of MD5(TCS-CUB13) (Figure 5.6C). These data suggest that the closed conformation impairs inhibitor access to the active site of MD5. Overall, experiments with MD5(TCS-CUB13) suggest that the closed conformation partially contributes to the resistance of ADAMTS13 to protease inhibitors by blocking access to the active site.

A. Percent aggrecan cleaved

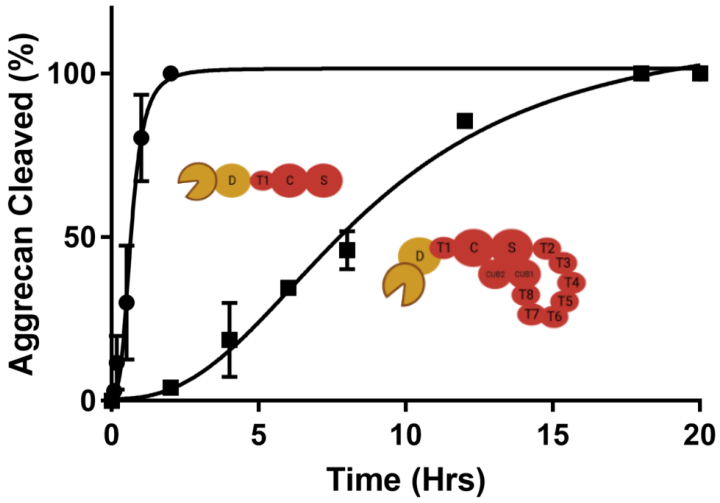

B. Aggrecan Western blot

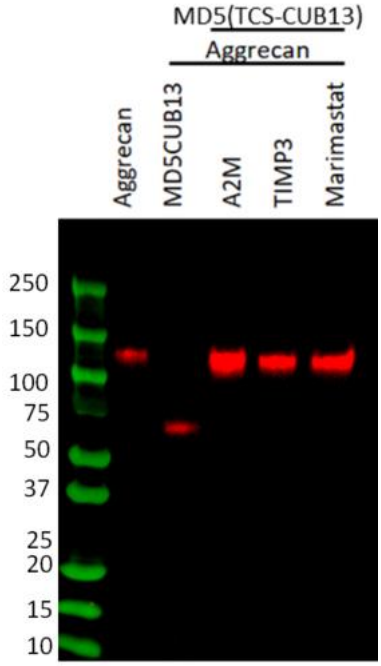

C. A2M Western blot

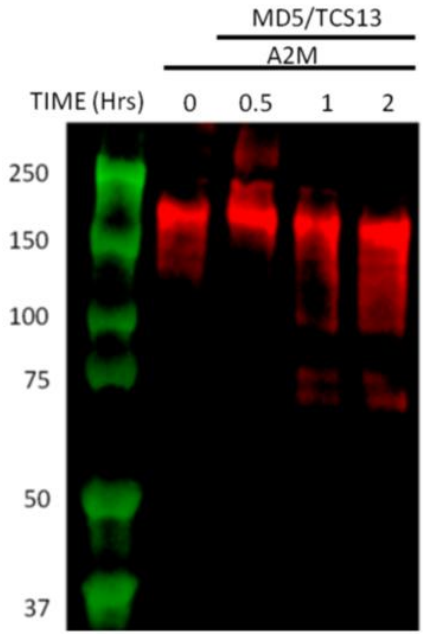

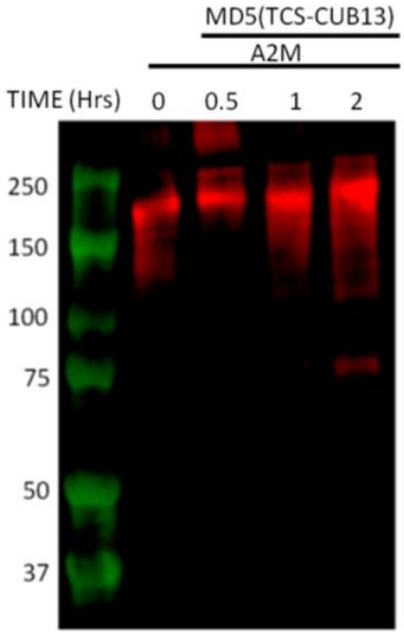

Figure 5.6. Investigating the resistance of MD5(TCS-CUB13) towards protease inhibitors. A. Time-course of MD5/TCS13 (25nM) and MD5(TCS-CUB13) (100 nM) chimeras with aggrecan (G1-IGD-G2) (100 nM). Expressed as percent aggrecan cleaved based on the presence of the cleaved aggrecan band 65 kDa by Western blot. Modeled using non-linear regression allosteric sigmoidal equation: $Y = V_{max}*X^h/(EC50^h+X^h)$. Where X: time (hours), Y: cleaved aggrecan (%), EC50: time at 50% aggrecan cleavage (half-maximal velocity), h: hillslope factor (no unit). N=3. Yellow: ADAMTS5; Red: ADAMTS13. **B.** Western blot of MD5(TCS-CUB13) (100 nM) incubated for 2 hours with either A2M, TIMP3, or Marimastat at concentration of 250 nM, followed by an 18 hour incubation of MD5(TCS-CUB13)/inhibitor complex with aggrecan (100 nM). Cleaved aggrecan band detected at 65 kDa using anti-aggrecan antibody. N=3. **C.** Western blot analysis of the cleaved form of A2M (50 nM) at 80 kDa in the presence of MD5(TCS-CUB13) (100 nM) (left) or MD5/TCS13 (25 nM) (right) at 0, 0.5, 1, 2 hours. N=3.

5.4 Engagement of the disintegrin domain

Although the closed conformation contributes to the protection of ADAMTS13 against protease inhibitors, our data suggests that features within and surrounding the active site are primarily responsible for protecting ADAMTS13 from inhibition. Although M13/DTCS5 was also resistant to protease inhibitors (Figure 5.4), the close proximity of the disintegrin domain to the metalloprotease domain may still be imposing a protective function in the chimera. Therefore, we designed two VWF peptides that specifically engage the disintegrin domain in an attempt to sensitize the MD deletion construct to inhibition (D-Peptide: SDEIKRLPGDIQ; T-VWF: TGNPASDEIKRLPGDIQ) (Figure 5.7A). Further, we designed a third peptide with a lysine substitution at P3' (K-VWF: KGNPASDEIKRLPGDIQ), based on previous work suggesting preference for positively charged residues at that position (Kretz et al., 2015).

To confirm binding to the exosite within the disintegrin domain, we first tested the capacity of these peptides to block VWF73 cleavage by MD. Each peptide elicited a dose-dependent decrease in the rate of FRETS-VWF73 cleavage (D-Peptide: IC50 4.74±0.23 mM, T-VWF: IC50 4.07±1.08 mM, and K-VWF: IC50 0.80±0.28 mM) (Figure 5.7B). These data are consistent with peptide binding to the disintegrin domain of ADAMTS13, and confirms previous data suggesting a preference for lysine at the P3' position of VWF73 (Kretz et al., 2015) (Figure 5.5B).

Next, each disintegrin-domain engaging peptide was incubated with MD for 2 hours to examine their capacity to sensitize MD to inhibition by molar excess A2M, TIMP3, or Marimastat. There was no inhibition of MD observed in the presence of these

peptides by any of the inhibitors tested (Figure 5.7C). These findings suggest that the disintegrin domain is not primarily responsible for protecting ADAMTS13 against inhibition. Further, these findings support the hypothesis that features within the metalloprotease domain protect ADAMTS13 against protease inhibitors.

A. Interaction between ADAMTS13 and VWF73

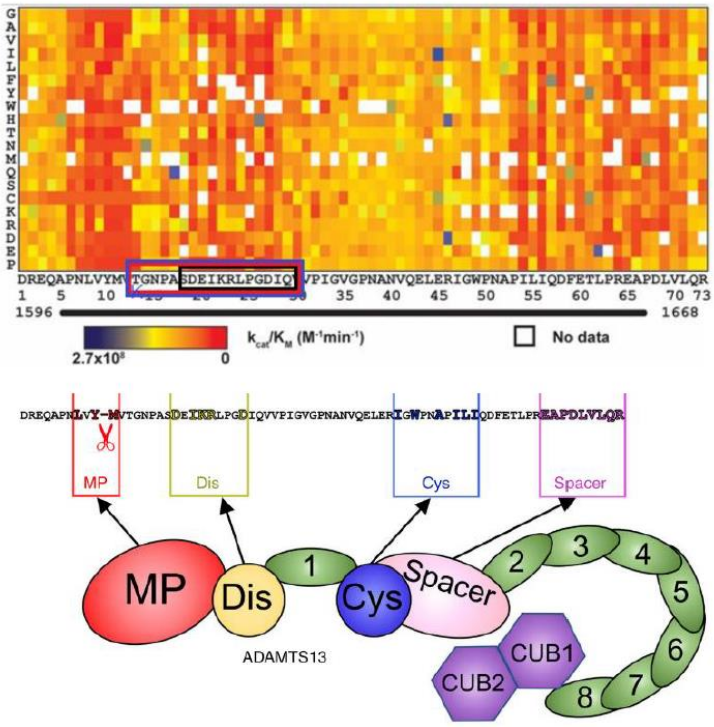

D-Peptide: SDEIKRLPGDIQ
T-VWF: TGNPASDEIKRLPGDIQ
K-VWF: KGNPASDEIKRLPGDIQ

B. VWF peptide titration

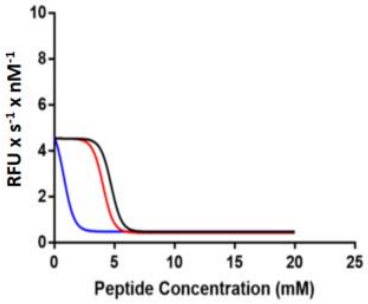

IC50: MD
D-Peptide: LogIC50 4.74±0.23
T-VWF: LogIC50 4.07±1.08
K-VWF: LogIC50 0.80±0.28

C. MD & VWF peptides w/ inhibitors

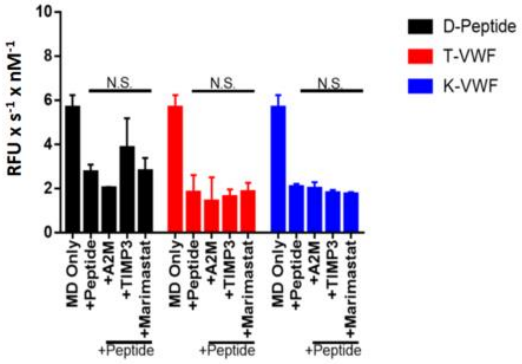

Figure 5.7. Peptide engagement of the disintegrin domain. A. Peptides were designed based on previous work examining the interaction between VWF73 and ADAMTS13 (top). Schematic of ADAMTS13 domains interacting with residues of VWF (bottom). D-Peptide: SDEIKRLPGDIQ; T-VWF: TGNPASDEIKRLPGDIQ; K-VWF: KGNPASDEIKRLPGDIQ (lysine substitution at P3' position); Red: inhibit cleavage; Blue: enhance cleavage. Adapted from Kretz et al. PNAS (2015) & Petri et al. Nat Comm (2019). **B.** Testing the capacity of disintegrin-engaging peptides to block VWF73 cleavage by MD (1 µM) in a dose-dependent manner (mM). The peptide inhibition was modelled by the non-linear regression equation: Y = (Top-Bottom)/(1+10^(X-LogIC50)) + Bottom. Where X: logmolar concentration (mM), Y: proteolytic activity (RFU x s^{-1} x nM^{-1}), Top and Bottom: plateaus in units of Y axis, and logIC50: peptide concentration at 50% proteolytic activity **C.** Incubation of peptides based on concentrations determined from IC50 with MD for 2 hours, followed by incubation with A2M, TIMP3, and Marimastat at 2.5 µM for 6 hours.

Chapter 6: Results – Identify and Examine the Contribution(s) of the Metalloprotease Domain in Protecting ADAMTS13 from Inhibition

6.1 Metalloprotease domain structure and sequence alignment

The amino acid sequences of ADAMTS 1, 4, 5, 7, and 12 were compared to ADAMTS13 using PRALINE. The sequence alignment revealed high consistency scores (~7 out of 10, with some regions being 10) within the MDT domains. Further, the consistency scores were moderate (~5 out of 10) within cysteine-rich and spacer domains among the ADAMTS family. The consistency scores were in line with the literature, which describes strong conservation within the MDTCS regions (Kelwick et al., 2015).

A closer look at the crystal structure of the metalloprotease domain and sequence alignment between ADAMTS13 and ADAMTS proteases reveals three unique features of interest: (i) the gatekeeper triad (R193, D217, and D252), (ii) the calcium-binding loop (R180-R193), and (iii) the variable loop (G231-S263) (Figure 6.1) (Petri et al., 2019). Residues R193, D217, and D252 form the "gatekeeper triad" through ionic interactions that have been hypothesized to obscure access to the S1' pocket that is critical in binding to the P1' methaionine of VWF (Petri et al., 2019), and is the target of inhibitors in other metalloproteases (including ADAMTS5) (Tortorella et al., 2009). The crystal structure of the metalloprotease domain suggests that the sides of the active site cleft are formed through interactions between the calcium-binding loop (R180-R193) and the variable loop G231-S263, and mediated by the side chains of R193, D217, and D252 which comprise the gatekeeper triad (Petri et al., 2019). Moreover, the crystal structure reveals that the active site cleft is occluded by the folding of the calcium-binding loop over the

S1’ pocket. The ionic interactions of the gatekeeper triad are hypothesized to stabilize the latent conformation of ADAMTS13 (Petri et al., 2019). Therefore, it is suggested that the ionic interactions among residues R193, D217, and D252 need to be overcome to gain access to the S1’ pocket (D252-P256), which is buried deep behind the gatekeeper triad (Petri et al., 2019).

In an attempt to sensitize ADAMTS13 to inhibition, we designed individual constructs targeting the gatekeeper triad, calcium-binding loop, and variable loop, as well as a construct that targets all three of these unique features by using MDTCS. MDTCS was selected over full-length ADAMTS13 and other constructs because the distal domains comprising the closed conformation are not required to study the role of the metalloprotease domain, but proximal domains serve as exosites necessary for detectable FRETS-VWF73 cleavage. To maintain the proteolytic activity of MDTCS towards FRETS-VWF73, we opted to swap these regions of interest with corresponding regions in ADAMTS5, which displays inhibition to protease inhibitors.

A. Molecular visualization of pertinent features of the metalloprotease domain

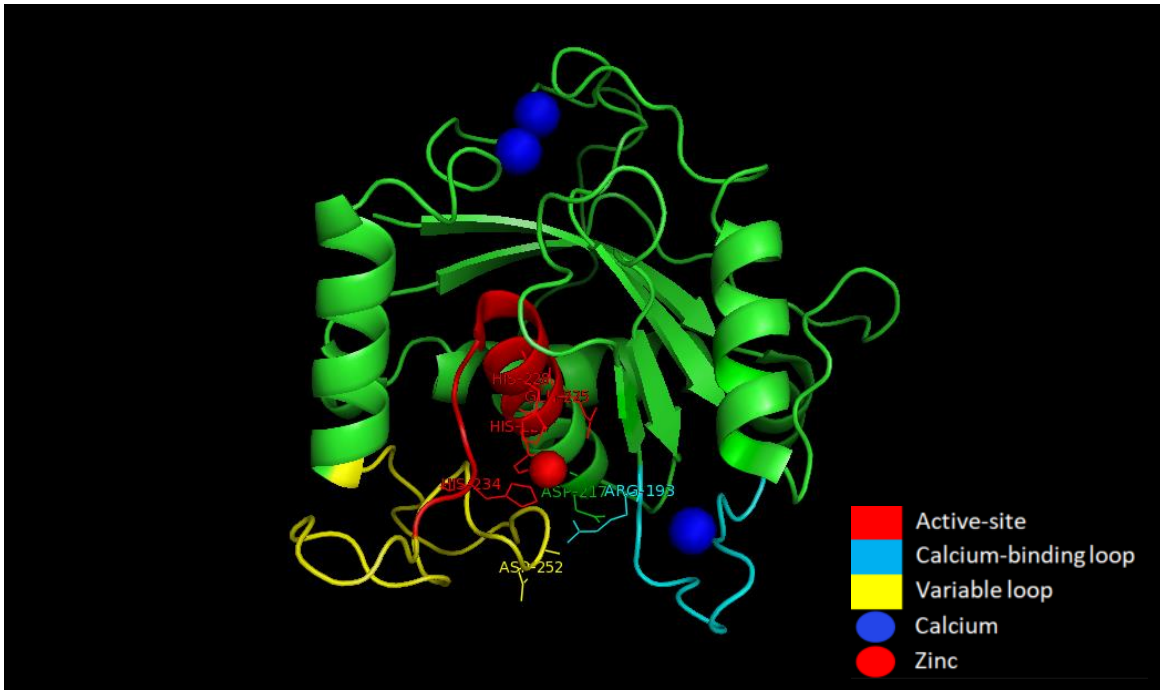

B. Sequence alignment of the active site region between ADAMTS members

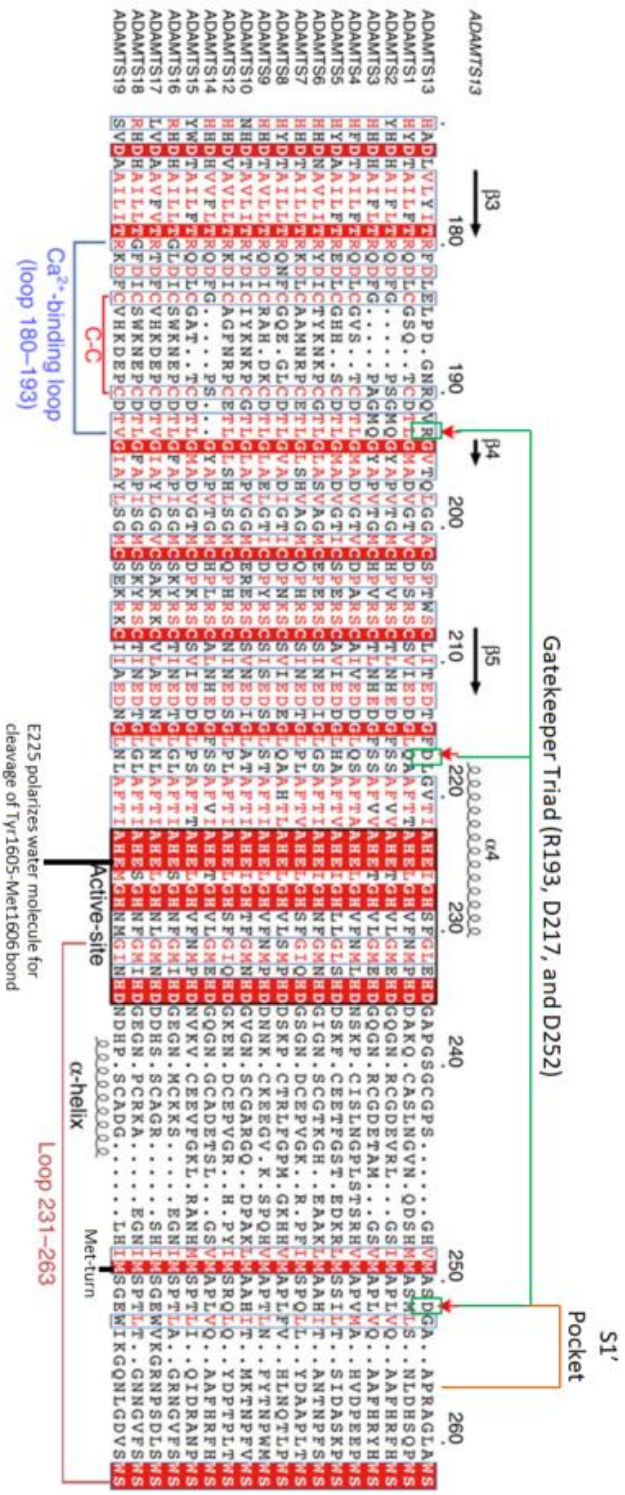

Figure 6.1. Metalloprotease domain structure and ADAMTS sequence alignment. A. Pertinent features of the Metalloprotease domain highlighted using PYMOL (PDB: 6QIG)**. B.** The sequence alignment between ADAMTS13 and ADAMTS proteases. The gatekeeper triad (R193, D217, and D252), calcium-binding loop (R180-R193) (cyan), and variable loop G231-S263 (yellow) are areas of interest. Sequence alignment adapted from: Petri et al., Nat Comm (2019).

6.2 Designing MDTCS metalloprotease domain mutants that are sensitive to inhibition

MDTCS metalloprotease domain mutants of the gatekeeper triad (R193A, D217A, and D252A), the variable loop (G236-P244 to ATS5 D421-F429), the calcium-binding loop with the gatekeeper triad (R180-R193 to ATS5 R367-L379), the gatekeeper triad with the calcium-binding loop and the variable loop (R180-R193 to ATS5 R367-L379, D217A, and G236-S263 to ATS5 D422-S453), and WT-MDTCS (Table 3.3) were transiently transfected into HEK 293T cells using Transport 5 reagent in OPTI-MEM. After 72 hours, the OPTI-MEM was collected, concentrated, and buffer exchanged into the ADAMTS13 reaction buffer. Western blot for V5 tag was used to verify the presence of each construct (Figure 6.2). All constructs were detected at their predicted molecular weight (80 kDa) (Figure 6.2). An ELISA capable of detecting different variants of ADAMTS13 was used to determine the concentration of each construct. The functional activity of each construct was verified using a FRETS-VWF73 assay. Nonetheless, degradation was also detected by Western blot (Figure 6.2). For purposes of studying inhibition, the effects of protein degradation on our interpretations were minimal. However, we acknowledge that protein degradation is a limitation of our protein expression technique. All MDTCS variants were first characterized for their capacity to cleave FRETS-VWF73 and data was fit to Michaelis-Menten equation (Section 3.11). From the Michaelis-Menten equation we determined the kinetic constants for proteolysis of FRETS-VWF73.

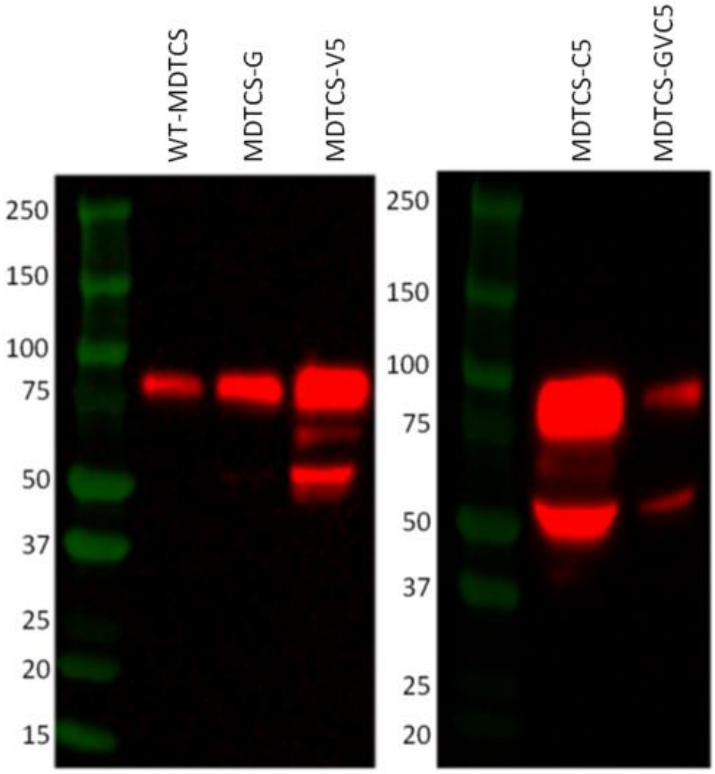

Figure 6.2. Verification of MDTCS metalloprotease domain mutants. Western blot for V5 tag. Verification of WT-MDTCS, MDTCS-G: gatekeeper triad mutant (R193A, D217A, and D252A), MDTCS-V5: variable loop (G236-P244 to ATS5 D421-F429), MDTCS-C5: calcium-binding loop with gatekeeper triad (R180-R193 to ATS5 R367-L379), and MDTCS-GVC5: gatekeeper triad with calcium-binding loop and variable loop (R180-R193 to ATS5 R367-L379, D217A, and G236-S263 to ATS5 D422-S453). Based on molecular weight, all constructs were detected at approximately 80 kDa, as expected. All constructs were concentrated, but not purified from OPTI-MEM. All gels were performed using a 4 to 20% polyacrylamide gel under reducing conditions.

6.3 MDTCS-G: The Gatekeeper triad

Collectively, our data suggests that the metalloprotease domain is primarily responsible for protecting ADAMTS13 from inhibition. Observations based on the crystal structure of ADAMTS13 suggest that ionic interaction among residues Arg193, Asp217, and Asp252 restrict access to the active site cleft of ADAMTS13 (Petri et al., 2019). The ionic interactions between these residues form the "gatekeeper triad" (Petri et al., 2019). The gatekeeper triad is hypothesized to protect the S1' pocket, and the passage between the disintegrin domain and the active site (Petri et al., 2019).

To examine the contribution of the gatekeeper triad in protecting the metalloprotease domain from protease inhibitors, each residue was mutated in MDTCS: R193A, D217A, and D252A. This variant, termed MDTCS-G neutralizes the ionic interaction of the gatekeeper triad, potentially opening access to the active site cleft (Figure 6.3A). The kinetic constants were determined for the proteolysis of FRETS-VWF73 by MDTCS-G using the Michaelis-Menten equation (Table 6.1). The k_{cat}/K_m value of MDTCS-G (128.77 RFU x s^{-1} x nM^{-1} x μM^{-1}) did not significantly differ from the k_{cat}/K_m value of WT-MDTCS (Figure 6.3B). Therefore, our data suggests that the mutagenesis of the gatekeeper triad does not affect the proteolytic efficiency and the capacity of MDTCS to cleave FRETS-VWF73. In addition, the kinetic constants of WT-ADAMTS13 were compared to WT-MDTCS (Table 6.1). The k_{cat}/K_m value of WT-ADAMTS13 was reduced by 2-fold (69.73 RFU x s^{-1} x nM^{-1} x μM^{-1}) in comparison to WT-MDTCS (Figure 6.3B). These data was consistent with previous litrature suggesting

that MDTCS cleaves FRETS-VWF73 with a 2-fold greater efficiency than WT-ADAMTS13 in the absence of the closed conformation (Gao et al., 2006).

Next, the susceptility of MDTCS-G to inhibition was tested. The activity of MDTCS-G was unaltered following a 6 hour incubation with 10-fold molar excess of A2M, TIMP3, or Marimastat (Figure 6.3C-D). Resistance towards A2M was confirmed using Western blot, since MDTCS-G was unable to cleave A2M (Figure 6.3E). This result is consistent with the inability of A2M to inhibit MDTCS-G proteolytic activity using the FRETS-VWF73. Collectively, these data suggest that the gatekeeper triad does not contribute to ADAMTS13 resistance to protease inhibitors.

A. PYMOL molecular visualization

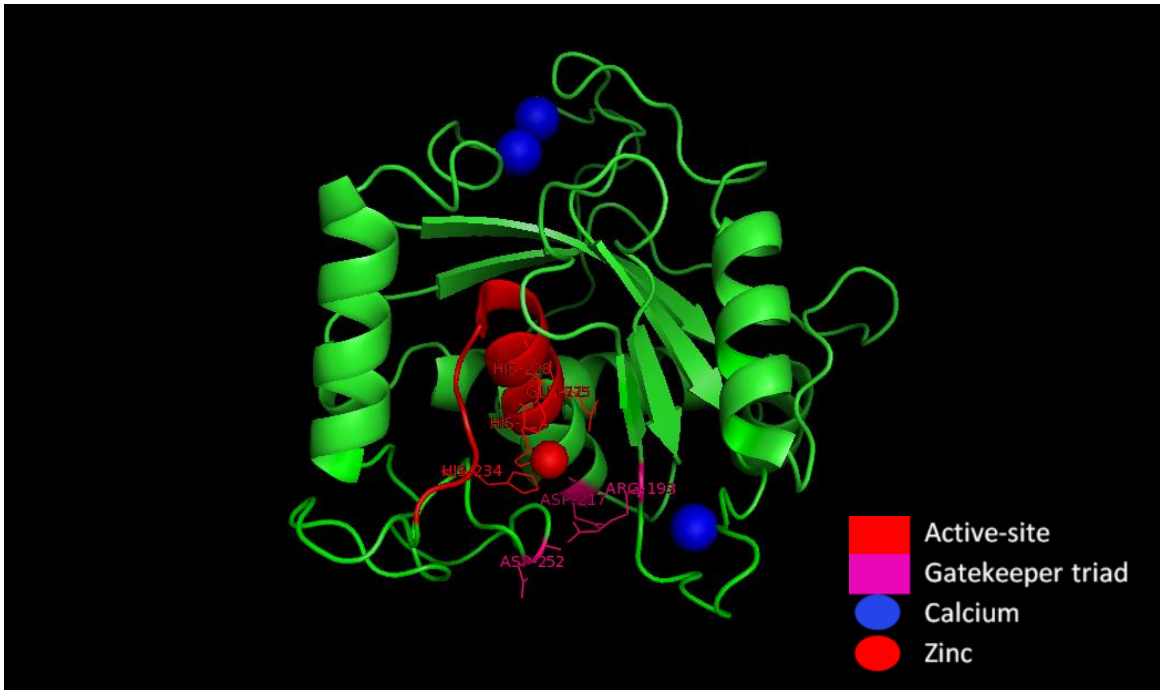

B. FRETS-VWF73 proteolysis modelled by Michaelis-Menten

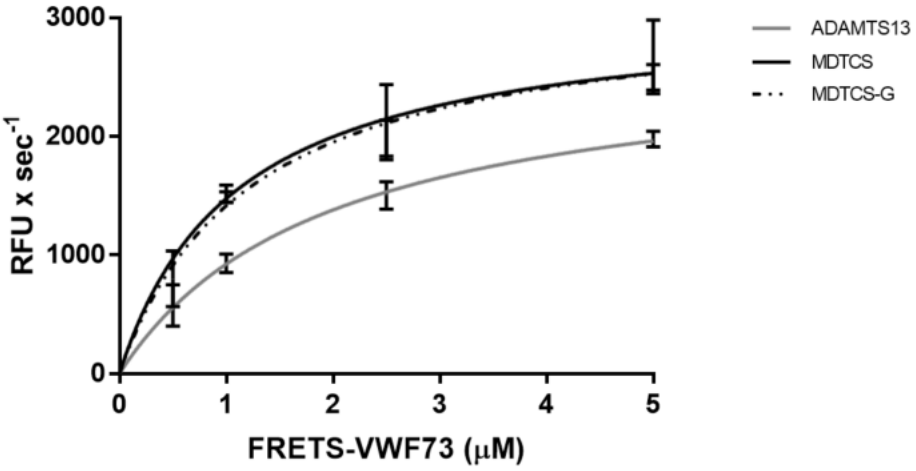

C. Raw proteolytic values of MDTCS and variants w/ or w/out inhibitors

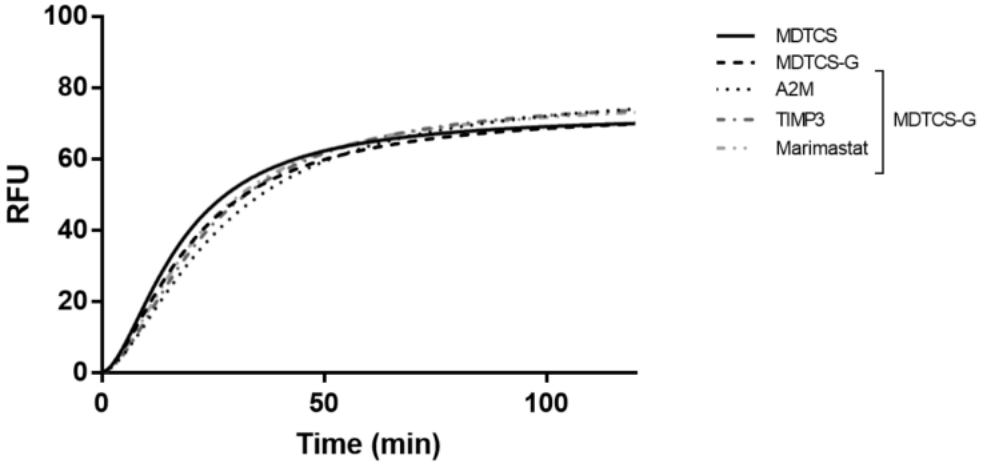

D. Analyzed proteolytic values

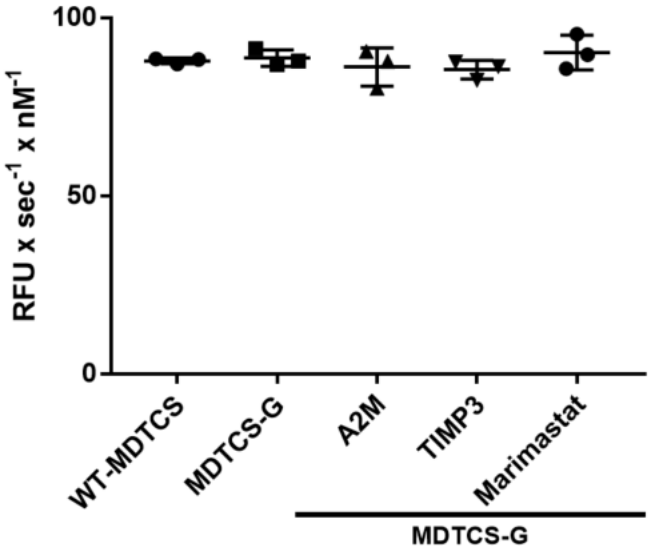

E. A2M Western blot

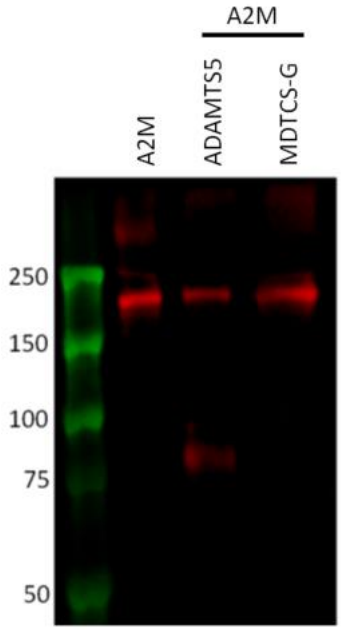

Figure 6.3. Characterizing gatekeeper triad mutant: MDTCS-G. A. Mutagenesis of the gatekeeper triad using alanine substitution; MDTCS-G (R193A, D217A, and D252A) (highlighted in pink). Molecular visualization using PYMOL (PDB: 6QIG)**. B.** Kinetic constants for FRETS-VWF73 proteolysis by WT-ADAMTS13, WT-MDTCS, and MDTCS-G at concentration of 20 nM with increasing concentration of FRETS-VWF73 (μM) using Michaelis-Menten equation: $Y = V_{max}*X/(K_m+X)$. **C.** Raw proteolytic values of FRETS-VWF73 (1 μM) by WT-MDTCS (20 nM), and MDTCS-G (20 nM) with and without A2M, TIMP3, or Marimastat (250 nM) incubated for 6 hours. Proteolytic cleavage expressed in RFU. Repersentative of three individual runs. **D.** Analyzed raw proteolytic values using linear regression of the initial slope of WT-MDTCS (20 nM), and MDTCS-G (20 nM) with and without A2M, TIMP3, or Marimastat (250 nM) incubated for 6 hours. Expressed as RFU x s^{-1} x nM^{-1}. **E.** Western blot was used to identify the cleaved form of A2M (250 nM) at 80 kDa using MDTCS-G (50 nM). ADAMTS5 (250 nM) was used as a positive control. All experiments were conducted at least three times.

Table 6.1. Kinetic constants for proteolysis of FRETS-VWF73 by WT-ADAMTS13, WT-MDTCS, and MDTCS-G. Data derived using Michaelis-Menten equation. Statistical analysis of V_{max} and K_m compared to WT-MDTCS values; ns $p > 0.05$, * $p \leq 0.05$, ** $p \leq 0.01$, *** $p \leq 0.001$, **** $p \leq 0.0001$.

	V_{max} (RFU x s^{-1})	**K_m (µM)**	**k_{cat} (RFU x s^{-1} x nM^{-1})**	**k_{cat}/K_m (RFU x s^{-1} x nM^{-1} x μM^{-1})**	**Fold change**
WT-ADAMTS13	2728±117*	1.96±0.20***	136.40±5.85	69.73	2.02↓
WT-MDTCS	3085±203	1.09±0.21	154.25±10.15	141.13	-
MDTCS-G	3142±192^{ns}	1.22±0.20^{ns}	157.10±9.60	128.77	1.10↓

6.4 MDTCS-C5: The calcium-binding loop

Examination of the MDTCS crystal structure revealed that the calcium-binding loop (L175-R193) resides in residues that compose the S1 specificity pocket and lacks a stabilizing disulfide bridge found in other ADAMTS proteases may result in flexibility that blocks access to the active site cleft of ADAMTS13 (Petri et al., 2019). Earlier attempts to delete the calcium-binding loop severely impaired the expression and secretion of this variant in HEK293 cells, thereby suggesting that the calcium-binding loop is important in the proper folding of ADAMTS13 (data not shown). To mitigate these limitations, we next designed a chimera that swapped the calcium-binding loop with ADAMTS5 (MDTCS R180-R193 to ATS5 R367-L379), termed MDTCS-C5, to examine the importance of this loop to ADAMTS13 resistance to inhibition (Figure 6.4A). Since ADAMTS5 is susceptible to inhibition, we hypothesized that its calcium-binding loop, which contains a disulfide bond and lacks a gatekeeper triad, would not auto-inhibit the ADAMTS13 active site.

The kinetic constants were determined for the proteolysis of FRETS-VWF73 by MDTCS-C5 using the Michaelis-Menten equation (Table 6.2). Swapping the calcium-binding loop with ADAMTS5 significantly reduced the K_m (2.70±0.64 μM) and k_{cat} (11.55±1.30 RFU x s^{-1} x nM^{-1}) of MDTCS-C5 compared to WT-MDTCS ($p \leq 0.0001$) (Figure 6.4B). Therefore, the catalytic efficiency of MDTCS-C5 was reduced by approximately 33-fold (k_{cat}/K_m: 4.28 RFU x s^{-1} x nM^{-1}) compared to WT-MDTCS (k_{cat}/K_m: 141.13 RFU x s^{-1} x nM^{-1} x μM) (Figure 6.4B and Table 6.2). Therefore, the

calcium-binding loop is crucial for determining the turnover rate and affinity for FRETS-VWF73.

Next, the effect of the calcium-binding loop on inhibition was examined. MDTCS-C5 was incubated with 10-fold molar excess of inhibitor for 6 hours before measuring residual activity using FRETS-VWF73. Marimastat may display potential capacity to attenuate MDTCS-C5 activity, but this was not statistically significant (Figure 6.4C-D). Neither A2M nor TIMP3 attenuated the proteolytic activity of MDTCS-C5 (Figure 6.4C-D). MDTCS-C5 was unable to cleave the bait region of A2M (Figure 6.4E), consistent with no change in the proteolytic activity. Together, these data suggest that the features of the calcium-binding loop of ADAMTS13 play an integral part in the recognition of VWF, but on its own the calcium-binding loop is not responsible for the protection of ADAMTS13 from protease inhibitors.

A. PYMOL molecular visualization

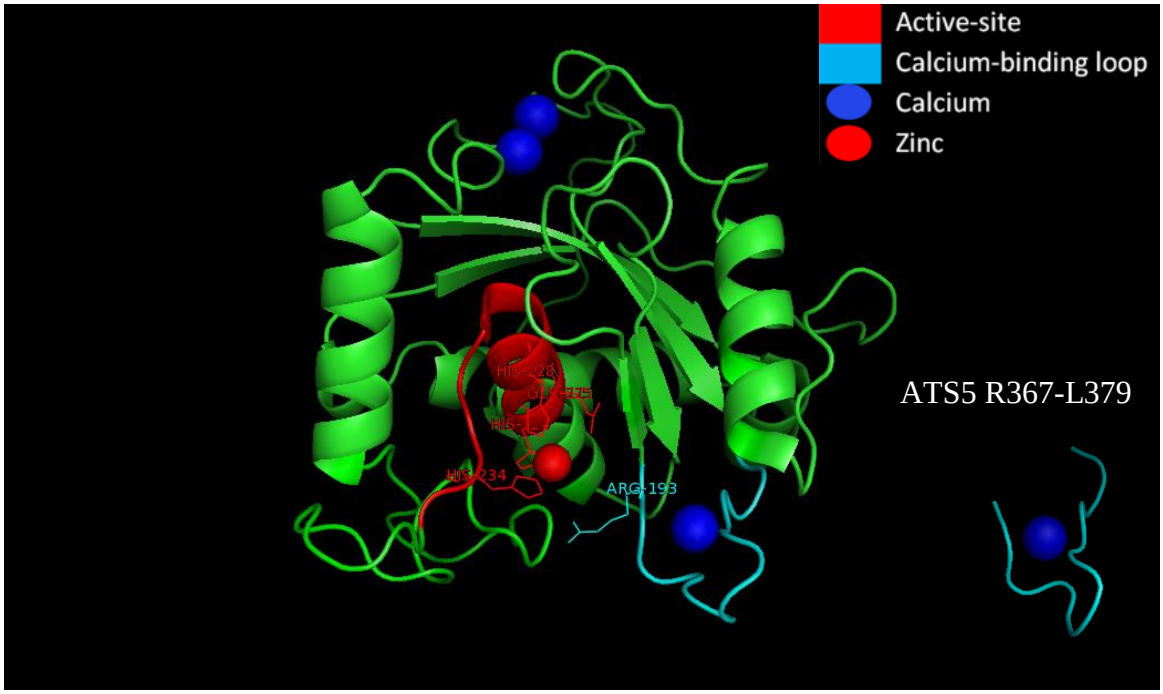

B. FRETS-VWF73 proteolysis modelled by Michaelis-Menten

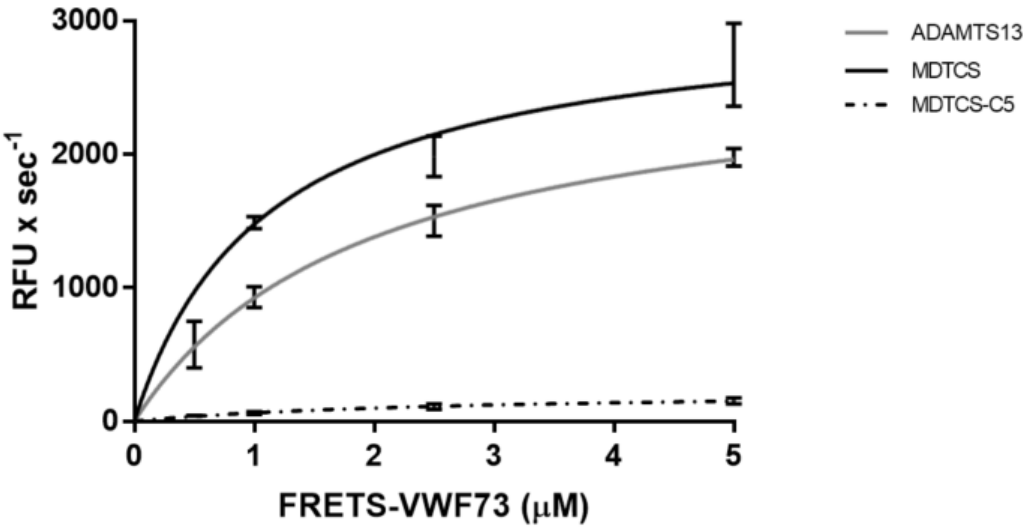

C. Raw proteolytic values of MDTCS and variants w/ or w/out inhibitors

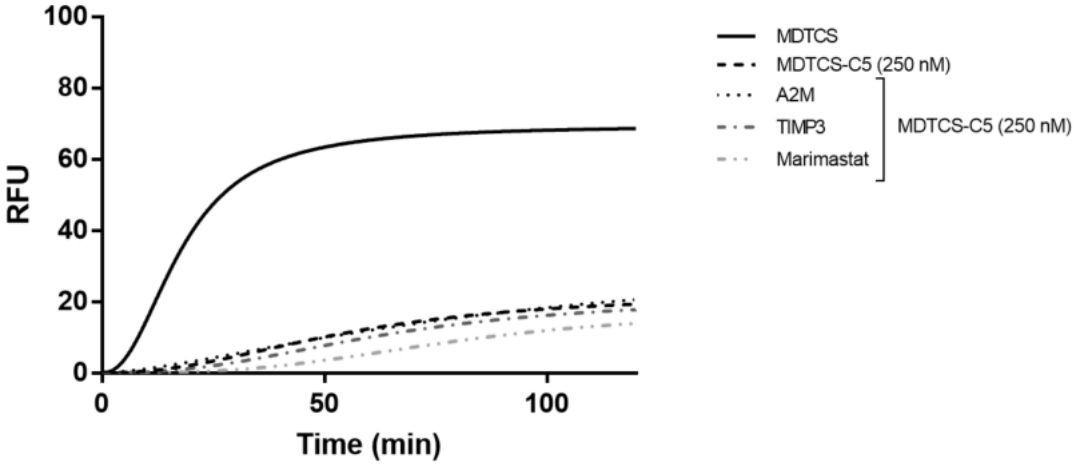

D. Analyzed proteolytic values

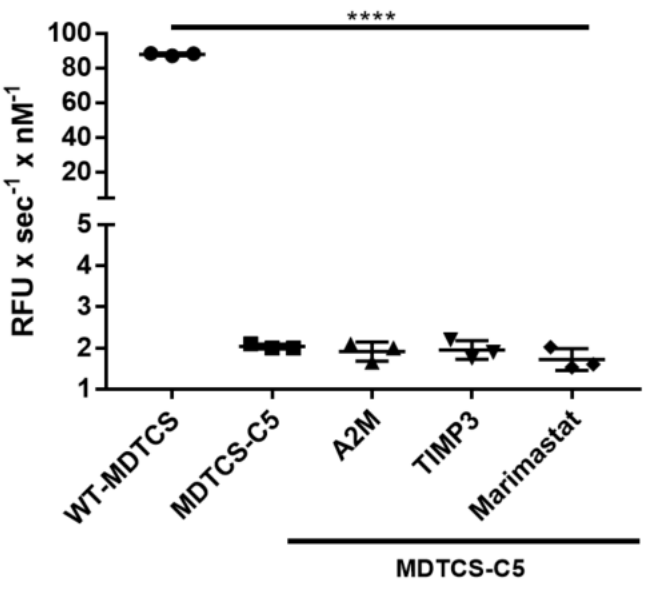

E. A2M Western blot

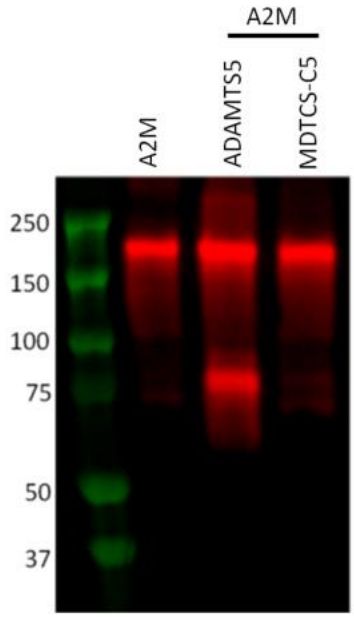

Figure 6.4. Characterizing the calcium-binding gatekeeper triad mutant: MDTCS-C5. A. Calcium-binding loop swap with ADAMTS5; MDTCS-C5 (R180-R193 to ATS5 R367-L379); highlighted in cyan. Molecular visualization using PYMOL (PDB: 6QIG). **B.** Kinetic constants for FRETS-VWF73 proteolysis by WT-ADAMTS13, WT-MDTCS, and MDTCS-C5 analyzed at concentration of 20 nM with increasing concentration of FRETS-VWF73 (μM) using Michaelis-Menten equation: $Y = V_{max}*X/(K_m+X)$. **C.** Raw proteolytic values of FRETS-VWF73 (1 μM) by WT-MDTCS (20 nM), and MDTCS-C5 (250 nM) with and without A2M, TIMP3, or Marimastat (2.5 μM) incubated for 6 hours. Proteolytic cleavage expressed in RFU. Repersentative of three individual runs. **D.** Analyzed raw proteolytic values using linear regression of the initial slope of WT-MDTCS (20 nM), and MDTCS-C5 (250 nM) with and without A2M, TIMP3, or Marimastat (2.5 μM) incubated for 6 hours. Expressed as RFU x s^{-1} x nM^{-1}. **E.** Western blot was used to identify the cleaved form of A2M (250 nM) at 80 kDa using MDTCS-C5 (250 nM). ADAMTS5 (250 nM) was used as a positive control. All experiments were conducted at least three times.

Table 6.2. Kinetic constants for proteolysis of FRETS-VWF73 by MDTCS-C5. Data derived using Michaelis-Menten equation. Statistical analysis of V_{max} and K_m compared to WT-MDTCS values; ns $p > 0.05$, * $p \leq 0.05$, ** $p \leq 0.01$, *** $p \leq 0.001$, **** $p \leq 0.0001$.

	V_{max} (RFU x s^{-1})	**K_m (µM)**	**k_{cat} (RFU x s^{-1} x nM^{-1})**	**k_{cat}/K_m (RFU x s^{-1} x nM^{-1} x μM^{-1})**	**Fold change**
WT-ADAMTS13	2728±117*	1.96±0.20***	136.40±5.85	69.73	2.02↓
WT-MDTCS	3085±203	1.09±0.21	154.25±10.15	141.13	-
MDTCS-C5	231±26****	2.70±0.64****	11.55±1.30	4.28	32.97↓

6.5 MDTCS-V5: Variable loop swap

Based on the crystal structure of the metalloprotease domain, the variable loop (G236-S263) borders the active site across from the calcium-binding loop (R180-R193) (Petri et al., 2019). Within the variable loop, residues G236-P244 help shape the active site cleft of ADAMTS13. In ADAMTS5, this feature is an alpha helix, which may lack the flexibility of the disordered loop in ADAMTS13. To study the role of the variable loop in protecting the ADAMTS13 active site from protease inhibitors, we swapped the variable loop of ADAMTS13 with the corresponding segment of the alpha helix in ADAMTS5, termed MDTCS-V5 (Figure 6.5A).

MDTCS-V5 was first characterized for its capacity to cleave FRETS-VWF73 using the Michaelis-Menten equation (Table 6.3). Swapping the variable loop in ADAMTS13 with the corresponding helix in ADAMTS5 significantly reduced k_{cat} (105.50±3.70 RFU x s^{-1} x nM^{-1}) ($p \leq 0.0001$), but not the K_m (1.25±0.13 µM) compared to WT-MDTCS (Figure 6.5B). MDTCS-V5 has a 1.67-fold reduction in catalytic efficiency (k_{cat}/K_m: 84.40 RFU x s^{-1} x nM^{-1} x μM^{-1}) compared to WT-MDTCS (k_{cat}/K_m: 141.13 RFU x s^{-1} x nM^{-1} x μM^{-1}). Therefore, swapping the variable loop from ADAMTS5 results in a k_{cat} effect that impacts the turnover rate, but not affinity for FRETS-VWF73.

Next, MDTCS-V5 was examined in inhibition assays to evaluate the contribution of the variable loop to ADAMTS13 resistance to protease inhibitors. Following a 6-hour incubation, the activity of MDTCS-V5 was not inhibited by 10-fold molar excess A2M, TIMP3, or Marimastat (Figure 6.5C-D). Resistance towards A2M was confirmed using Western blot by verifying the cleaved form of A2M at 80 kDa. MDTCS-V5 was unable to

cleave A2M (Figure 6.5E), consistent with no significant change detected with FRETS-VWF73. These data suggest that segment G236-P244 of the variable loop plays a minor role in substrate turnover, but is not responsible for the protection of ADAMTS13 from natural and synthetic metalloprotease inhibitors.

A. PYMOL molecular visualization

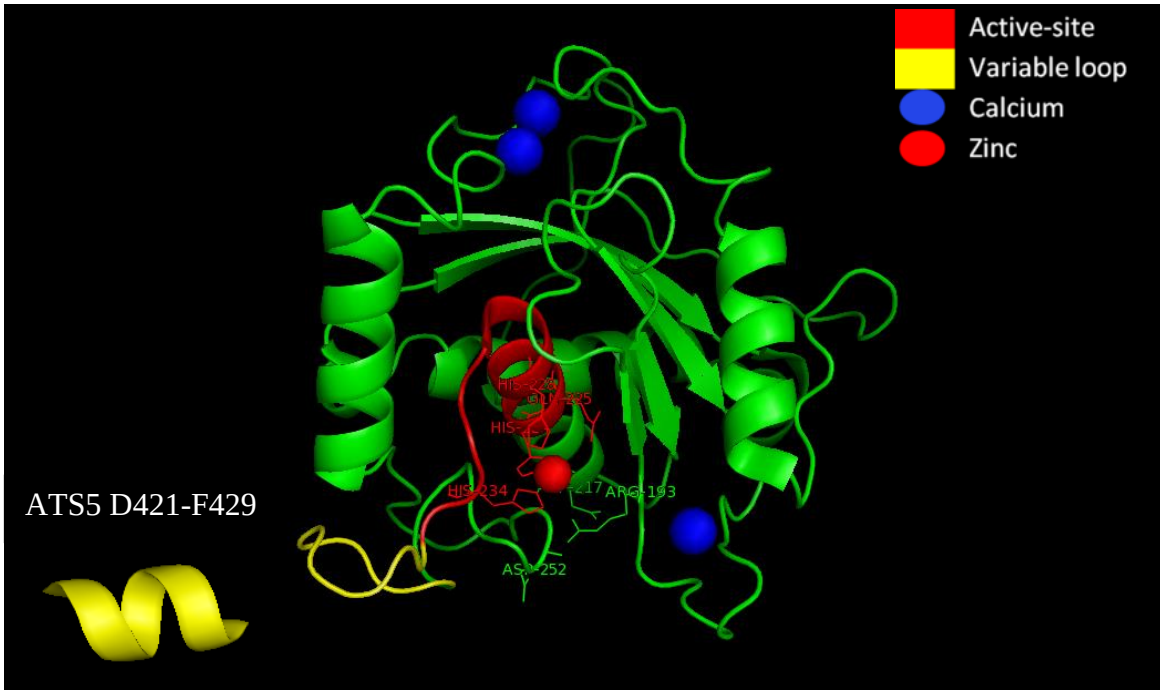

B. FRETS-VWF73 proteolysis modelled by Michaelis-Menten

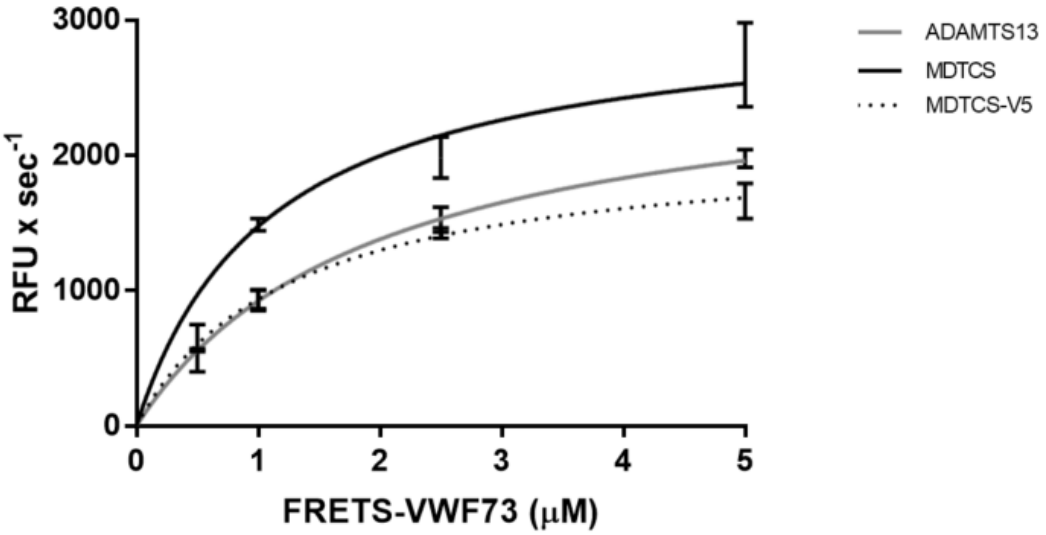

C. Raw proteolytic values of MDTCS and variants w/ or w/out inhibitors

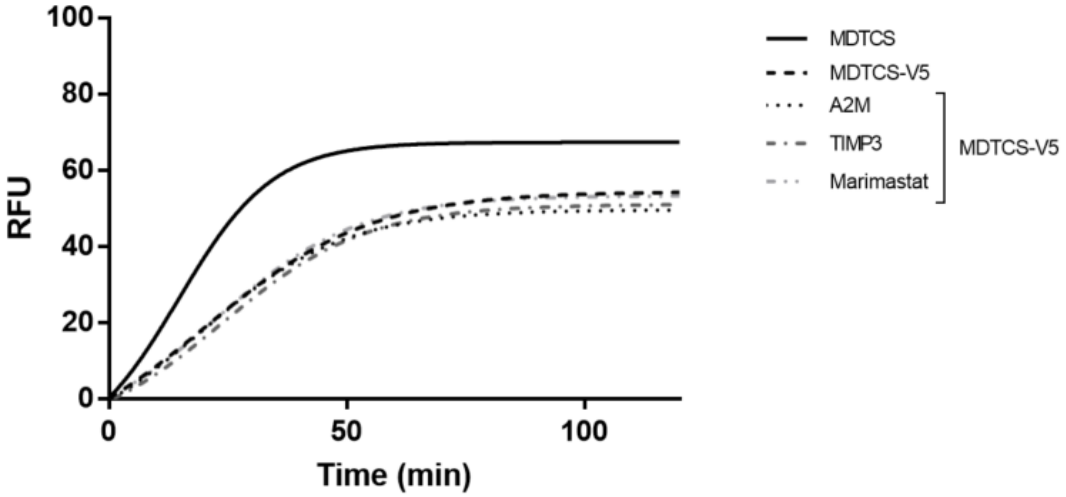

D. Analyzed proteolytic values

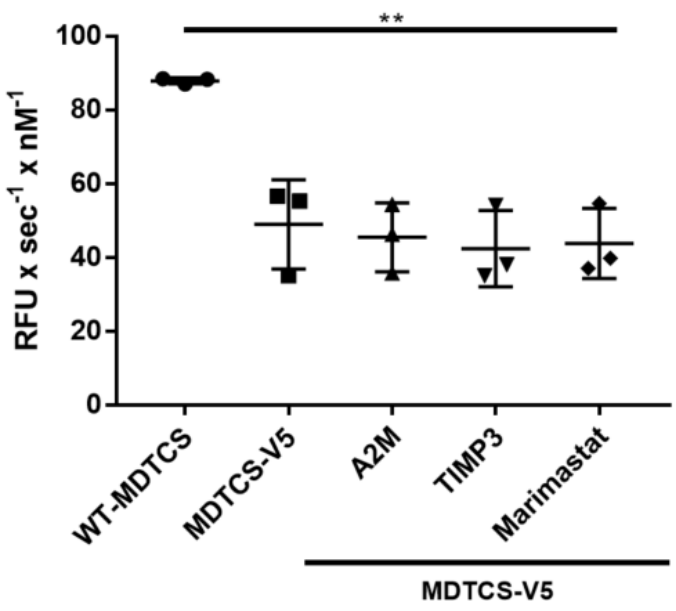

E. A2M Western blot

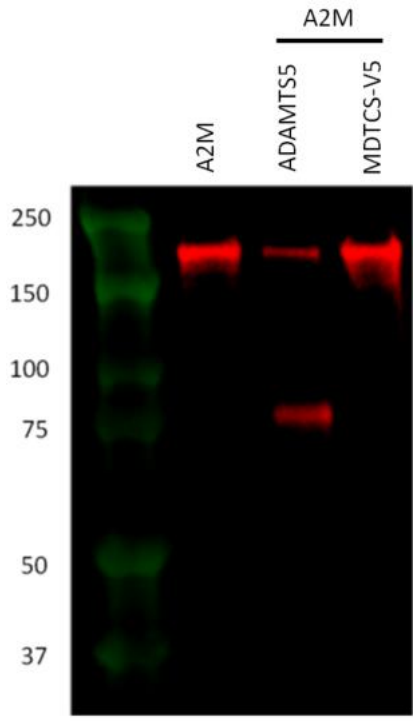

Figure 6.5. Characterizing the variable loop mutant: MDTCS-V5. A. G236-P244 segment of the variable loop of ADAMTS13 swapped with the corresponding segment D421-F429 from ADAMTS5 (highlighted in yellow) in MDTCS; MDTCS-V5 (G236-P244 to ATS5 D421-F429). Molecular visualization using PYMOL (PDB: 6QIG). **B.** Kinetic constants for FRETS-VWF73 proteolysis by WT-ADAMTS13, WT-MDTCS, and MDTCS-V5 analyzed at concentration of 20 nM with increasing concentration of FRETS-VWF73 (µM) using Michaelis-Menten equation: $Y = V_{max}*X/(K_m+X)$. **C.** Raw proteolytic values of FRETS-VWF73 (1 µM) by WT-MDTCS (20 nM), and MDTCS-V5 (20 nM) with and without A2M, TIMP3, or Marimastat (250 nM) incubated for 6 hours. Proteolytic cleavage expressed in RFU. Repersentative of three individual runs. **D.** Analyzed raw proteolytic values using linear regression of the initial slope of WT-MDTCS (20 nM), and MDTCS-V5 (20 nM) with and without A2M, TIMP3, or Marimastat (250 nM) incubated for 6 hours. Expressed as RFU x s^{-1} x nM^{-1}. **E.** Western blot was used to identify the cleaved form of A2M (250 nM) at 80 kDa using MDTCS-V5 (250 nM). ADAMTS5 (250 nM) was used as a positive control. All experiments were performed at least three times.

Table 6.3. Kinetic constants for proteolysis of FRETS-VWF73 by MDTCS-V5. Data dervied from using Michaelis-Menten equation. Statistical analysis of V_{max} and K_m compared to WT-MDTCS values; ns $p > 0.05$, * $p \leq 0.05$, ** $p \leq 0.01$, *** $p \leq 0.001$, **** $p \leq 0.0001$.

	V_{max} (RFU x s^{-1})	**K_m (µM)**	**k_{cat} (RFU x s^{-1} x nM^{-1})**	**k_{cat}/K_m (RFU x s^{-1} x nM^{-1} x μM^{-1})**	**Fold change**
WT-ADAMTS13	2728±117*	1.96±0.20***	136.40±5.85	69.73	2.02↓
WT-MDTCS	3085±203	1.09±0.21	154.25±10.15	141.13	-
MDTCS-V5	2110±74****	1.25 ± 0.13^{ns}	105.50±3.70	84.40	1.67↓

6.6 MDTCS-GVC5: Gatekeeper triad, variable loop, and calcium-binding loop

Collectively, the sequence alignment among ADAMTS proteases and the crystal structure of ADAMTS13 and ADAMTS5, highlight three areas of interest within the metalloprotease domain that may protect ADAMTS13 from inhibition: I) the gatekeeper triad (R193, D217, D252), II) the variable loop (G236-S263), and III) the calcium-binding loop (R180-R193). Based on these observations, we designed a chimera termed MDTCS-GVC5, which swapped residues R180-R193 to ATS5 R367-L379, D217A, and G236-S263 to ATS5 D422-S453. All three features were targeted simultaneously to increase the potential for inhibition (Figure 6.6A).

The kinetic parameters were determined for the proteolysis of FRETS-VWF73 by MDTCS-GVC5 using the Michaelis-Menten equation. MDTCS-GVC5 cleavage of VWF73 has a significantly reduced K_m (1.84±0.31 μM) ($p \leq 0.001$) and k_{cat} (43.05±3.00 RFU x s^{-1} x nM^{-1}) ($p \leq 0.0001$) compared to WT-MDTCS (Figure 6.6B and Table 6.4). As a result, the catalytic efficiency of MDTCS-GVC5 for VWF73 was reduced by 6.03-fold (k_{cat}/K_m: 23.40 RFU x s^{-1} x nM^{-1} x μM^{-1}) compared to WT-MDTCS (k_{cat}/K_m: 141.13 RFU x s^{-1} x nM^{-1} x μM^{-1}) (Table 6.4). Interestingly, targeting all three features in MDTCS-GVC5 exhibited more efficient proteolytic activity than MDTCS-C5 which only swapped the calcium-binding loop (Figure 6.4B and Figure 6.6B; Table 6.2 and Table 6.4). Collectively, our findings from these metalloprotease mutants suggest that the calcium-binding loop plays a crucial role in determining catalytic efficiency, and the overall catalytic performance is less reduced when all segments of the active site cleft,

such as the variable loop and the calcium-binding loop are from the same protease (e.g. ADAMTS5).

Next, MDTCS-GVC5 was incubated with 10-fold molar excess A2M, TIMP3, or Marimastat for 6 hours to examine its susceptibility to inhibition. The presence of A2M or TIMP3 did not reduce MDTCS-GVC5 proteolysis of FRETS-VWF73 (Figure 6.6C-D). Resistance to A2M was confirmed using Western blot assessing the cleaved form of A2M at 80 kDa. MDTCS-GVC5 was unable to cleave A2M (Figure 6.6E), consistent with no significant change detected with FRETS-VWF73. Interestingly, incubation with Marimastat showed statistically significant reduced FRETS-VWF73 activity (1.25±0.17 RFU x s^{-1} x nM^{-1}) compared to no inhibitor control (16.38±1.26 RFU x s^{-1} x nM^{-1}) ($p \leq 0.0001$) (Figure 6.6C-D).

Next, we determined the kinetic parameters of MDTCS-GVC5 for FRETS-VWF73 in the presence of Marimastat to better characterize inhibition. The k_{cat} (14.35±1.40 RFU x s^{-1} x nM^{-1}) of MDTCS-GVC5 was significantly reduced in the presence of Marimastat compared to the absence of Marimastat (43.05±3.00 RFU x s^{-1} x nM^{-1}) ($p \leq 0.001$) (Figure 6.6F and Table 6.5). However, in the presence of Marimastat the K_m (1.65±0.40 µM) of MDTCS-GVC5 was not affected (Figure 6.6F and Table 6.5). The catalytic efficiency of MDTCS-GVC5 (k_{cat}/K_m: 8.70 RFU x s^{-1} x nM^{-1} x μM^{-1}) was reduced by 16.22-fold compared to WT-MDTCS (k_{cat}/K_m: 141.13 RFU x s^{-1} x nM^{-1} x μM^{-1}), and by 2.69-fold compared to MDTCS-GVC5 without Marimastat (k_{cat}/K_m: 23.37 RFU x s^{-1} x nM^{-1} x μM^{-1}) (Figure 6.6F and Table 6.5). Therefore, these data suggest that the variable loop (G231-S263) and the calcium-binding loop (R180-R193) are crucial for

determining the proteolytic parameters of ADAMTS13, and contribute to the protection of ADAMTS13 to protease inhibitors. Further, the inhibitory effects of Marimastat on MDTCS-GVC5 affect the substrate turnover, which is consistent with a direct active site inhibitor.

A. PYMOL molecular visualization

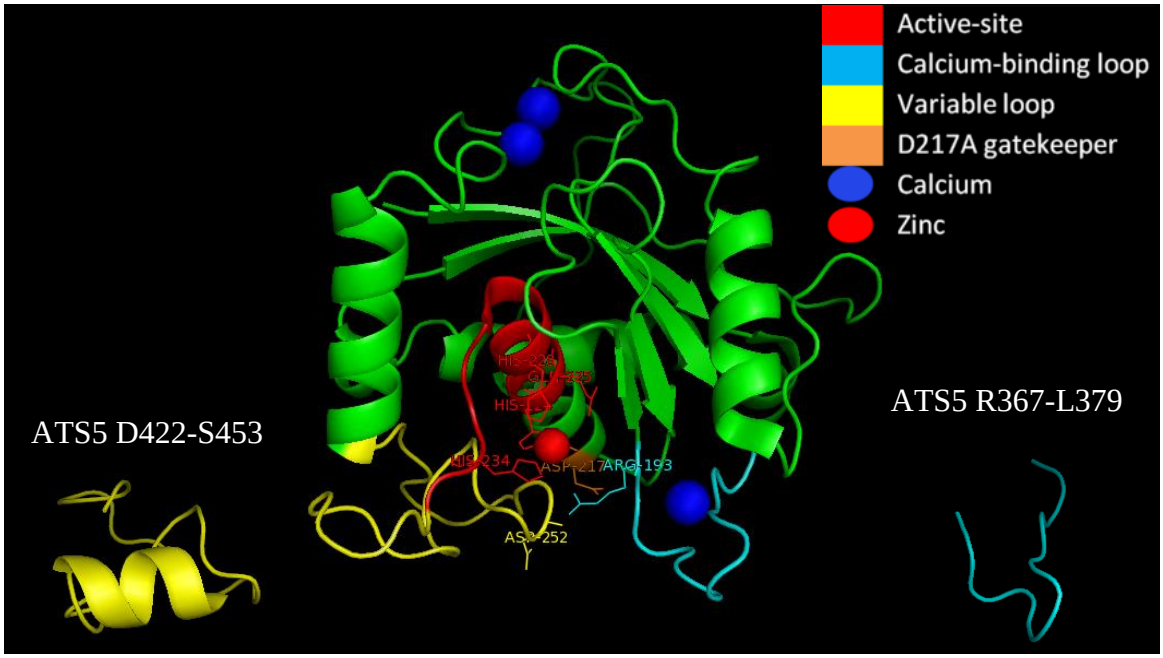

B. FRETS-VWF73 proteolysis modelled by Michaelis-Menten

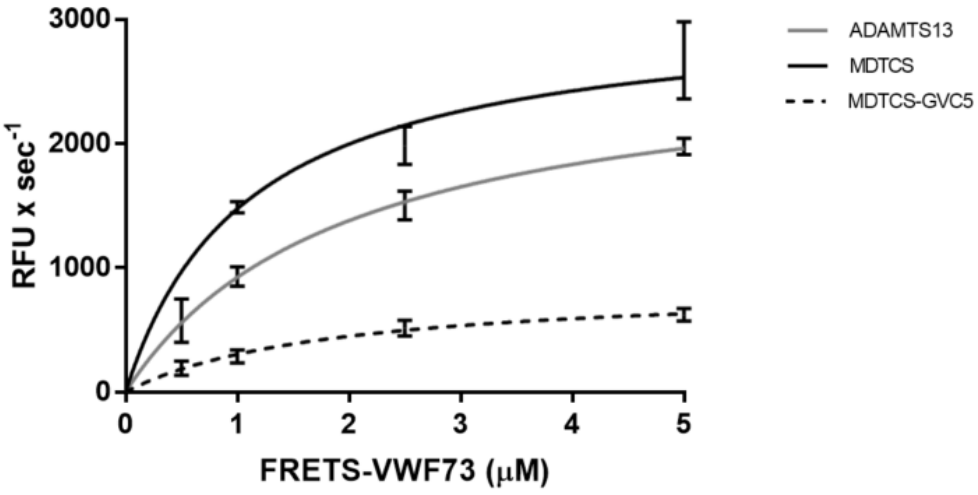

C. Raw proteolytic values of MDTCS and variants w/ or w/out inhibitors

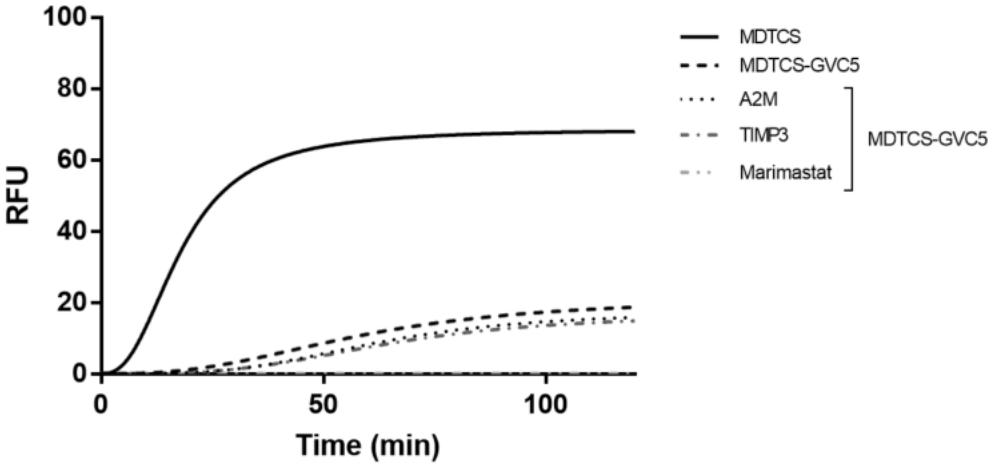

D. Analyzed proteolytic values

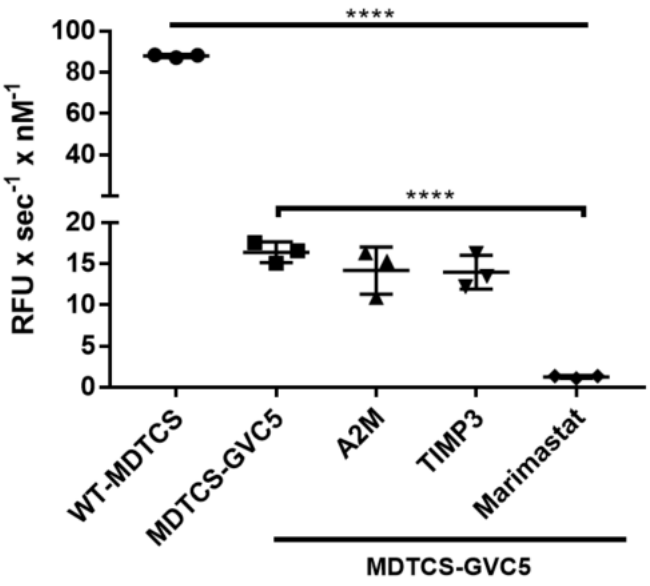

E. A2M Western blot

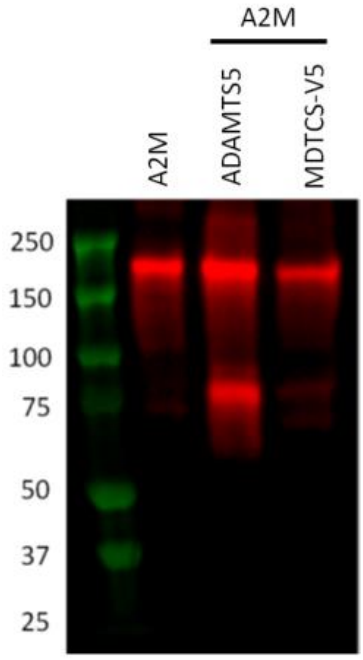

F. FRETS-VWF73 proteolysis modelled by Michaelis-Menten (Marimastat)

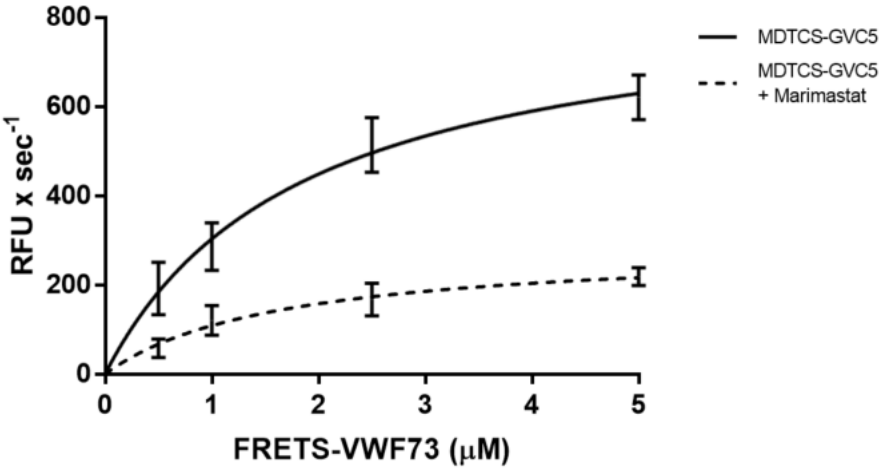

Figure 6.6. Characterizing the combination of the gatekeeper triad, the calcium-binding loop, and the variable loop mutant: MDTCS-GVC5. A. The calcium-binding loop residues R180-R190 were swapped with their corresponding residues R367-L379 in ADAMTS5 (cyan), residue D217 was swapped for alanine to eliminate the gatekeeper triad (orange), and the variable loop residues G236-S263 were swapped with their corresponding residues D422-S453 in ADAMTS5 (yellow) in MDTCS; MDTCS-GVC5 (R180-R193 to ATS5 R367-L379, D217A, and G236-S263 to ATS5 D422-S453) Molecular visualization using PYMOL (PDB: 6QIG). **B.** Kinetic constants for FRETS-VWF73 proteolysis by WT-ADAMTS13, WT-MDTCS, and MDTCS-GVC5 analyzed at concentration of 20 nM with increasing concentration of FRETS-VWF73 (µM) using Michaelis-Menten equation: $Y = V_{max}*X/(K_m+X)$. **C.** Raw proteolytic values of FRETS-VWF73 (1 µM) by WT-MDTCS (20 nM), and MDTCS-GVC5 (20 nM) with and without A2M, TIMP3, or Marimastat (250 nM) incubated for 6 hours. Proteolytic cleavage expressed in RFU. Repersentative of three individual runs. **D.** Analyzed raw proteolytic values using linear regression of the initial slope of WT-MDTCS (20 nM), and MDTCS-GVC5 (20 nM) with and without A2M, TIMP3, or Marimastat (250 nM) incubated for 6 hours. Expressed as RFU x s^{-1} x nM^{-1}. **E.** Western blot was used to identify the cleaved form of A2M (250 nM) at 80 kDa using MDTCS-GVC5 (250 nM). ADAMTS5 (250 nM) was used as a positive control. **F.** Kinetic constants for FRETS-VWF73 proteolysis by MDTCS-GVC5 (20 nM) with and without Marimastat (250 nM) in the presence of increasing concentration of FRETS-VWF73 (µM) using Michaelis-Menten equation: $Y = V_{max}*X/(K_m+X)$. All experiments were performed at least three times.

Table 6.4. Kinetic constants for proteolysis of FRETS-VWF73 by MDTCS-GVC5. Data derived using Michaelis-Menten equation. Statistical analysis of V_{max} and K_m compared to WT-MDTCS values; ns $p > 0.05$, * $p \leq 0.05$, ** $p \leq 0.01$, *** $p \leq 0.001$, **** $p \leq 0.0001$.

	V_{max} (RFU x s^{-1})	**K_m (µM)**	**k_{cat} (RFU x s^{-1} x nM^{-1})**	**k_{cat}/K_m (RFU x s^{-1} x nM^{-1} x μM^{-1})**	**Fold change**
WT-ADAMTS13	2728±117*	1.96±0.20***	136.40±5.85	69.73	2.02↓
WT-MDTCS	3085±203	1.09±0.21	154.25±10.15	141.13	-
MDTCS-GVC5	861±60****	1.84±0.31***	43.05±3.00	23.40	6.03↓

Table 6.5. Kinetic constants for proteolysis of FRETS-VWF73 by MDTCS-GVC5 in the presence of Marimastat. Data derived using Michaelis-Menten equation. Statistical analysis of V_{max} and K_m compared to MDTCS-GVC5 values; ns $p > 0.05$, * $p \leq 0.05$, ** $p \leq 0.01$, *** $p \leq 0.001$, **** $p \leq 0.0001$.

	V_{max} (RFU x s^{-1})	**K_m (µM)**	**k_{cat} (RFU x s^{-1} x nM^{-1})**	**k_{cat}/K_m (RFU x s^{-1} x nM^{-1} x μM^{-1})**	**Fold change**
WT-MDTCS	3085±203	1.09±0.21	154.25±10.15	141.13	-
MDTCS-GVC5	861±60	1.84±0.31	43.05±3.00	23.40	-
MDTCS-GVC5 + Marimastat (250 nM)	287±28***	1.65±0.40^{ns}	14.35±1.40	8.70	16.22↓ (WT-MDTCS) 2.69↓ (MDTCS-GVC5)

6.7 Marimastat inhibition comparison between ADAMTS5 versus MDTCS-GVC5

Marimastat has shown to bind a broad range of metalloproteinases through interactions with the S1' specificity pocket, which stabilize binding to the active site zinc ion (Tortorella et al., 2009). Our findings from Section 6.6 suggest that the calcium-binding loop (R180-193) and the variable loop (G236-S263) contain features that limit Marimastat interaction with ADAMTS13. By swapping these loops with ADAMTS5, including the gatekeeper triad, we were able to sensitize MDTCS-GVC5 to Marimastat. Herein we compare the inhibition characteristics between ADAMTS5 and MDTCS-GVC5 to determine the degree to which Marimastat was able to inhibit MDTCS-GVC5, relative to ADAMTS5.

An ADAMTS5 reaction time course with aggrecan was first performed in the absence of Marimastat. The EC50 of ADAMTS5 was determined at 26±3 minutes (Figure 6.7A). From the time-course experiment, we determined that aggrecan consumption by ADAMTS5 was complete by 60 minutes (Figure 6.7A). ADAMTS5 was reacted with increasing concentrations of Marimastat, followed by aggrecan for 60 minutes. Cleavage of intact aggrecan was quantified from the Western blot and the residual activity was expressed as a percentage. This analysis revealed that Marimastat inhibited ADAMTS5 with IC50 value of 1.64±0.31 nM (Figure 6.7B). The inhibitory effect of Marimastat on ADAMTS5 was consistent with previous literature (Tortorella et al., 2009). In contrast, the IC50 of Marimastat inhibition of MDTCS-GVC5 using FRETS-VWF73 was 42.59±5.20 nM (Figure 6.7B). Therefore, our data suggests that

Marimastat was significantly more potent against ADAMTS5 than MDTCS-GVC5 ($p \leq 0.001$). These data suggest that MDTCS-GVC5 is susceptible to inhibition by small molecule inhibitors of metalloproteases like Marimastat, but is not susceptible to natural protease inhibitors like A2M or TIMPs. Future studies will examine whether additional features with the metalloprotease or disintegrin domain confer additional protection.

A. ADAMTS5-aggrecan time course

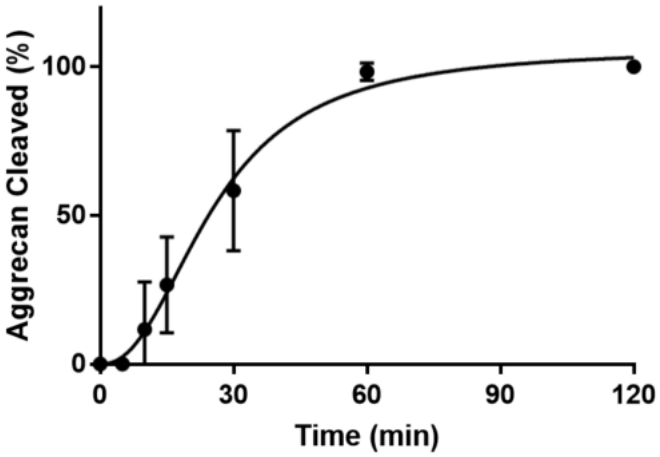

B. Marimastat IC50 at 60 minutes

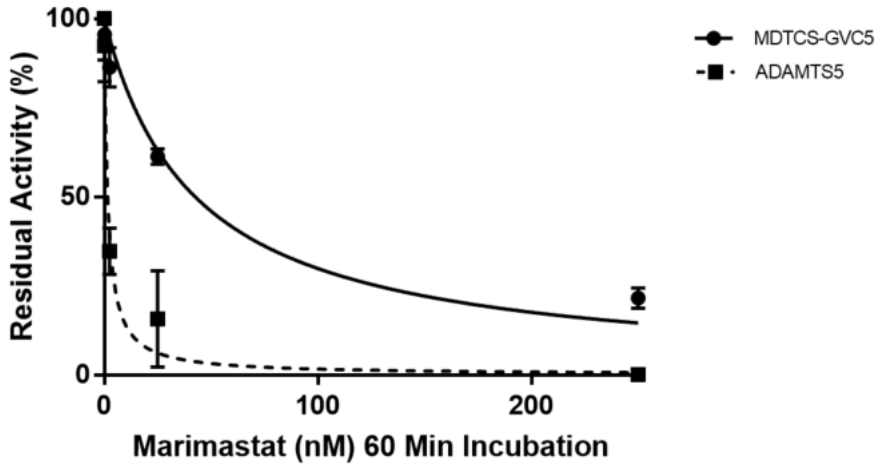

Figure 6.7. Characterizing Marimastat inhibition between ADAMTS5 and MDTCS-GVC5. A. ADAMTS5-aggrecan time-course to verify the time required for ADAMTS5 (20 nM) to completely cleave 100 nM of aggrecan. Percent aggrecan cleavage was determined by quantifying the cleavage of intact aggrecan at 120 kDa by Western blotting relative to no protease. The data was modelled using non-linear regression equation: Y = V_{max}*X^h/(EC50^h+X^h). **B.** Incubation of Marimastat at concentrations of 0 nM, 0.250 nM, 2.5 nM, 25 nM, and 250 nM with ADAMTS5 (20 nM) and aggrecan (100 nM) for 60 minutes, and assessed for the cleavage of aggrecan after 60 minutes relative to no Marimastat by Western blot. MDTCS-GVC5 (20 nM) was incubated with increasing Marimastat concentrations (0 nM, 0.250 nM, 2.5 nM, 25 nM, and 250 nM), and evaluated proteolysis using FRETS-VWF73 (1 μM) after 60 minutes. Reactions were modelled by using the non-linear equation: Y = 100/(1+X/IC50). Residual activity was expressed as a percent. All experiments were performed at least three times.

Table 6.6. Comparison of Marimastat IC50 value between ADAMTS5 and MDTCS-GVC5; ns $p > 0.05$, * $p \leq 0.05$, ** $p \leq 0.01$, *** $p \leq 0.001$, **** $p \leq 0.0001$.

	IC50: Marimastat (nM)
ADAMTS5	1.64±0.31***
MDTCS-GVC5	42.59±5.20

Chapter 7: Discussion

ADAMTS13 is a unique protease with properties that set it apart from the other ADAMTS family members and coagulation proteases. Remarkably, ADAMTS13 is constitutively secreted as an active protease, and exhibits a prolonged half-life of several days, while displaying remarkable specificity for VWF, with no known off-target proteolysis. By contrast, other members of the ADAMTS family and serine proteases in the coagulation system require proteolytic activation, are rapidly inactivated by natural protease inhibitors, cleave multiple substrates, and have relatively shorter half-lives in the range of minutes to hours (Furlan et al., 1999; Gao et al., 2006; Scully et al., 2017; South et al., 2016). Uncovering the mechanism(s) that regulate ADAMTS13 is urgently needed as recombinant ADAMTS13 advances through clinical trials for treatment of congenital TTP, and is a promising therapeutic to treat stroke and other microvascular thrombotic illnesses (de Maat et al., 2021). The goal of this project was to define the resistance of ADAMTS13 to natural and synthetic protease inhibitors and explore the mechanism behind this unique property.

To answer the aforementioned questions, we constructed ADAMTS13 deletion mutants to determine which domain(s) of ADAMTS13 are responsible for conveying resistance against protease inhibitors. We first verified that FL-ADAMTS13 is indeed resistant towards protease inhibitors (Figure 4.2). The deletion constructs showed that MDTCS and MD are protected from inhibition (Figures 4.3 and 4.4). We observed a 2-fold increase in MDTCS activity compared to FL-ADAMTS13, confirming that the closed conformation has an auto-inhibitory effect on the cleavage of FRETS-VWF73,

consistent with previous studies (Figure 6.3B, Table 7.1) (Gao et al., 2012; Muia et al., 2014). Removal of –TCS exosites significantly impaired the proteolytic activity of MD demonstrating the importance of these exosites on VWF recognition. Resistance of MD towards protease inhibitors suggests that the unique features of the active site region contribute to the resistance of ADAMTS13.

As a result of impaired expression, we were unable to truncate past the disintegrin domain in order to solely study the role of the metalloprotease domain. Moreover, removal of the disintegrin domain would further impair ADAMTS13 activity below FRETS-VWF73 detection threshold (data not shown). To overcome this limitation and study the metalloprotease domain of ADAMTS13, we designed a chimera with the exosites of ADAMTS5, including the disintegrin domain (M13/DTCS5). Chimeric constructs between ADAMTS5 and ADAMTS13 were designed to evaluate the roles of the active site and the closed conformation on ADAMTS13 resistance against protease inhibitors. ADAMTS5 was inhibited by protease inhibitors (Figure 5.2), which was consistent with previous studies (Fan & Kassiri, 2020; Kashiwagi et al., 2001; Meisel & Chang, 2017; Murphy, 2011; Rasmussen & McCann, 1997; Tortorella et al., 2004). More specifically, we found that A2M, TIMP3, and Marimastat were potent inhibitors of ADAMTS5, and were therefore selected for all subsequent experiments (Figure 5.2). Chimeras containing the active site from ADAMTS13 (MD13/TCS5 and M13/DTCS5) were resistant towards all protease inhibitors (Figure 5.3 and 5.4), whereas chimeras containing the active site from ADAMTS5 (MD5/TCS13 and MD5(TCS-CUB13)) were inhibited (Figure 5.5 and 5.6). These findings again suggest that the metalloprotease

domain of ADAMTS13 is primarily responsible for protecting it from inhibition, which is consistent with our domain truncation studies. M13/DTCS5 displayed an approximate 3000-fold decrease in proteolytic activity compared to WT-MDTCS for FRETS-VWF73, suggesting that -DTCS domains of ADAMTS13 are important exosites for binding and anchoring VWF for proteolysis (Figure 5.4). These findings are consistent with previous studies showing that domains –DTCS are critical for substrate specificity, and mutations or removal of these domains significantly impair the proteolytic activity of ADAMTS13 (Akiyama et al., 2009; De Groot et al., 2015; Petri et al., 2019; Zander et al., 2015). Our data suggests that while the absence of these domains result in a significant decrease in proteolytic activity, these domains are not directly responsible for protecting ADAMTS13 from inhibition (Table 7.1).

While these studies demonstrate that the metalloprotease domain itself is resistant to inhibitors, we also tested whether long-range conformational changes in ADAMTS13 confer additional protections to the protease domain. Using the chimeric construct MD5(TCS-CUB13), we observed a 50-fold reduction in the rate of aggrecan cleavage and a slower rate of inhibition compared to MD5/TCS13 (Figure 5.6). The crystal structure suggests that the closed conformation confers a “global” latency, whereby non-covalent interactions between the C-terminal CUB domains and the central spacer domain cause structural constraint on the active site of ADAMTS13 (Kim et al., 2021). Moreover, the global latency induced by the closed conformation attenuates ADAMTS13 activity; however, the spacer-CUB domain interaction can be readily disrupted by the D4-CK domains of multimeric VWF, thereby resulting in the “open” conformation, and

activating ADAMTS13 (South et al., 2017). Using murine monoclonal antibodies targeting the spacer domain, kinetic analysis during the open conformation, revealed a k_{cat} effect that enhanced the proteolytic activity rather than substrate binding effect (K_m) (Schelpe et al., 2020). The k_{cat} effect suggests that the active site may be affected when ADAMTS13 is in its closed conformation, but becomes conformationally activated by VWF through spacer domain interactions (Schelpe et al., 2020). From an evolutionary standpoint, the notion that a 2-fold k_{cat}/K_m effect on the proteolysis of FRETS-VWF73 between ADAMTS13 and truncated MDTCS does not represent a substantial impact on ADAMTS13 regulation. We hypothesized that the closed conformation served other function(s), such as protecting ADAMTS13 against inhibition. Our findings with MD5(TCS-CUB13) coincide with previous suggestions that the conformation quiescence of ADAMTS13 may serve to protect ADAMTS13 from off-target proteolysis (South et al., 2016). We suggest that the closed conformation not only masks important VWF-binding exosites on the spacer domain through non-covalent interactions, but it also confers long-range effects on the metalloprotease domain, consistent with studies by Schelpe *et al*. and South *et al*. To add, the relatively large structural composition of the closed conformation may further restrict access to the exosites and the active site through steric hindrance. These proposals are consistent with 3D protein structure computations (AlphaFold, DeepMind and EMBL-EBI), which predict that domains TSP5-8 of the closed conformation restrict active site and exosite accessibility (Jumper et al., 2021; Varadi et al., 2022). The AlphaFold computations of ADAMTS13 predict that TSP5-8 domains are brought into proximity of the metalloprotease and disintegrin domains

because of spacer-CUB interactions of the closed conformation. The TSP5-8 domains are anterior to metalloprotease domain, and then run parallel and inferior to MDTCS (Jumper et al., 2021; Varadi et al., 2022) (Figure 7.1). As a result, accessibility to the protease domain may be blocked, which may further explain the reduction in proteolytic activity and reduced rate of inhibition observed with MD5(TCS-CUB13). Therefore, based on our MD5(TCS-CUB13) and MD5/TCS13 data, we suggest that the closed conformation attenuates the proteolytic activity of ADAMTS13, as well the accessibility of the active site to protease inhibitors. Nonetheless, the closed conformation contributes to the resistance of ADAMTS13 against protease inhibition, but this is not the primary mechanism. Removal of the closed conformation was not sufficient to sensitize ADAMTS13 to natural or synthetic protease inhibitors (Figure 4.3 and 4.4), and MD5(TCS-CUB13) was still prone to inhibition, albeit at a slower rate.

Engagement of proximal domains near the active site of ADAMTS13 is essential for full-length VWF and VWF73 cleavage (Gao et al., 2008). Recently, it was shown that ADAMTS13 was incapable of cleaving any of the 64 million, 6 amino acid peptides in a phage display library (Kretz et al., 2018). However, when this library was inserted into P3-P3' of VWF73, 1670 cleaved peptide sequences were identified (Kretz et al., 2018). The findings suggest that VWF residues outside the P3-P3' interval must engage with exosites on ADAMTS13 to gain access to its active site. Previous studies found that mutations in the disintegrin domain resulted in a 5- to 20- fold decrease in catalytic efficiency (k_{cat}/K_m) towards the A2 domain of VWF (De Groot et al., 2009). Additionally, disruptions in the disintegrin domain that interact with VWF resulted in a 700-fold

decrease in proteolytic activity (Petri et al., 2019). The disintegrin domain has also shown to play an important role in determining cleavage parameters (k_{cat}) because the exosite on the disintegrin domain plays an important role in orienting VWF toward the active site in ADAMTS13, and subsequent substrate-induced protease activation steps that follow (De Groot et al., 2009). The role of the exosites on the disintegrin domain is different from the cysteine-rich and spacer domains, which confer a K_m effect on VWF cleavage, suggesting that they are primarily responsible for docking ADAMTS13 onto the shear-unfolding A2 domain.

Based on these findings, we attempted to sensitize MD to inhibition by designing various VWF peptides that engaged the disintegrin domain exosite. In doing so, we hypothesized that the engagement of the disintegrin domain should cause a conformational change that activates ADAMTS13, thereby granting inhibitors access to the active site. However, multiple disintegrin-engaging peptides were unable to sensitize ADAMTS13 to inhibition (Figure 5.7). This suggests that the disintegrin domain binding alone is not sufficient to activate the ADAMTS13 metalloprotease domain. This is consistent with experiments performed with M13/DTCS5, which demonstrated that the resistance to protease inhibitors can be primarily explained by features within the ADAMTS13 metalloprotease domain alone (Figure 5.4). It is possible that further conformational changes are required in order for the active site to fully mature. For instance, the S3 subsite interacts with the P3 residue L1603 in VWF, which may help to position the P1-P1’ scissile bond proximal to the catalytic zinc within the active site for proteolysis (Crawley et al., 2011). Evidently, mutation of the P3 residue, L1603N resulted

in a 218-fold reduction in ADAMTS13 proteolysis of VWF96 and a 66-fold reduction in k_{cat} (Petri et al., 2019). Therefore, the S3-P3 interaction is critical to substrate turnover. Future studies should examine the importance of the S3 subsite engagement to the maturation of the ADAMTS13 active site, and its subsequent susceptibility to inhibition. Overall, our studies demonstrate that engagement of the disintegrin domain alone does not sensitize ADAMTS13 to inhibition, which contributes to our understanding of how substrate-induced protease activation serves to regulate ADAMTS13 activity.

Our data suggests that features within the metalloprotease domain protect ADAMTS13 from inhibitors. One potential mechanism to explain this unique property of ADAMTS13 may be adapted from the known role of the prodomain in maintaining ADAMTS protease latency. ADAMTS proteases (and metzincins generally) are synthesized as zymogens, which need to be activated by proteolytic removal of the prodomain (Longpré & Leduc, 2004). The prodomain can contain multiple furin-recognition sites that can be processed by furin-like proprotein convertases, thereby activating the protease from its zymogen state (Longpré & Leduc, 2004). The function of the prodomain of these proteases is 2-fold; to mediate proper protein folding and to maintain latency until proteolytic removal of the prodomain activates these proteases (Kelwick et al., 2015; Longpré & Leduc, 2004). Latency of metzincin proteases, including ADAMTS proteases, is maintained by the formation of an intramolecular complex between a free cysteine residue in the prodomain and the catalytic zinc ion in the active site (Van Wart & Birkedal-Hansen, 1990). This intramolecular complex, referred to as the “cysteine-switch”, blocks the active site until proteolytic removal by furin-like

proprotein convertases (Van Wart & Birkedal-Hansen, 1990). In ADAMTS13 the prodomain serves neither of these functions, and its removal is not required for ADAMTS13 to cleave VWF (Kelwick et al., 2015; Majerus et al., 2003). ADAMTS13 is active once folding is completed in the endoplasmic reticulum (Majerus et al., 2003). Additionally, the prodomain of ADAMTS13 contains 41 residues, compared to the approximate 200 residues in most ADAMTS proteases (Majerus et al., 2003), suggesting it is a non-functional and vestigial feature of ADAMTS13 evolution. However, ADAMTS13 exhibits all the features of a zymogen with respect to capacity to be inhibited, unless it is activated by its substrate VWF. We hypothesize that loops guarding the ADAMTS13 active site occlude the catalytic zinc, which reside in a manner similar to the cysteine-switch mechanism of the prodomain in other metzincin proteases. While these loops are sufficient to prevent inhibitors from accessing the active site, they are rapidly displaced by VWF in an interaction that is facilitated by extensive exosite interactions. In support of this hypothesis, the crystal structure of ADAMTS13 and the sequence alignment of ADAMTS proteases reveal three distinct features of the metalloprotease domain: (i) the gatekeeper triad (R193, D217, and D252), (ii) the variable loop (G231-S263), and (iii) the calcium-binding loop (R180-R193) (Figure 6.1 and Figure 7.2). The investigations into these features contributed to our improved understanding of ADAMTS13 regulation and substrate recognition.

Alanine substitutions of gatekeeper residues D193, D217, and D252 did not affect the kinetic parameters (k_{cat} or K_m) for the proteolysis of FRETS-VWF73 compared to WT-MDTCS (Figure 6.3 C-D and Table 7.2). Moreover, our observations suggest that the

ionic interactions between these charged residues do not protect ADAMTS13 from protease inhibitors (Figure 6.3 C-E), as suggested by previous studies (Kim et al., 2021; Petri et al., 2019). The ionic interactions of the gatekeeper triad may provide additional stabilization to the active site cleft formed by the calcium-binding loop and the variable loop, but this function is not reflected in changes to substrate recognition or susceptibility to inhibition. Alternatively, the ionic interactions of the gatekeeper triad observed in the crystal structure of MDTCS may be an artifact of the large Fab fragment binding to the calcium-binding loop in the metalloprotease domain that was required for its crystallization. The Fab fragment may have induced a conformational change that reinforced an otherwise transient or weak ionic interaction between residues R193, D217, and D252 in ADAMTS13.

The active site cleft of ADAMTS13 is flanked by the calcium-binding loop (R180-R193) and the variable loop (G236-S263). The catalytic motif in the centre of the active site cleft is marked by the S1 and S1’ specificity pockets, but is otherwise devoid of overt pockets that would accept other substrate residues in the P3-P3’ (Crawley et al., 2011; Kelwick et al., 2015; Petri et al., 2019; South et al., 2014). The variable loop extends to include residues that compose the S1’ specificity pocket (D252-P256), which accommodates the P1’ residue (M1606) of VWF (Crawley et al., 2011; Petri et al., 2019). The calcium-binding loop extends to include two of five residues that compose the S1 specificity pocket (L185 and V192), which accommodates the P1 residue (Y1605) of VWF (Crawley et al., 2011; Petri et al., 2019). The remaining three residues of the S1 subsite (L147, L151, and V195) flank the calcium-binding loop and are oriented towards

the catalytic motif (Crawley et al., 2011; Petri et al., 2019). The crystal structure of ADAMTS5 suggests that its active site and the S1' specificity pocket remains accessible to inhibitors, such as Marimastat (Tortorella et al., 2009) (Figure 7.3). To date, ADAMTS13 is the only known member of the ADAMTS family to display a restricted active site (Kretz et al., 2015; Petri et al., 2019). We hypothesize that the folding of the variable loop and the calcium-binding loop across the active site cleft restricts access to the active site cleft of ADAMTS13, similar to the function of the prodomain of other metzincin proteases. In support of this hypothesis, comparison of the crystal structures and sequences between the metalloprotease domains of ADAMTS5 and ADAMTS13 suggests that the variable loop and the calcium-binding loop of ADAMTS13 may display a high degree of flexibility (Figure 6.1B and Figure 7.2). In particular, the variable loop of ADAMTS5 contains an alpha helix at position G236-P244 in ADAMTS13, thereby lacking the flexibility that is likely found in the disordered loop of ADAMTS13. Further, the calcium-binding loop of ADAMTS5 contains a disulfide bond between positions 184 and 190, thereby providing rigidity to the loop. Interestingly, the disulfide bond at this position is conserved in the ADAMTS family, but does not exist in ADAMTS13. Therefore, we propose that the absence of the alpha helix in the variable loop, and the lack of a disulfide bond between positions 184 and 190 in the calcium-binding loop, provide the necessary flexibility for both loops to restrict access to the active site cleft of ADAMTS13.

As expected, swapping the variable loop and the calcium-binding loop from ADAMTS5 into MDTCS13 impaired the proteolysis of FRETS-VWF73 (Table 7.2).

Swapping the sequence responsible for the alpha helix (D421-F429) from the variable loop of ADAMTS5 did not produce the same pronounced k_{cat} and K_m effects as observed with swapping the calcium-binding loop from ADAMTS5. This observation is consistent with the importance of the calcium-binding loop in forming the S1 specificity pocket required for VWF docking to ADAMTS13. Nonetheless, MDTCS-V5 displayed a 2-fold reduction in k_{cat} and no change in K_m compared to WT-MDTCS (Table 7.2). Therefore, residues G236-P244 within the variable loop of ADAMTS13 may affect the turnover of VWF, but not the affinity of ADAMTS13 for VWF. Swapping the calcium-binding loop of ADAMTS13 with ADAMTS5 revealed a 13-fold decrease in k_{cat}, a 2-fold increase in K_m, and a 33-fold decrease in the catalytic efficiency of MDTCS-C5 compared to WT-MDTCS. These findings were consistent with a previous mutagenesis study (Gardner et al., 2009). By swapping the calcium-binding loop of ADAMTS13 with ADAMTS5, we propose that this change may have caused a disruption in the S1 specificity pocket, resulting in a reduction in both the turnover rate and affinity for VWF. Since the calcium-binding loop was swapped and not removed, this suggests that the calcium-binding loop of ADAMTS13 is very specific to the ADAMTS13/VWF interaction, and not a general defect in proteolytic activity. Interestingly, we did not observe a synergistic reduction in enzyme function when combining the variable loop and the calcium-binding loop swaps. Swapping both the variable loop and the calcium-binding loop together resulted in the catalytic efficiency of MDTCS-GVC5 to be less reduced (6-fold) than swapping only the calcium-binding loop (33-fold) (Table 7.2). Since the active site cleft (including the S1 and S1' specificity pockets) were composed by segments solely from ADAMTS5, these

segments may have been better coordinated for active site functionality in the double mutant than observed with either of the single variants of ADAMTS13. Therefore, we suggest that the variable loop and the calcium-binding loop of ADAMTS5 are conformationally complementary to each other, which may explain the absence of a synergistic reduction in proteolytic activity when we swapped both the variable loop and the calcium-binding loop from ADAMTS5.

Regarding inhibition, swapping each loop individually did not sensitize MDTCS to inhibition. When both the loops were swapped with their corresponding segments from ADAMTS5, we were able to sensitize MDTCS-GVC5 to Marimastat (Figure 6.6 D and F). The kinetic analysis of MDTCS-GVC5 in the presence of Marimastat reveal a 3-fold reduction in k_{cat} and no change in K_m compared to MDTCS-GVC5 in the absence of Marimastat (Table 7.2). The pronounced k_{cat} effect and an absent K_m effect is consistent with a direct inhibitor specifically targeting the catalytic zinc ion of the active site (Tortorella et al., 2009). As previously mentioned, the crystal structure of ADAMTS5 in the presence of Marimastat suggests that the active site cleft and the S1' specificity pocket remain accessible (Tortorella et al., 2009) (Figure 7.3). By swapping the same regions that compose the active site cleft of ADAMTS5 that were shown to remain unrestricted (the variable loop and the calcium-binding loop) into MDTCS13 we were able to sensitize MDTCS-GVC5 to Marimastat. However, A2M and TIMP3 were unable to inhibit MDTCS-GVC5 despite both being inhibitors of ADAMTS5 (Figure 6.6 C-E). These findings suggest that swapping the active site cleft from ADAMTS5 only partially opened the access to the active site cleft. We propose that the relative small size of

Marimastat (331.41 g/mol) allowed Marimastat to enter the partial opening to the active cleft of MDTCS-GVC5 induced by swapping the calcium-binding loop and the variable loop from ADAMTS5, whereas both A2M (800,000 g/mol) and TIMP3 (30,000 g/mol) are much larger inhibitors. Direct comparison of Marimastat inhibition between ADAMTS5 and MDTCS-GVC5 found Marimastat to inhibit ADAMTS5 with higher potency than MDTCS-GVC5 (Figure 6.7B). This finding further supports the active site cleft being only partially opened in MDTCS-GVC5.

Once in the active site cleft, Marimastat covalently binds to the catalytic zinc ion, and forms non-covalent interactions with residues residing in the active site cleft, including the conserved catalytic glutamic acid in the catalytic motif (Tortorella et al., 2009). Consequently, this results in the inhibition of ADAMTS5 and other members of the ADAMTS protease family (Tortorella et al., 2009). The crystal structure of ADAMTS5 in complex with Marimastat demonstrates non-covalent interactions with residues D377, T378, G380, E411, S440, S441, and L443 in ADAMTS5. Several of these residues were carried over from ADAMTS5 in the MDTCS-GVC5 variant that was susceptible to Marimastat inhibition. Therefore, Marimastat likely engaged MDTCS-GVC5 residues D377/T378 in the calcium-binding loop, residues S440/S441/L443 in the variable loop, and with E225, which is the conserved catalytic glutamic acid found in all ADAMTS members. We propose that swapping the variable loop and the calcium-binding loop from ADAMTS5 allowed for Marimastat to access the active site cleft, including these residues, which would otherwise be restricted in ADAMTS13 by folding of these loops across the active site cleft. Anchoring of Marimastat or similar inhibitors to

these residues that are in close proximity to the catalytic zinc can only occur when inhibitors can gain access to the active site cleft. Specificity of inhibitors is determined by subtle and indirect factors, such as ring shape, ring rigidity, specificity pocket size, and protein conformation flexibility, rather than specific inhibitory interaction, such as zinc chelation (Tortorella et al., 2009). These indirect factors, particularly conformation flexibility, may explain the resistance of ADAMTS13 to protease inhibitors. This characteristic is consistent with our data suggesting that in ADAMTS13 the calcium-binding loop and the variable loop protect access to the active site cleft by folding across it. Swapping the variable loop and the calcium-binding loop from ADAMTS5 may impact the conformation flexibility of the metalloprotease domain of MDTCS13, thereby allowing partial access to the active site cleft. However, these conformational changes may not be sufficient to allow access of larger inhibitors like A2M and TIMPs, which may explain why these macromolecular inhibitors were still unable to inhibit MDTCS-GVC5.

Since MDTCS-GVC5 remained resistant towards A2M and TIMP3, this finding suggests that there are other feature(s) of ADAMTS13 that continue to protect it from these natural macromolecular protease inhibitors. The crystal structure of ADAMTS13 yields further clues into the resistance of ADAMTS13 to protease inhibitors. Posterior to the active site cleft, residues P317-L354 of the disintegrin domain form two loops at the base of the active site cleft (Figure 7.2B). A previous study targeting this region of the disintegrin domain showed that these loops bind to VWF and help position the scissile bond towards the active site cleft of ADAMTS13 (De Groot et al., 2009). However, these

two disordered loops are also likely to be very flexible, and may contribute to the protection of the MDTCS-GVC5 against A2M and TIMPs. Future studies will explore the contribution of residues P317-L354 of the disintegrin domain of ADAMTS13 in protecting against macromolecular inhibitors, such as A2M and TIMPs. Taken together, the closed conformation confers global latency, while the metalloprotease domain confers local latency, which collectively restricts the accessibility of protease inhibitors to the active site cleft, thereby protecting ADAMTS13 from inhibition. The findings here present novel insight into the mechanism by which ADAMTS13 is resistance to protease inhibitors.

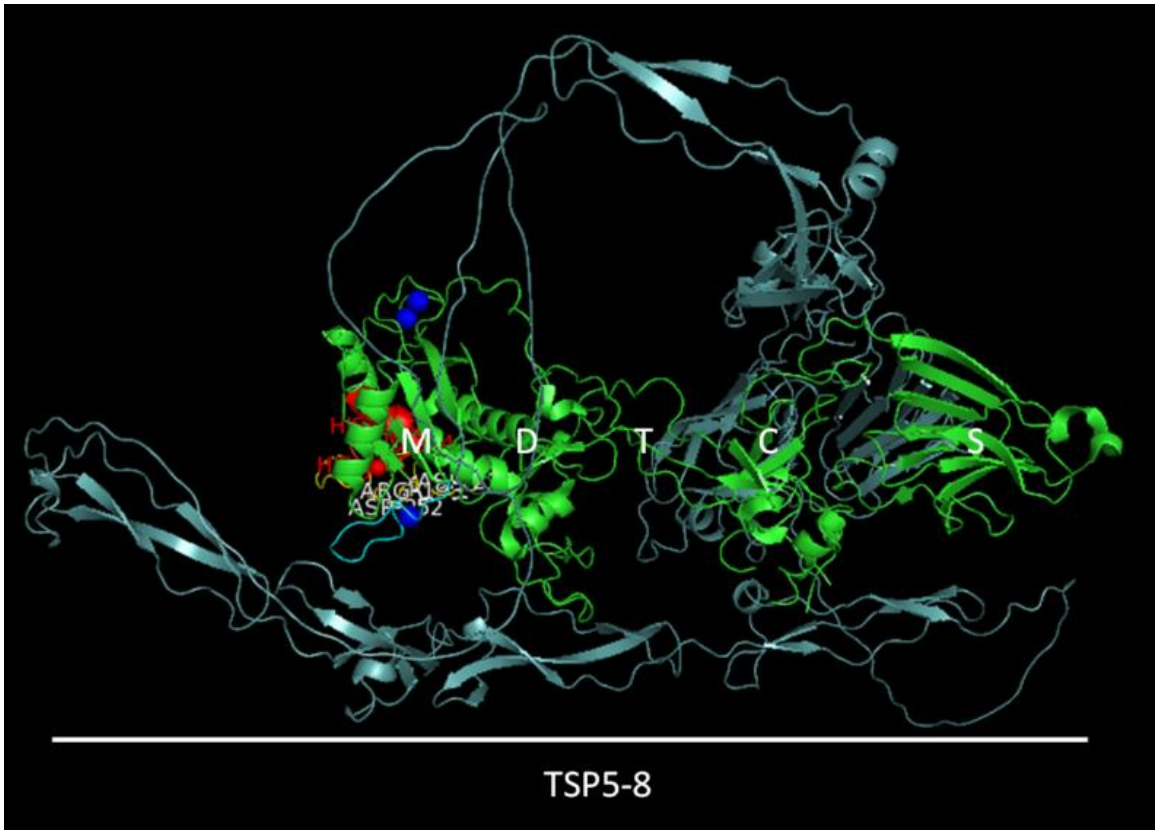

Figure 7.1 AlphaFold computational prediction of ADAMTS13 structure. Lateral view of the closed conformation interacting with MDTCS domains. Computational prediction of the structure of ADAMTS13 suggests that TSP5-8 domains of the closed conformation are anterior to metalloprotease domain, and then run parallel and inferior to MDTCS. The AlphaFold model suggests that the closed conformation restricts the active site and exosite accessibility. MDTCS is shown in green; closed conformation is shown in teal. Molecular visualization using PYMOL (PDB: 6QIG – ADAMTS13; AF-Q76LX8-F1-model_v2 – AlphaFold prediction).

A.

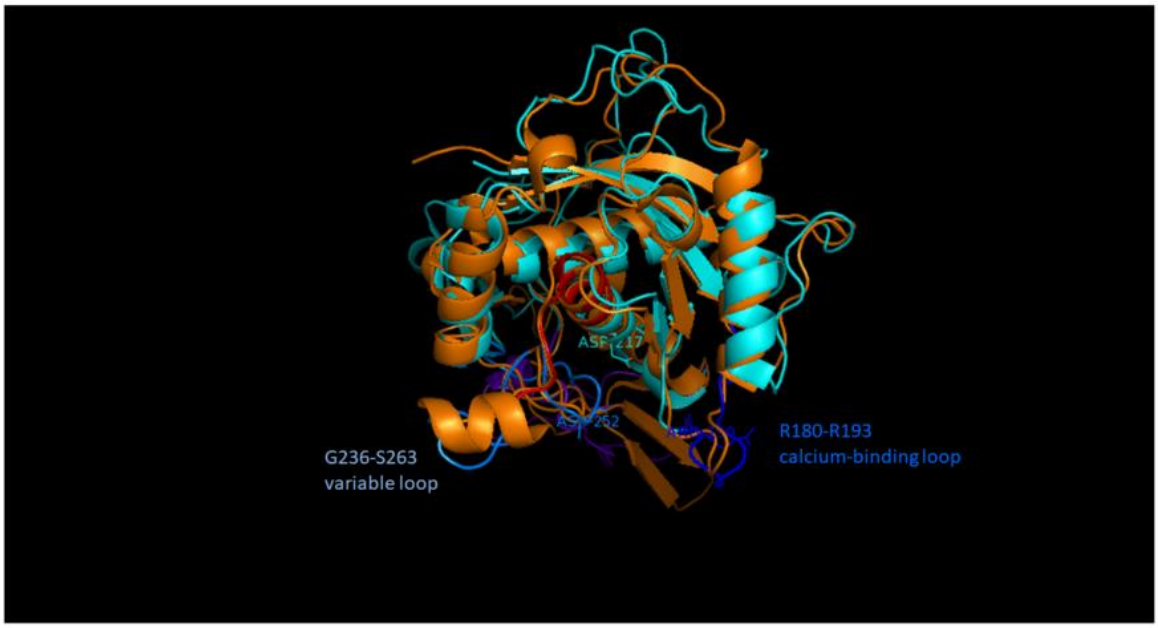
G236-S263
variable loop
R180-R193
calcium-binding loop

B.


P317-L354
Disintegrin Domain

Figure 7.2. Crystal structure of ADAMTS13 overlapped with the crystal structure of ADAMTS5. A. Anterior view of the active site of ADAMTS13 overlaid with ADAMTS5. **B.** Lateral view of the active of ADAMTS13 overlaid with ADAMTS5. ADAMTS13 is shown in cyan, ADAMTS5 is shown in orange, and their active site residues are shown in red. The gatekeeper triad (R193, D217, and D252), the variable loop (G236-S263) (marine), and the calcium-binding loop (R180-R193) (blue) are unique features of ADAMTS13 that contribute to the protection of ADAMTS13 against protease inhibitors. The residues P317-L354 form two loops (purple) within the disintegrin domain of ADAMTS13, which may further protect ADAMTS13 from protease inhibitors. Molecular visualization using PYMOL (PDB: 6QIG – ADAMTS13; 3HY7 – ADAMTS5).

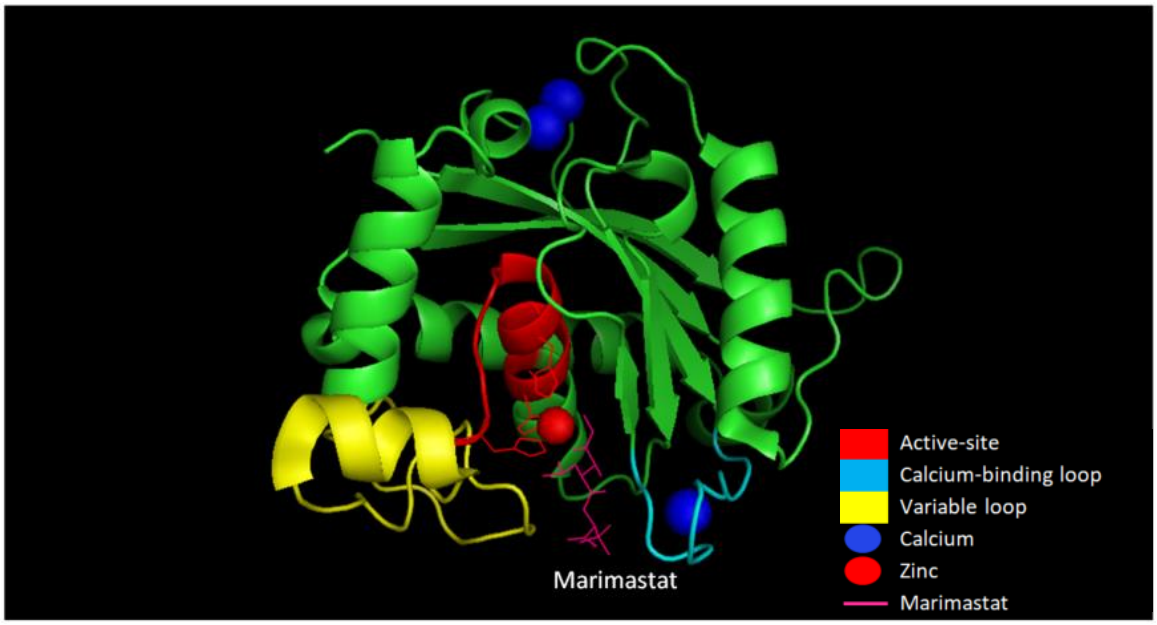

Figure 7.3. Crystal structure of ADAMTS5 in the presence of Marimastat. Marimastat is able to gain access to the active site cleft of ADAMTS5. The variable loop (yellow) and the calcium-binding loop (cyan) restrict access to the active site cleft of ADAMTS13, but not ADAMTS5. Active site shown in red and Marimastat shown in pink. Molecular visualization using PYMOL (PDB: 3HY7).

Table 7.1. Specific activity for each domain truncation and chimeric construct containing the active site from ADAMTS13. Statistical analysis compared to row shaded in grey; ns $p > 0.05$, * $p \leq 0.05$, ** $p \leq 0.01$, *** $p \leq 0.001$, **** $p \leq 0.0001$.

	Proteolytic Activity (RFU x s^{-1} x nM)	**Fold change**
WT-ADAMTS13	51.52±3.98	
WT-MDTCS	92.73±4.82****	1.80 (↑)
MD	2.83±0.33****	32.77 (↓)

	Proteolytic Activity (RFU x s^{-1} x nM)	**Fold change**
WT-MDTCS	92.73±4.82	
MD13/TCS5	1.77±0.19****	52.39 (↓)
M13/DTCS5	0.03±0.02****	3091.00 (↓)

	Proteolytic Activity (RFU x s^{-1} x nM)	**Fold change**
WT-MDTCS	87.92±0.75	
MDTCS-G	88.67±2.30^{ns}	1.01 (↑)
MDTCS-C5	2.17±0.75****	40.52 (↓)
MDTCS-V5	48.97±12.11****	1.80 (↓)
MDTCS-GVC5	17.37±1.38****	5.06 (↓)

Table 7.2. Kinetic analysis of WT-ADAMTS13, WT-MDTCS, and MDTCS metalloprotease domain mutants. Statistical analysis of V_{max} and K_m compared to WT-MDTCS values. Effects of Marimastat on MDTCS-GVC5 also compared to MDTCS-GVC5 in the absence of Marimastat; ns $p > 0.05$, * $p \leq 0.05$, ** $p \leq 0.01$, *** $p \leq 0.001$, **** $p \leq 0.0001$.

	V_{max} (RFU x s^{-1})	**K_m (µM)**	**k_{cat} (RFU x s^{-1} x nM^{-1})**	**k_{cat}/K_m (RFU x s^{-1} x nM^{-1} x μM^{-1})**	**Fold change**
WT-ADAMTS13	2728±117*	1.96±0.20***	136.40±5.85	69.73	2.02↓
WT-MDTCS	3085±203	1.09±0.21	154.25±10.15	141.13	-
MDTCS-G	3142±192ns	1.22±0.20ns	157.10±9.60	128.77	1.10↓
MDTCS-C5	231±26****	2.70±0.64****	11.55±1.30	4.28	32.97↓
MDTCS–V5	2110±74****	1.25±0.13^{ns}	105.50±3.70	84.40	1.67↓
MDTCS-GVC5	861±60****	1.84±0.31***	43.05±3.00	23.40	6.03↓
MDTCS-GVC5 + Marimastat (250 nM)	287±28****	1.65±0.40*	14.35±1.40	8.70	16.22↓
MDTCS-GVC5	861±60	1.84±0.31	43.05±3.00	23.37	-
MDTCS-GVC5 + Marimastat (250 nM)	287±28***	1.65±0.40^{ns}	14.35±1.40	8.70	2.69↓

Chapter 8: Limitations and Future Directions

A limitation of our study is the protein purification technique. Total protein stains and Western blots show impurities and degradation with our Q-Sepharose and Ni-NTA purified constructs. The combination of Q-Sepharose and Ni-NTA did increase the purity of our constructs compared to our preliminary purifications, which were purified using only Ni-NTA; however, the final protein product was not highly pure (>90%). To increase our purity yield, all future purifications will be conducted using the Strep-tag II/Strep Tactin system because this system provides significantly improved specificity in a single step. We have redesigned some of our important constructs to include an N-terminal Strep-tag II (WSHPQFEK). Extended protein collection period increases protein yield; however this also increases protein degradation even in the presence of protease inhibitors. Currently, we collect conditioned media every 48-72 hours in the presence of protease inhibitors (AEBSF) to limit protein degradation. To further limit degradation, we will change our protocol to collect condition media at 48 hours. These changes should improve the overall purity of our constructs. We do acknowledge the importance of having highly purified recombinant protein; however, the impurities and degradation did not affect our interpretation of studying the inhibition of our constructs. More importantly, we verified that each construct was proteolytically active and confirmed that each construct performed similar to values reported in previous literature.

Another limitation of our study is the narrow detection threshold of the FRETS-VWF73 assay. The FRETS-VWF73 assay is designed to measure the activity of full-length ADAMTS13 or truncated MDTCS. Removing or swapping crucial exosites of

ADAMTS13 prevents adequate binding to FRETS-VWF73, thereby resulting in significant loss in proteolytic activity that is below the detection limit of this assay. To meet the detection threshold, we had to increase the concentrations of our domain truncation and chimeric constructs. However, we also increased the concentration of inhibitors to maintain protease-inhibitor ratios throughout the study. Alternatively, since we have determined the K_m value of pertinent constructs, we can use that value of FRETS-VWF73 to measure the activity of that particular construct.

Lastly, we acknowledge that quantification of aggrecan Western blots is not an accurate assessment of proteolysis by ADAMTS5 or its chimeras. Western blots lack the sensitivity required for precise measurement of proteolytic activity. Since no FRET-based aggrecan substrate is currently available for ADAMTS5, we opted to study the inhibition of our ADAMTS5 constructs using a Western blot approach. Through this approach, we assessed for the loss of the intact form of aggrecan and/or gain of the cleaved form of A2M relative to aggrecan, in the absence of protease. For the purpose of studying inhibition, the precise measurements of proteolysis were not necessary because we were still able to distinguish differences among various experimental conditions. Nonetheless, we attempted to address and limit the shortcomings of our study, so these limitations do not affect the interpretations of our results.

In terms of future directions, the MD5(TCS-CUB13) chimera tested the impact of the closed conformation by swapping the MD domains of ADAMTS13 with ADAMTS5. We found that the closed conformation significantly reduced the proteolytic activity, and partially contributed to the resistance of ADAMTS13 to protease inhibitors by blocking

access to the active site. The Western blot detected MD5(TCS-CUB13) at the correct predicted molecular weight, and our results showed evidence of resistance towards protease inhibitors, as predicted with the addition of the closed conformation. However, we did not verify the interaction between the spacer domain and the CUB domains, indicative of the closed conformation. Therefore, we intend on confirming the spacer-CUB interaction by using an ELISA-based technique specifically designed to test the spacer-CUB interaction through collaboration with our colleague Dr. Karen Vanhoorelbeke (KU Leuven, Belgium).

We attempted to sensitize the MD construct using segments of VWF that engaged the disintegrin domain exosite. These VWF peptides were unable to sensitize MD to inhibition. Existing literature shows that following disintegrin domain engagement, VWF engages the N-terminal S3 subsite in the metalloprotease domain, prior to the cleavage of its scissile bond (Crawley et al., 2011). Therefore, future studies that examine ADAMTS13 resistance to protease inhibition using this exosite engagement approach should include an additional N-terminal peptide that engages the S3 subsite. Peptides engaging the S3 subsite, in addition to engaging the disintegrin domain, may activate ADAMTS13 from its latent form, thereby allowing inhibitor access to the active site cleft.

In the present study, we describe the novel mechanism by which ADAMTS13 shows no off-target proteolysis and is resistant to protease inhibitors. The variable loop (G236-S263) and the calcium-binding loop (R180-R193) both contribute to the resistance of ADAMTS13 to protease inhibition by restricting access to its active site cleft. The global latency induced by the closed confirmation prevents further access to the active

site cleft. Swapping the variable loop and the calcium-binding loop with the corresponding loop from ADAMTS5 partially opened the access to the active site cleft. Analysis of the crystal structures and sequences between ADAMTS5 and ADAMTS13 disintegrin domains suggests that residues P317-L354 may also contribute to the resistance of ADAMTS13 to protease inhibitors (Figure 7.2B). These residues form two unique loops at the base of the active site cleft, and are important in positioning VWF for proteolysis (De Groot et al., 2009). Therefore, we suggest that residues P317-L354 of the disintegrin domain may also contribute to the resistance of ADAMTS13 to protease inhibitors. Thus, we propose that future studies focus on the contribution of residues P317-L354 of the disintegrin domain, in addition to the variable loop, the calcium-binding loop, and the closed conformation of ADAMTS13.

Chapter 9: Conclusion

Collectively our findings suggest that the resistance of ADAMTS13 to protease inhibitors occurs at multiple levels. Consistent with recent findings by Petri *et al.*, we also propose that the closed conformation confers global latency and the metalloprotease domain confers the local latency of ADAMTS13. In addition to attenuating ADAMTS13 proteolytic activity, we suggest that the closed conformation also contributes to the resistance of ADAMTS13 against protease inhibitors. The closed conformation limits the accessibility of the active site to protease inhibitors, which was evident by a diminished rate of proteolysis and inhibition. We further suggest that the local latency of ADAMTS13 is maintained by the flexibility of the variable loop (G236-S263) and the calcium-binding loop (R180-R193), which allows these loops to fold across the active site cleft, thereby protecting ADAMTS13 from protease inhibitors. We propose that these loops which guard the active site cleft, including the catalytic zinc, reside in a manner similar to the propeptide in other metzincin proteases. Additionally, residues P317-L354 in the disintegrin domain may further protect ADAMTS13 from protease inhibitors, which may be of future interest. For inhibition or proteolysis to occur, exosites need to be engaged by a substrate, and cause conformational change that converts ADAMTS13 from its latent form to an active protease. To date, VWF is the only known substrate of ADAMTS13, and only VWF has shown the capacity to readily displace these loops through extensive exosite interactions, resulting in its proteolysis. Remarkably, we are the first group to sensitize ADAMTS13 to protease inhibitors. Altogether, our findings here present novel insight into the mechanism by which ADAMTS13 is resistant to protease

inhibition, and advances our understanding of ADAMTS13 regulation and substrate recognition.

Chapter 10: References

Abou-ismail, M. Y., Diamond, A., Kapoor, S., Arafah, Y., & Nayak, L. (2020). The hypercoagulable state in COVID-19: Incidence, pathophysiology, and management. *Thrombosis Research*, *194*, 101–115.

Ai, J., Smith, P., Wang, S., Zhang, P., & Zheng, X. L. (2005). The Proximal Carboxyl-terminal Domains of ADAMTS13 Determine Substrate Specificity and Are All Required for Cleavage of von Willebrand Factor. *J Biol Chem*, *280*(33), 29438–29434.

Akiyama, M., Takeda, S., Kokame, K., Takagi, J., & Miyata, T. (2009). Crystal structures of the noncatalytic domains of ADAMTS13 reveal multiple discontinuous exosites for von Willebrand factor. *Proceedings of the National Academy of Sciences of the United States of America*, *106*(46), 19274–19279.

Andersen, G. R., Koch, T. J., Dolmer, K., Sottrup-jensen, L., & Nyborg, J. (1995). Low Resolution X-ray Structure of Human Methylamine-treated A2- Macroglobulin. *The Journal of Biological Chemistry*, *270*(42), 25133–25141.

Apte, S. S. (2004). A disintegrin-like and metalloprotease (reprolysin type) with thrombospondin type 1 motif: the ADAMTS family. *Int J Biochem Cell Bio*, *36*, 981–985.

Asakura, H., & Ogawa, H. (2021). COVID-19-associated coagulopathy and disseminated intravascular coagulation. *International Journal of Hematology*, *113*(1), 45–57.

Azfar, M. F., Khan, M. F., Habib, S. S., Aseri, Z. Al, Zubaidi, A. M., Aguila, D. O., Suriya, M. O., & Ullah, H. (2017). Prognostic value of ADAMTS13 in patients with severe sepsis and septic shock. *Clin Invest Med*, *40*(2), 49–58.

Banno, F., Chauhan, A. K., Kokame, K., Yang, J., Miyata, S., Wagner, D. D., & Miyata, T. (2009). The distal carboxyl-terminal domains of ADAMTS13 are required for regulation of in vivo thrombus formation. *Blood*, *113*(21), 5323–5329.

Berg, J., Tymoczko, J., & Stryer, L. (2002). Proteases: Facilitating a Different Reaction. In *Biochemistry* (5th ed.).

Bernardo, A., Ball, C., Nolasco, L., Moake, J. F., & Dong, J. (2019). Effects of inflammatory cytokines on the release and cleavage of the endothelial cell – derived ultralarge von Willebrand factor multimers under flow. *Blood*, *104*(1), 100–107.

Berntorp, E., Peake, I., Laffan, M., Montgomery, R., Windyga, J., Goodeve, A., Petrini, P., Von Depka, M., Miesbach, W., Lillicrap, D., Federici, A. B., Lassila, R., & White, G. (2012). von Willebrand's disease: a report from a meeting in the Aland islands. *Haemophilia*, *18*(Suppl. 6), 1–13.

Biltoft, D., Gram, J. B., Larsen, A., Münster, A. M. B., Sidelmann, J. J., Skjoedt, K., & Palarasah, Y. (2017). Fast form alpha-2-macroglobulin - A marker for protease activation in plasma exposed to artificial surfaces. *Clinical Biochemistry*, *50*(18), 1203–1208.

Blair, P., & Flaumenhaft, R. (2009). Platelet α–granules: Basic biology and clinical correlates. *Blood Rev.*, *23*(4), 177–189.

Bondeson, J., Wainwright, S., Hughes, C., & Caterson, B. (2008). The regulation of the ADAMTS4 and ADAMTS5 aggrecanases in osteoarthritis: A review. *Clinical and Experimental Rheumatology*, *26*(1), 139–145.

Cataland, S. R., & Wu, H. M. (2015). Acquired thrombotic thrombocytopenic purpura: New therapeutic options and their optimal use. *Journal of Thrombosis and Haemostasis*, *13*(S1), S223–S229.

Chapin, J. C., & Hajjar, K. A. (2015). Fibrinolysis and the control of blood coagulation. *Blood Reviews*, *29*(1), 17–24.

Chen, Y., Yuan, Y., & Li, W. (2018). Sorting machineries: How platelet-dense granules differ from α-granules. *Bioscience Reports*, *38*(5), 1–9.

Coppo, P., & Lämmle, B. (2020). Animal models of thrombotic thrombocytopenic purpura: the tales from zebrafish. *Haematologica*, *105*(4), 861–863.

Crawley, J. T. B., De Groot, R., Xiang, Y., Luken, B. M., & Lane, D. A. (2011). Unraveling the scissile bond: How ADAMTS13 recognizes and cleaves von Willebrand factor. *Blood*, *118*(12), 3212–3221.

Dangott, L. J.; Cunningham, L. W. (1982). Residual A2-macroglobulin in fetal calf serum and properties of its complex with thrombin. *Biochemical and Biophysical Research Communications*, *107*(4), 1243–1251.

De Groot, R., Bardhan, A., Ramroop, N., Lane, D. A., & Crawley, J. T. B. (2009). Essential role of the disintegrin-like domain in ADAMTS13 function. *Blood*, *113*(22), 5609–5616.

De Groot, R., Lane, D. A., & Crawley, J. T. B. (2010). The ADAMTS13 metalloprotease domain: Roles of subsites in enzyme activity and specificity. *Blood*, *116*(16), 3064–3072.

De Groot, R., Lane, D. A., & Crawley, J. T. B. (2015). The role of the ADAMTS13 cysteine-rich domain in VWF binding and proteolysis. *Blood*, *125*(12), 1968–1975.

de Maat, S., Clark, C., Barendrecht, A. D., Smits, S., van Kleef, N. D., El Otmani, H., Waning, M., van Moorsel, M. V. A., Szardenings, M., Delaroque, N., Vercruysse, K., Urbanus, R. T., Sebastian, S., Lenting, P. J., Hagemeyer, C. E., Renné, T.,

Vanhoorelbeke, K., Tersteeg, C., & Maas, C. (2021). Microlyse; a thrombolytic agent that targets VWF for clearance of microvascular thrombosis. *Blood*.

Deforche, L., Roose, E., Vandenbulcke, A., Vandeputte, N., Feys, H. B., Springer, T. A., Mi, L. Z., Muia, J., Sadler, J. E., Soejima, K., Rottensteiner, H., Deckmyn, H., De Meyer, S. F., & Vanhoorelbeke, K. (2015). Linker regions and flexibility around the metalloprotease domain account for conformational activation of ADAMTS-13. *Journal of Thrombosis and Haemostasis*, *13*(11), 2063–2075.

Demircan, K., Yonezawa, T., Takigawa, T., Topcu, V., Erdogan, S., Ucar, F., Armutcu, F., Yigitoglu, M. R., Ninomiya, Y., & Hirohata, S. (2013). ADAMTS1, ADAMTS5, ADAMTS9 and aggrecanase-generated proteoglycan fragments are induced following spinal cord injury in mouse. *Neuroscience Letters*, *544*, 25–30.

Dempfle, C. (2004). Coagulopathy of sepsis. *Thromb Haemost.*, *91*, 213–224.

Di Stasio, E., Lancellotti, S., Peyvandi, F., Palla, R., Mannucci, P. M., & De Cristofaro, R. (2008). Mechanistic studies on ADAMTS13 catalysis. *Biophysical Journal*, *95*(5), 2450–2461.

Dorman, G., Cseh, S., Hajdu, I., Barna, L., Konya, D., Kupai, K., Kovacs, L., & Ferdinandy, P. (2010). Matrix metalloproteinase inhibitors: A critical appraisal of design principles and proposed therapeutic utility. *Drugs*, *70*(8), 949–964.

Fan, D., & Kassiri, Z. (2020). Biology of Tissue Inhibitor of Metalloproteinase 3 (TIMP3), and Its Therapeutic Implications in Cardiovascular Pathology. *Frontiers in Physiology*, *11*(June), 1–16.

Feldman, S. R., Gonias, S. L., & Pizzo, S. V. (1985). Model of alpha 2-macroglobulin structure and function. *Proceedings of the National Academy of Sciences of the United States of America*, *82*(17), 5700–5704.

Feys, H. B., Anderson, P., Vanhoorelbeke, K., Majerus, E., & Sadler, J. (2009). Multi-step binding of ADAMTS13 to VWF. *J Thromb Haemost*, *7*(12).

Fleischmann, C., Scherag, A., Adhikari, N., Hartog, C., Tsaganos, Y., Schlattmann, P., Angus, D., & Reinhart, K. (2016). Assessment of Global Incidence and Mortality of Hospital-treated Sepsis. *Am J Respir Crit Care Med*, *193*(3), 259–272.

Franchini, M., & Mannucci, P. M. (2008). Advantages and limits of ADAMTS13 testing in thrombotic thrombocytopenic purpura. *Blood Transfusion = Trasfusione Del Sangue*, *6*(3), 127–135.

Fujimura, Y., Titani, K., Holland, L. Z., Roberts, J. R., Kostel, P., Ruggeri, Z. M., & Zimmerman, T. S. (1987). A heparin-binding domain of human von Willebrand factor. *Journal of Biological Chemistry*, *262*(4), 1734–1739.

Furlan, M., Robles, R., Morselli, B., Sandoz, P., & Lämmle, B. (1999). Recovery and half-life of von Willebrand factor-cleaving protease after plasma therapy in patients with thrombotic thrombocytopenic purpura. *Thrombosis and Haemostasis*, *81*(1), 8–13.

Gailani, D., & Renné, T. (2007). The intrinsic pathway of coagulation: A target for treating thromboembolic disease? *Journal of Thrombosis and Haemostasis*, *5*(6), 1106–1112.

Gale, A. (2011). Current understanding of hemostasis. *Toxicol Pathol* ., *39*(1), 273–280.

Gao, W., Anderson, P. J., Majerus, E. M., Tuley, E. A., & Sadler, J. E. (2006). Exosite interactions contribute to tension-induced cleavage of von Willebrand factor by the antithrombotic ADAMTS13 metalloprotease. *Proc Natl Acad Sci U S A*, *103*(50), 19099–19104.

Gao, W., Anderson, P. J., & Sadler, J. E. (2008). Extensive contacts between ADAMTS13 exosites and von Willebrand factor domain A2 contribute to substrate specificity. *Blood*, *112*(5), 1713–1719.

Gao, W., Zhu, J., Westfield, L. A., Tuley, E. A., Anderson, P. J., & Sadler, J. E. (2012). Rearranging exosites in noncatalytic domains can redirect the substrate specificity of ADAMTS proteases. *Journal of Biological Chemistry*, *287*(32), 26944–26952.

Garcia-Ferrer, I., Arêde, P., Gómez-Blanco, J., Luque, D., Duquerroy, S., Castón, J. R., Goulas, T., & Gomis-Rüth, F. X. (2015). Structural and functional insights into *Escherichia coli* α_2 -macroglobulin endopeptidase snap-trap inhibition. *Proceedings of the National Academy of Sciences*, *112*(27), 8290–8295.

Gardner, M. D., Chion, C. K. N. K., Groot, R. De, Shah, A., Crawley, J. T. B., & Lane, D. A. (2009). A functional calcium-binding site in the metalloprotease domain of ADAMTS13. *Blood*, *113*(5), 1149–1157.

Garland, K. S., Reitsma, S. E., Shirai, T., Zilberman-Rudenko, J., Tucker, E. I., Gailani, D., Gruber, A., McCarty, O. J. T., & Puy, C. (2017). Removal of the C-Terminal Domains of ADAMTS13 by Activated Coagulation Factor XI induces Platelet Adhesion on Endothelial Cells under Flow Conditions. *Frontiers in Medicine*, *4*(December).

Gerhardt, S., Hassall, G., Hawtin, P., McCall, E., Flavell, L., Minshull, C., Hargreaves, D., Ting, A., Pauptit, R. A., Parker, A. E., & Abbott, W. M. (2007). Crystal Structures of Human ADAMTS-1 Reveal a Conserved Catalytic Domain and a Disintegrin-like Domain with a Fold Homologous to Cysteine-Rich Domains. *Journal of Molecular Biology*, *373*(4), 891–902.

Giansily-Blaizot, M., & Schved, J.-F. (2017). Recombinant human factor VIIa (rFVIIa) in hemophilia: mode of action and evidence to date. *Therapeutic Advances in*

Hematology, *8*(12), 345–352.

Gill, J., Endres-Brooks, J., Bauer, P., Marks, W., & Montgomery, R. R. (1987). The effect of ABO blood group on the diagnosis of von Willebrand disease. *Blood*, *69*(6), 1691–1695.

Golias, C., Charalabopoulos, A., Stagikas, D., Charalabopoulos, K. A., & Batistatou, A. (2007). The kinin system - bradykinin: Biological effects and clinical implications. Multiple role of the kinin system-bradykinin. *Hippokratia*, *11*(3), 124–128.

Gomis-Rth, F.-X., Maskos, K., Betz, M., Bergner, A., Huber, R., Suzuki, K., Yoshida, N., Nagase, H., Brew, K., Bourenkov, G. P., Bartunik, H., & Bode, W. (1997). Mechanism of inhibition of the human matrix metalloproteinase stromelysin-1 by TIMP-1. *Nature*, *389*, 77–81.

Gorodetsky, R., Mou, X., Blankenfeld, A., & Marx, G. (1993). Platelet multielemental composition, lability, and subcellular localization. *American Journal of Hematology*, *42*(3).

Grover, S. P., & Mackman, N. (2019). Intrinsic pathway of coagulation and thrombosis: Insights from animal models. *Arteriosclerosis, Thrombosis, and Vascular Biology*, *39*(3), 331–338.

Guo, C., Tsigkou, A., & Lee, M. H. (2016). ADAMTS13 and 15 are not regulated by the full length and N-terminal domain forms of TIMP-1, -2, -3 and -4. *Biomedical Reports*, *4*(1), 73–78.

Harter, K., Levine, M., & Henderson, S. (2015). Anticoagulation Drug Therapy: A Review. *Western Journal of Emergency Medicine*, *26*(1), 11–17.

Heijdra, J. M., Cnossen, M. H., & Leebeek, F. W. G. (2017). Current and Emerging Options for the Management of Inherited von Willebrand Disease. *Drugs*, *77*(14), 1531–1547.

James, P. D., & Goodeve, A. C. (2011). Von Willebrand disease. *Genetics in Medicine*, *13*(5), 365–376.

Jin, S. Y., Skipwith, C. G., & Zheng, X. L. (2010). Amino acid residues Arg659, Arg660, and Tyr 661 in the spacer domain of ADAMTS13 are critical for cleavage of von Willebrand factor. *Blood*, *115*(11), 2300–2310.

Jumper, J., Evans, R., Pritzel, A., Green, T., Figurnov, M., Ronneberger, O., Tunyasuvunakool, K., Bates, R., Žídek, A., Potapenko, A., Bridgland, A., Meyer, C., Kohl, S. A. A., Ballard, A. J., Cowie, A., Romera-Paredes, B., Nikolov, S., Jain, R., Adler, J., … Hassabis, D. (2021). Highly accurate protein structure prediction with AlphaFold. *Nature*, *596*(7873), 583–589.

Kashiwagi, M., Tortorella, M., Nagase, H., & Brew, K. (2001). TIMP-3 Is a Potent Inhibitor of Aggrecanase 1 (ADAM-TS4) and Aggrecanase 2 (ADAM-TS5). *Journal of Biological Chemistry*, *276*(16), 12501–12504.

Kelwick, R., Desanlis, I., Wheeler, G. N., & Edwards, D. R. (2015). The ADAMTS (A Disintegrin and Metalloproteinase with Thrombospondin motifs) family. *Genome Biology*, *16*, 113–129.

Kessler, T., Zhang, L., Liu, Z., Yin, X., Huang, Y., Wang, Y., Fu, Y., Mayr, M., Ge, Q., Xu, Q., Zhu, Y., Wang, X., Schmidt, K., De Wit, C., Erdmann, J., Schunkert, H., Aherrahrou, Z., & Kong, W. (2015). ADAMTS-7 inhibits re-endothelialization of injured arteries and promotes vascular remodeling through cleavage of thrombospondin-1. *Circulation*, *131*(13), 1191–1201.

Khan, M. M., Motto, D. G., Lentz, S. R., & Chauhan, A. K. (2012). ADAMTS13 reduces VWF-mediated acute inflammation following focal cerebral ischemia in mice. *Journal of Thrombosis and Haemostasis*, *10*(8), 1665–1671.

Kim, H. J., Xu, Y., Petri, A., Vanhoorelbeke, K., Crawley, J. T. B., & Emsley, J. (2021). Crystal structure of ADAMTS13 CUB domains reveals their role in global latency. *Science Advances*, *7*(April).

Kirtava, A., Crudder, S., Dilley, A., Lally, C., & Evatt, B. (2004). Trends in clinical management of women with von Willebrand disease: a survey of 75 women enrolled in haemophilia treatment centres in the United States. *Haemophilia*, *10*(2), 158–161.

Kokame, K., Nobe, Y., Kokubo, Y., Okayama, A., & Miyata, T. (2005). FRETS-VWF73, a first fluorogenic substrate for ADAMTS13 assay. *British Journal of Haematology*, *129*(1), 93–100.

Kremer Hovinga, J. A., Vesely, S. K., Terrell, D. R., Lämmle, B., & George, J. N. (2010). Survival and relapse in patients with thrombotic thrombocytopenic purpura. *Blood*, *115*(8), 1500–1511.

Kremer Hovinga, J. A., Zeerleder, S., Kessler, P., Wit, T. R. D. E., Van, J. A., Wuillemin, W. A., & Lammle, B. (2007). ADAMTS-13, von Willebrand factor and related parameters in severe sepsis and septic shock. *Journal of Thrombosis and Haemostasis*, *5*, 2284–2290.

Kretz, C. A., Dai, M., Soylemez, O., Yee, A., Desch, K. C., Siemieniak, D., Tomberg, K., Kondrashov, F. A., Meng, F., & Ginsburg, D. (2015). Massively parallel enzyme kinetics reveals the substrate recognition landscape of the metalloprotease ADAMTS13. *Proceedings of the National Academy of Sciences of the United States of America*, *112*(30), 9328–9333.

Kretz, C. A., Tomberg, K., Van Esbroeck, A., Yee, A., & Ginsburg, D. (2018). High throughput protease profiling comprehensively defines active site specificity for

thrombin and ADAMTS13. *Scientific Reports*, *8*(1), 1–13.

Kuno, K., Terashima, Y., & Matsushima, K. (1999). ADAMTS-1 is an active metalloproteinase associated with the extracellular matrix. *Journal of Biological Chemistry*, *274*(26), 18821–18826.

Lancellotti, S., Peyvandi, F., Pagliari, M., Cairo, A., Abdel-Azeim, S., Chermak, E., Lazzareschi, I., Mastrangelo, S., Cavallo, L., Oliva, R., & De Cristofaro, R. (2015). The D173G mutation in ADAMTS-13 causes a severe form of congenital thrombotic thrombocytopenic purpura. *Thrombosis and Haemostasis*, *115*(1), 51–62.

Lankof, H., van Hoeij, M., Schiphorst, M. E., Bracke, M., Wu, Y. P., Ijsseldijk, M. J., Vink, T., de Groot, P. G., & Sixma, J. J. (1996). A3 domain is essential for interaction of von Willebrand factor with collagen type III. *Thromb Haemost*, *75*(6), 950–958.

Lattuada, A., Rossi, E., Calzarossa, C., Candolfi, R., & Mannucci, P. (2003). Mild to moderate reduction of a von Willebrand factor cleaving protease (ADAM-TS13) in pregnant women with HELLP microangiopathic syndrome. *Haematologica*, *88*(09), 1002–1012.

Leebeek, F. W. G., & Eikenboom, J. C. J. (2016). Von Willebrand's Disease. *New England Journal of Medicine*, *375*(21), 2067–2080.

Lenting, P. J., Christophe, O. D., & Denis, C. V. (2015). von Willebrand factor biosynthesis, secretion, and clearance: connecting the far ends. *Blood*, *125*(13), 2019–2028.

Lerolle, N., Dunois-Larde, C., Badirou, I. ., Motto, D. G., Bruneval, P., Diehl, J.-L., Denis, C. V., & Baruch, D. (2009). von Willebrand factor is a major determinant of ADAMTS-13 decrease during mouse sepsis induced by cecum ligation and puncture. *J Thromb Haemost*, *7*, 843–850.

Levi, M., Scully, M., & Singer, M. (2018). The role of ADAMTS-13 in the coagulopathy of sepsis. *Journal of Thrombosis and Haemostasis*, *16*, 646–651.

Levy, G. G., Motto, D. G., & Ginsburg, D. (2015). Review in translational hematology ADAMTS13 turns 3. *Blood*, *16*(1), 11–18.

Levy, G. G., Nichols, W. C., Lian, E. C., Foroud, T., McClintick, J. N., McGee, B. M., Yang, A. Y., Siemieniak, D. R., Stark, K. R., Gruppo, R., Sarode, R., Shurin, S. B., Chandrasekaran, V., Stabler, S. P., Sabio, H., Bouhassira, E. E., Upshaw, J. D., Ginsburg, D., & Tsai, H. M. (2001). Mutations in a member of the ADAMTS gene family cause thrombotic thrombocytopenic purpura. *Nature*, *413*(6855), 488–494.

Lillicrap, D., & James, P. (2009). Von Willebrand Disease: An introduction for the primary care physician. *Treatment of Hemophilia*, *47*.

Lippi, G., Favaloro, E., Franchini, M., & Guidi, G. (2009). Milestones and perspectives in Hemostasis and coagulation. *Semin.Thromb.Hemost.*, *1*(35), 9–22.

Lippi, G., Pasalic, L., & Favaloro, E. J. (2015). Detection of mild inherited disorders of blood coagulation: Current options and personal recommendations. *Expert Review of Hematology*, *8*(4), 527–542.

Longpré, J.-M., & Leduc, R. (2004). Identification of Prodomain Determinants Involved in ADAMTS-1 Biosynthesis. *Journal of Biological Chemistry*, *279*(32), 33237–33245.

Luan, Y., Kong, L., Howell, D. R., Ilalov, K., Fajardo, M., Bai, X., Di Cesare, P. E., Goldring, Mary, B., Abramson, S. B., & Liu, C. (2008). Inhibition of ADAMTS-7 and ADAMTS-12 Degradation of Cartilage Oligomeric Matrix Protein by Alpha-2-Macroglobulin. *Osteoarthristis Cartilage*, *16*(11), 1413–1420.

Lynch, C. J., Cawte, A. D., Millar, C. M., Rueda, D., & Lane, D. A. (2017). A common mechanism by which type 2A von Willebrand disease mutations enhance ADAMTS13 proteolysis revealed with a von Willebrand factor A2 domain FRET construct. *PLoS ONE*, *12*(11), 1–21.

Mackman, N., Tilley, R. E., & Key, N. S. (2007). Role of the extrinsic pathway of blood coagulation in hemostasis and thrombosis. *Arteriosclerosis, Thrombosis, and Vascular Biology*, *27*(8), 1687–1693.

Madhusudhan, T., Kerlin, B. A., & Isermann, B. (2016). The emerging role of coagulation proteases in kidney disease. *Nature Reviews Nephrology*, *12*(2), 94–109.

Majerus, E. M., Zheng, X., Tuley, E. A., & Sadler, J. E. (2003). Cleavage of the ADAMTS13 propeptide is not required for protease activity. *Journal of Biological Chemistry*, *278*(47), 46643–46648.

Majumdar, M., Askew, R., Schelling, S., Stedman, N., Blanchet, T., Hopkins, B., Morris, E., & Glasson, S. (2007). Double-knockout of ADAMTS-4 and ADAMTS-5 in mice results in physiologically normal animals and prevents the progression of osteoarthritis. *Arthritis Rheum*, *56*(11), 3670–3674.

Matsui, T., & Hamako, J. (2016). von Willebrand factor and von Willebrand disease. *[Rinsho Ketsueki] The Japanese Journal of Clinical Hematology*, *57*(10), 2113–2123.

Matsushita, T., & Sadler, J. E. (1995). Identification of amino acid residues essential for von Willebrand factor binding to platelet glycoprotein ib: Charged-to-alanine scanning mutagenesis of the A1 domain of human von Willebrand factor. *Journal of Biological Chemistry*, *270*(22), 13406–13414.

McGrath, R. T., McRae, E., Smith, O. P., & O'Donnell, J. S. (2010). Platelet von

Willebrand factor - Structure, function and biological importance. *British Journal of Haematology*, *148*(6), 834–843.

McKinnon, T. A. J., Goode, E. C., Birdsey, G. M., Nowak, A. A., Chan, A. C. K., Lane, D. A., & Laffan, M. A. (2010). Specific N-linked glycosylation sites modulate synthesis and secretion of von Willebrand factor. *Blood*, *116*(4), 640–648.

Meisel, J. E., & Chang, M. (2017). Selective small-molecule inhibitors as chemical tools to define the roles of matrix metalloproteinases in disease. *Biochimica et Biophysica Acta - Molecular Cell Research*, *1864*(11), 2001–2014.

Moake, J. F. (2002). Thrombotic microangiopathies. *New England Journal of Medicine*, *347*(8), 589–600.

Moschcowitz, E. (1925). An acute febrile pleiochromic anemia with hyaline thrombosis of the terminal arterioles and capillaries: an undescribed disease. *Mt Sinai J Med*, *70*(5), 352–355.

Mosyak, L., Georgiadis, K., Shane, T., Svenson, K., Hebert, T., McDonagh, T., Mackie, S., Olland, S., Lin, L., Zhong, X., Kriz, R., Reifenberg, E. L., Collins-Racie, L. A., Corcoran, C., Freeman, B., Zollner, R., Marvell, T., Vera, M., Sum, P.-E., … Somers, W. (2008). Crystal structures of the two major aggrecan degrading enzymes, ADAMTS4 and ADAMTS5. *Protein Science*, *17*(1), 16–21.

Muia, J., Zhu, J., Gupta, G., Haberichter, S. L., Friedman, K. D., Feys, H. B., Deforche, L., Vanhoorelbeke, K., Westfield, L. A., Roth, R., Tolia, N. H., Heuser, J. E., & Sadler, J. E. (2014). Allosteric activation of ADAMTS13 by von Willebrand factor. *Proceedings of the National Academy of Sciences of the United States of America*, *111*(52), 18584–18589.

Murphy, G. (2011). Tissue inhibitors of metalloproteinases. *Genome Biology*, *12*(11).

Ono, T., Mimuro, J., Madoiwa, S., Soejima, K., Kashiwakura, Y., Ishiwata, A., & Takano, K. (2006). Severe secondary deficiency of von Willebrand factor – cleaving protease (ADAMTS13) in patients with sepsis-induced disseminated intravascular coagulation : its correlation with development of renal failure. *Blood*, *107*(2), 528–535.

Palta, S., Saroa, R., & Palta, A. (2014). Overview of the coagulation system. *Indian Journal of Anaesthesia*, *58*(5), 515–523.

Patick, A. K., & Potts, K. E. (1998). Protease inhibitors as antiviral agents. *Clinical Microbiology Reviews*, *11*(4), 614–627.

Periayah, M., Halim, A., & Saad, A. (2017). Mechanism action of platelets and crucial blood coagulation pathways in Hemostasis. *International Journal of Hematology-Oncology and Stem Cell Research*, *11*(4), 319–327.

Petri, A., Kim, H. J., Xu, Y., de Groot, R., Li, C., Vandenbulcke, A., Vanhoorelbeke, K., Emsley, J., & Crawley, J. T. B. (2019). Crystal structure and substrate-induced activation of ADAMTS13. *Nature Communications*, *10*(1), 1–16.

Peyvandi, F., Garagiola, I., & Baronciani, L. (2011). Role of von Willebrand factor in the haemostasis. *Blood Transfusion*, *9*(SUPPL. 2), 3–8.

Pillai, V. G., Bao, J., Zander, C. B., Mcdaniel, J. K., Chetty, P. S., Seeholzer, S. H., Bdeir, K., Cines, D. B., & Zheng, X. L. (2016). Human neutrophil peptides inhibit cleavage of von Willebrand factor by ADAMTS13 : a potential link of inflammation to TTP. *Blood*, *128*(1), 110–120.

Pipe, S. W., Montgomery, R. R., Pratt, K. P., Lenting, P. J., & Lillicrap, D. (2016). Life in the shadow of a dominant partner: the FVIII-VWF association and its clinical implications for hemophilia A. *Blood*, *128*(16), 2007–2016.

Pos, W., Crawley, J. T. B., Fijnheer, R., Voorberg, J., Lane, D. A., & Luken, B. M. (2010). An autoantibody epitope comprising residues R660, Y661, and Y665 in the ADAMTS13 spacer domain identifies a binding site for the A2 domain of VWF. *Blood*, *115*(8), 1640–1649.

Prechel, M. M., & Walenga, J. M. (2013). Emphasis on the Role of PF4 in the Incidence, Pathophysiology and Treatment of Heparin Induced Thrombocytopenia. *Thrombosis Journal*, *11*(1), 1–9.

Qu, A., & Leahy, D. J. (1995). Crystal structure of the I-domain from the CD11a/CD18 (LFA-1 ab2) integrin. *Proceedings of the National Academy of Sciences*, *92*(22), 10277–10281.

Rasmussen, H., & McCann, P. (1997). Matrix Metalloproteinase Inhibition as a Novel Anticancer Strategy: A Review with Special Focus on Batimastat and Marimastat. *Pharmacol. Ther*, *75*(1), 69–75.

Rehman, A. A., Ahsan, H., & Khan, F. H. (2013). Alpha-2-macroglobulin: A physiological guardian. *Journal of Cellular Physiology*, *228*(8), 1665–1675.

Reiter, R. A., Varadi, K., Turecek, P. L., Jilma, B., & Knöbl, P. (2005). Changes in ADAMTS13 (von-Willebrand-factor-cleaving protease) activity after induced release of von Willebrand factor during acute systemic inflammation. *Thromb Haemost*, *93*, 554–558.

Rock, G. A., Shumak, K. H., Buskard, N. A., Blanchette, V. S., Kelton, J. G., Nair, R. C., Spasoff, R. A., & Group, & T. C. A. S. (1991). Comparison of plasma exchange with plasma infusion in the treatment of thrombotic thrombocytopenic purpura. *The New England Journal of Medicine*, *325*(6), 393–397.

Romão De Souza, V., Beatriz Cavalcante De Oliveira, A., Maria Vanderlei, A., Queiroz

Da Mota Silveira Aroucha, A., Pontes Duarte, B., Nunes Machado, A., Netto Chaer, L., Wanderley De Barros Correia, C., Da Conceição De Barros Correia, M., & Freire Hazin Costa, M. (2018). Inherited thrombotic thrombocytopenic purpura mimicking immune thrombocytopenic purpura during pregnancy: A case report. *Journal of Medical Case Reports*, *12*(1), 1–6.

Romijn, R. A., Bouma, B., Wuyster, W., Gros, P., Kroon, J., Sixma, J. J., & Huizinga, E. G. (2001). Identification of the Collagen-binding Site of the von Willebrand Factor A3-domain. *Journal of Biological Chemistry*, *276*(13), 9985–9991.

Romijn, R. A., Westein, E., Bouma, B., Schiphorst, M. E., Sixma, J. J., Lenting, P. J., & Huizinga, E. G. (2003). Mapping the collagen-binding site in the von Willebrand factor-A3 domain. *Journal of Biological Chemistry*, *278*(17), 15035–15039.

Roose, E., Schelpe, A. S., Joly, B. S., Peetermans, M., Verhamme, P., Voorberg, J., Greinacher, A., Deckmyn, H., De Meyer, S. F., Coppo, P., Veyradier, A., & Vanhoorelbeke, K. (2018). An open conformation of ADAMTS-13 is a hallmark of acute acquired thrombotic thrombocytopenic purpura. *Journal of Thrombosis and Haemostasis*, *16*(2), 378–388.

Rudzińska, M., Daglioglu, C., Savvateeva, L. V., Kaci, F. N., Antoine, R., & Zamyatnin, A. A. (2021). Current status and perspectives of protease inhibitors and their combination with nanosized drug delivery systems for targeted cancer therapy. *Drug Design, Development and Therapy*, *15*, 9–20.

Ruggeri, Z. M. (2003). Von Willebrand factor, platelets and endothelial cell interactions. *Journal of Thrombosis and Haemostasis*, *1*(7), 1335–1342.

Sadler, J. E. (1998). Biochemistry and genetics of von Willebrand factor. *Annu. Rev. Bioichem*, *67*, 395–424.

Sadler, J. E. (2008). Von Willebrand factor, ADAMTS13, and thrombotic thrombocytopenic purpura. *Blood*, *112*(1), 11–18.

Sadler, J. E. (2015). What's new in the diagnosis and pathophysiology of thrombotic thrombocytopenic purpura. *ASH Education Program Book*, 631–636.

Schelpe, A. S., Petri, A., Roose, E., Pareyn, I., Deckmyn, H., De Meyer, S. F., Crawley, J. T. B., & Vanhoorelbeke, K. (2020). Antibodies that conformationally activate ADAMTS13 allosterically enhance metalloprotease domain function. *Blood Advances*, *4*(6), 1072–1080.

Scully, M., Cataland, S. R., Peyvandi, F., Coppo, P., Knöbl, P., Kremer Hovinga, J. A., Metjian, A., de la Rubia, J., Pavenski, K., Callewaert, F., Biswas, D., De Winter, H., & Zeldin, R. K. (2019). Caplacizumab Treatment for Acquired Thrombotic Thrombocytopenic Purpura. *New England Journal of Medicine*, *380*(4), 335–346.

Scully, M., Knöbl, P., Kentouche, K., Rice, L., Windyga, J., Schneppenheim, R., Kremer Hovinga, J. A., Kajiwara, M., Fujimura, Y., Maggiore, C., Doralt, J., Hibbard, C., Martell, L., & Ewenstein, B. (2017). Recombinant ADAMTS-13: First-in-human pharmacokinetics and safety in congenital thrombotic thrombocytopenic purpura. *Blood*, *130*(19), 2055–2063.

Shieh, H.-S., Mathis, K. J., Williams, J. M., Hills, R. L., Wiese, J. F., Benson, T. E., Kiefer, J. R., Marino, M. H., Carroll, J. N., Leone, J. W., Malfait, A.-M., Arner, E. C., Tortorella, M. D., & Tomasselli, A. (2008). High Resolution Crystal Structure of the Catalytic Domain of ADAMTS-5 (Aggrecanase-2). *Journal of Biological Chemistry*, *283*(3), 1501–1507.

Shiltagh, N., Kirkpatrick, J., Cabrita, L. D., McKinnon, T. A. J., Thalassinos, K., Tuddenham, E. G. D., & Hansen, D. F. (2014). Solution structure of the major factor VIII binding region on von Willebrand factor. *Blood*, *123*(26), 4143–4151.

Sing, C. E., & Alexander-Katz, A. (2010). Elongational flow induces the unfolding of von willebrand factor at physiological flow rates. *Biophysical Journal*, *98*(9), L35–L37.

Singer, M., Seymour, C. W., Manu, S.-H., Duetschman, C. S., Opal, S. M., Rubenfeld, G. D., Poll, T. Van Der, Vincent, J., & Angus, D. C. (2016). The Third International Consensus Definitions for Sepsis and Septic Shock (Sepsis-3). *JAMA*, *315*(8), 801–810.

Smith, S. A., Travers, R. J., & Morrissey, J. H. (2016). Initiation of clotting cascade. *Critical Reviews in Biochemistry and Molecular Biology*, *50*(4), 326–336.

Soejima, K., Nakamura, H., Hirashima, M., Morikawa, W., Nozaki, C., & Nakagaki, T. (2006). Analysis on the molecular species and concentration of circulating ADAMTS13 in Blood. *J Biochem*, *139*(1), 147–154.

Solecka, B. A., Weise, C., Laffan, M. A., & Kannicht, C. (2016). Site-specific analysis of von Willebrand factor O-glycosylation. *Journal of Thrombosis and Haemostasis*, *14*(4), 733–746.

Somerville, R. P. T., Jungers, K. A., & Apte, S. S. (2004). Discovery and characterization of a novel, widely expressed metalloprotease, ADAMTS10, and its proteolytic activation. *Journal of Biological Chemistry*, *279*(49), 51208–51217.

South, K., Freitas, M. O., & Lane, D. A. (2016). Conformational quiescence of ADAMTS-13 prevents proteolytic promiscuity. *Journal of Thrombosis and Haemostasis*, *14*(10), 2011–2022.

South, K., Freitas, M. O., & Lane, D. A. (2017). A model for the conformational activation of the structurally quiescent metalloprotease ADAMTS13 by von Willebrand factor. *Journal of Biological Chemistry*, *292*(14), 5760–5769.

South, K., Luken, B. M., Crawley, J. T. B., Phillips, R., Thomas, M., Collins, R. F., Deforche, L., Vanhoorelbeke, K., & Lane, D. A. (2014). Conformational activation of ADAMTS13. *Proceedings of the National Academy of Sciences of the United States of America*, *111*(52), 18578–18583.

Springer, T. A. (2014). von Willebrand factor, Jedi knight of the bloodstream. *Blood*, *124*(9), 1412–1425.

Steinhubl, S. R., Tan, W. A., Foody, J. M., & Topol, E. J. (1999). Incidence and Clinical Course of Thrombotic Thrombocytopenic Purpura Due to Triclopidine Follwing Cornonary Stenting. *JAMA*, *281*(9), 806–810.

Stokol, T., Millar, P., Adarraga, J., Wong, C., Babcock, G., Mazhar, B., Felippe, J., & Warnick, L. (2013). *Hemostasis*. EClinpath Cornell University.

Swystun, L. L., & Lillicrap, D. (2018). Genetic regulation of plasma von Willebrand factor levels in health and disease. *J Thromb Haemost*, *16*(12), 2375–2390.

Tallant, C., Marrero, A., & Gomis-Rüth, F. X. (2010). Matrix metalloproteinases: Fold and function of their catalytic domains. *Biochimica et Biophysica Acta - Molecular Cell Research*, *1803*(1), 20–28.

Terrell, D. R., Vesely, S. K., Kremer Hovinga, J. A., Lämmle, B., & George, J. N. (2010). Different disparities of gender and race among the thrombotic thrombocytopenic purpura and hemolytic-uremic syndromes. *American Journal of Hematology*, *85*(11), 844–847.

Tjernberg, P., Vos, H. L., Castaman, G., Bertina, R. M., & Eikenboom, J. C. J. (2004). Dimerization and multimerization defects of von Willebrand factor due to mutated cysteine residues. *Journal of Thrombosis and Haemostasis*, *2*(2), 257–265.

Tortorella, M. D., Arner, E. C., Hills, R., Easton, A., Korte-Sarfaty, J., Fok, K., Wittwer, A. J., Liu, R. Q., & Malfait, A. M. (2004). A2-Macroglobulin Is a Novel Substrate for ADAMTS-4 and ADAMTS-5 and Represents an Endogenous Inhibitor of These Enzymes. *Journal of Biological Chemistry*, *279*(17), 17554–17561.

Tortorella, M. D., Tomasselli, A. G., Mathis, K. J., Schnute, M. E., Woodard, S. S., Munie, G., Williams, J. M., Caspers, N., Wittwer, A. J., Malfait, A.-M., & Shieh, H.-S. (2009). Structural and inhibition analysis reveals the mechanism of selectivity of a series of aggrecanase inhibitors. *The Journal of Biological Chemistry*, *284*(36), 24185–24191.

Uemura, M., Fujimura, Y., Ko, S., Matsumoto, M., Nakajima, Y., & Fukui, H. (2010). Pivotal role of ADAMTS13 function in liver diseases. *International Journal of Hematology*, *91*(1), 20–29.

Uemura, M., Tatsumi, K., Matsumoto, M., Fujimoto, M., Matsuyama, T., Ishikawa, M.,

& Iwamoto, T. (2005). Localization of ADAMTS13 to the stellate cells of human liver. *Blood*, *106*(3), 922–924.

Upreti, H., Kasmani, J., Dane, K., Braunstein, E. M., Streiff, M. B., Shanbhag, S., Moliterno, A. R., Sperati, C. J., Gottesman, R. F., Brodsky, R. A., Kickler, T. S., & Chaturvedi, S. (2019). Reduced ADAMTS13 activity during TTP remission is associated with stroke in TTP survivors. *Blood*, *134*(13), 1037–1045.

Urban, S., & Dickey, S. W. (2011). The rhomboid protease family: A decade of progress on function and mechanism. *Genome Biology*, *12*(10).

Van Wart, H. E., & Birkedal-Hansen, H. (1990). The cysteine switch: a principle of regulation of metalloproteinase activity with potential applicability to the entire matrix metalloproteinase gene family. *Proceedings of the National Academy of Sciences*, *87*(14), 5578–5582.

Varadi, M., Anyango, S., Deshpande, M., Nair, S., Natassia, C., Yordanova, G., Yuan, D., Stroe, O., Wood, G., Laydon, A., Žídek, A., Green, T., Tunyasuvunakool, K., Petersen, S., Jumper, J., Clancy, E., Green, R., Vora, A., Lutfi, M., … Velankar, S. (2022). AlphaFold Protein Structure Database: massively expanding the structural coverage of protein-sequence space with high-accuracy models. *Nucleic Acids Research*, *50*(D1), D439–D444.

Versteeg, H. H., Heemskerk, J. W. M., Levi, M., & Reitsma, P. H. (2013). New Fundamentals in Hemostasis. *Physiological Reviews*, *93*(1), 327–358.

Visse, R., & Nagase, H. (2003). Matrix metalloproteinases and tissue inhibitors of metalloproteinases: Structure, function, and biochemistry. *Circulation Research*, *92*(8), 827–839.

Wagner, D. D. (1990). Cell biology of von Willebrand factor. *Annu. Rev. Cell Biol.*, *6*, 217–246.

Wendelboe, A. M., & Raskob, G. E. (2016). Global Burden of Thrombosis: Epidemiologic Aspects. *Circulation Research*, *118*(9), 1340–1347.

Wu, K. K., & Thiagarajan, P. (1996). Role of endothelium in thrombosis and hemostasis. *Annual Review of Medicine*, *47*, 315–331.

Xu, A. J., & Springer, T. A. (2012). Calcium stabilizes the von Willebrand factor A2 domain by promoting refolding. *Proceedings of the National Academy of Sciences of the United States of America*, *109*(10), 3742–3747.

Zanardelli, S., Chion, A. C. K., Groot, E., Lenting, P. J., McKinnon, T. A. J., Laffan, M. A., Tseng, M., & Lane, D. A. (2009). A novel binding site for ADAMTS13 constitutively exposed on the surface of globular VWF. *Blood*, *114*(13), 2819–2828.

Zander, C., Cao, W. J., & Zhang, X. (2015). ADAMTS13 and von Willebrand factor interactions. *Curr Opin Hematol*, *2*(5), 452–459.

Zhang, P., Pan, W., Rux, A. H., Sachais, B., & X.L. Zheng. (2007). The cooperative activity between the carboxyl-terminal TSP1 repeats and the CUB domains of ADAMTS13 is cruical for recognition of von Willebrand factor under flow. *Blood*, *110*(6), 1887–1894.

Zhang, Q., Zhou, Y. F., Zhang, C. Z., Zhang, X., Lu, C., & Springer, T. A. (2009). Structural specializations of A2, a force-sensing domain in the ultralarge vascular protein von Willebrand factor. *Proceedings of the National Academy of Sciences of the United States of America*, *106*(23), 9226–9231.

Zhang, X., Halvorsen, K., Zhang, C. Z., Wong, W. P., & Springer, T. A. (2009). Mechanoenzymatic cleavage of the ultralarge vascular protein von willebrand factor. *Science*, *324*(5932), 1330–1334.

Zheng, X. L. (2013). Structure-function and regulation of ADAMTS13. *J Thromb Haemost*, *11*(1), 11–21.

Zhou, M., Dong, X., Baldauf, C., Chen, H., Zhou, Y., Springer, T. A., Luo, X., Zhong, C., Gräter, F., & Ding, J. (2011). A novel calcium-binding site of von Willebrand factor A2 domain regulates its cleavage by ADAMTS13. *Blood*, *117*(17), 4623–4631.

Zhou, Y. F., & Springer, T. A. (2014). Highly reinforced structure of a C-terminal dimerization domain in von Willebrand factor. *Blood*, *123*(12), 1785–1793.

Chapter 11: Appendix

Table 10.1. Summary of the effects of A2M, TIMPs, and Marimastat on all constructs, chimeras, and variants. Green – resistant; yellow – partial inhibition, red – inhibited.

	A2M	TIMP1	TIMP2	TIMP3	TIMP4	Marimastat
Deletion Constructs						
ADAMTS13						
MDTCS						
MD						
Chimeras						
ADAMTS5						
MD13/TCS5						
MD5/TCS13						
MD5(TCS-CUB13)						
Disintegrin Domain Engagement						
MDTCS + D-PEPTIDE						
MDTCS + T-VWF						
MDTCS + K-VWF						
MD + D-PEPTIDE						
MD + T-VWF						
MD + K-VWF						
Metalloprotease Domain Mutations (MDTCS)						
Gatekeeper Triad						
Calcium-binding loop and Gatekeeper (R193) with ADAMTS5						
Variable loop swap with ADAMTS5						
Gatekeeper triad, calcium-binding loop, and variable loop swap with ADAMTS5						

Table 10.2. Summary of pertinent construct information, including the type of expression vector, mammalian cell line, purification/detection tag(s), and selection/induction compound(s).

Construct	Vector	Cell type	Tag	Selection
FL-ADAMTS13	pcDNA 4/TO	HEK 293T REX	His, V5	Zeo, Blast, induce with tet
FL-ADAMTS13	pcDNA 3.1(+)	HEK 293T	Strep, V5	G418
MDTCS	pcDNA 3.1-LIC	HEK 293T	His	Zeo
MDTCS	pcDNA 3.1(+)	HEK 293T	Strep, V5	G418
MD	pcDNA 3.1-LIC	HEK 293T	His	Zeo
MD13/TCS5	pcDNA 4/TO	HEK 293T	His, V5	Zeo, induce with tet, add heparin
M13/DTCS5	pcDNA 3.1(+)	HEK 293T	Strep, V5	G418
MD5/TCS13	pcDNA 4/TO	HEK 293T	His, V5	Zeo, induce with tet
MD5(TCS-CUB13)	pcDNA 4/TO	HEK 293T	His, V5	Zeo, induce with tet
MDTCS (R193A, D217A, and D252A)	pcDNA 3.1(+)	HEK 293T	Strep, V5	G418
MDTCS (G236-P244 to ATS5 D421-F429)	pcDNA 3.1(+)	HEK 293T	Strep, V5	G418
MDTCS (R180-R193 to ATS5 R367-L379)	pcDNA 3.1(+)	HEK 293T	Strep, V5	G418
MDTCS (R180-R193 to ATS5 R367-L379, D217A, and G236-S263 to ATS5 D422-S453)	pcDNA 3.1(+)	HEK 293T	Strep, V5	G418